RICE UNIVERSITY

In Vivo and *In Vitro* Remodeling of a Small Intestinal Submucosa Extracellular Matrix Cardiac Patch in an Ovine Model and Splashing Bioreactor

Brandi Braud Scully

A THESIS SUBMITTED
IN PARTIAL FULFILLMENT OF THE
REQUIREMENTS FOR THE DEGREE

Master of Science

APPROVED, THESIS COMMITTEE

K. Jane Grande-Allen, Ph.D.
Associate Professor, Department of Bioengineering
Adjunct Associate Professor, Department of Surgery
Rice University and Baylor College of Medicine
Committee Chair

David L.S. Morales, M.D.
Associate Professor, Departments of Surgery and Pediatrics
Adjunct Associate Professor, Bioengineering
Baylor College of Medicine and Rice University

Jeffrey G. Jacot, Ph.D.
Assistant Professor, Department of Bioengineering
Assistant Professor of Surgery, Division of Congenital Heart Surgery
Texas Children's Hospital and Rice University

Daniel Harrington, Ph.D.
Faculty Fellow, Department of Biochemistry and Cell Biology
Rice University

Charles D. Fraser, Jr., M.D.
Professor, Departments of Surgery and Pediatrics
Adjunct Professor, Bioengineering
Baylor College of Medicine and Rice University
Donovan Chair and Chief of Congenital Heart Surgery
Surgeon-In-Chief, Texas Children's Hospital

HOUSTON, TEXAS, MAY 2012

ABSTRACT

In Vivo and *In Vitro* Remodeling of a Small Intestinal Submucosa Extracellular Matrix Cardiac Patch in an Ovine Model and Splashing Bioreactor

by

Brandi Braud Scully

Previous studies have demonstrated that surgical patches comprised of small intestinal submucosa (SIS)-derived extracellular matrix (ECM) have biological remodeling potential in various tissues. In this series of experiments, the remodeling potential of a commercially available cardiac SIS-ECM patch was examined in both *in vivo* and *in vitro* models.

This thesis begins by introducing the clinical need for a tissue-engineered cardiovascular scaffold that can grow with the patient and avoid the morbidity associated with currently available synthetic and biological materials. Such a patch would transform the surgical repair of congenital heart disease, in particular of patients with tetralogy of Fallot and in the repair of mitral regurgitation.

The *in vivo* study investigated histological, mechanical, and bioelectrical properties of an SIS-ECM patch implanted in the ovine right-ventricular outflow tract (RVOT), and the histological and mechanical properties of the same patch implanted in the descending aorta and main pulmonary artery of a juvenile ovine. We found the juvenile ovine model to be a suitable model for evaluation of SIS-ECM patch remodeling, as seen by *in vivo* echocardiography, electrical mapping, and *ex vivo* optical mapping for the RVOT patch and mechanical testing, histology and

immunohistochemistry for patches placed in all three positions.

The *in vitro* study looked at an SIS-ECM patch pretreated with pepsin, seeded with mitral valve interstitial cells (MVICs), and exposed to mechanical stimulation in a splashing bioreactor for one week. Greater cell integration and proliferation and greater tissue cohesion was seen in the pepsin-treated SIS-ECM, while groups without mechanical stimulation demonstrated a stiffening effect for the bioreactor.

In sheep, the SIS-ECM patch appears capable of remodeling to resemble native, functional ventricular tissue, but further validation of this patch material is required. Bioreactors can play an important role in validation of this promising scaffold material.

Tissue-engineered scaffolds are unique in their complete ontological metamorphosis (from scaffold material to part of the patient's own tissue) and pose distinctive ethical challenges that must be responsibly managed. Contract studies, such as the research presented in chapters 3-5, that are funded by the medical device industry require close scrutiny and precautions to avoid conflicts of interest.

ACKNOWLEDGMENTS

A grateful mind
By owing owes not, but still pays, at once
Indebted and discharged
-Paradise Lost, IV.55-57

No one can be more surprised than I am that I have written a thesis and completed the coursework for an M.S. in Bioengineering. I would like to point out that the first thesis I wrote as a Rice student was a *tad* different; it was a senior thesis for the English department entitled "The Debt Immense of Endless Gratitude: John Milton's Indebtedness to William Shakespeare." A common theme in my life has been the doing of things that would completely surprise my younger self. So I begin this thesis in the same manner that I began my last one, by quoting Lucifer in *Paradise Lost* at his most introspective. I interpret Milton's words above as meaning that the only way to discharge your debt to someone is to fully recognize it. I am extremely grateful to the many people who have mentored me and shaped my life in unexpected ways.

I thank my thesis committee for their guidance in this undertaking, and especially Dr. Grande-Allen for welcoming a novice medical student into her lab and for her encouragement and support on projects large and small, including pursuing an M.S. The fact that she could have me running a bioreactor in a few months is a testament to what an extraordinary mentor she is. I am proud to have been a member of the lab and have thoroughly enjoyed the collegial and warm atmosphere. I would like to thank everyone in the Grande-Allen lab, in particular Dr. Christopher Durst and Hubert Tseng, who taught me almost everything in the lab and who continue to amaze me with their breadth of knowledge and zeal for scientific discovery. Thank you also to everyone in the Pediatric Cardiac Bioengineering Laboratory, who allowed me to take over a lab bench

with the optical mapping setup, and the veterinarians and everyone at the Experimental Surgery and Surgery Training Laboratories, without whom the surgeries would have never happened. In addition, these studies would not have been possible without the undergraduates I worked with: Minsuk Kwak, Kendra Erskine, Chris Fan, and Bagrat Grigoryan.

This all began over seven years ago, when I was a Michael E. DeBakey Summer Surgery Intern in the Congenital Heart Surgery Department at Texas Children's Hospital. I thank Dr. Fraser for his mentorship of me ever since, and for sponsoring me for the American Association for Thoracic Surgery's Summer Intern Scholarship that helped to fund this work. I continue to be inspired by his example of leadership and relentless pursuit of excellence.

It was during this internship that I also met Dr. Morales, and I cannot possibly do justice to the countless hours he has spent mentoring me, and his impact on my life. I have learned more than I would have ever thought possible. I am grateful for the many opportunities our collaboration has given me, including getting to know his amazing family. I am looking forward to seeing the results of the next phase of this study, and hope that in 15 years I will be changing my patients' lives as he does his.

Credit also goes to my incredibly supportive family, who have given me the gift of a wonderful childhood and a first-rate education: my mother, for her unwavering belief that I can do anything, my father, the first engineer in my life, who showed me there's a right way to do everything, from dribbling a basketball to building a gingerbread house, my grandmother, who continues to feed me on a weekly basis, my grandfather, who has

never missed a game, and my twin brother, the reason I played with legos instead of dolls.

To Peter: thank you for keeping me company in lab in the middle of the night, teaching me multivariable calculus, listening to every hypothesis, reading every paragraph, and for asking me out eight years ago. Our son is by far the best thing that we have ever done. I love him and you, and home is wherever the three of us are.

These projects were funded in part by CorMatrix Cardiovascular, Inc and an American Association for Thoracic Surgery Summer Intern Scholarship.

TABLE OF CONTENTS

LIST OF FIGURES

LIST OF TABLES

LIST OF ABBREVIATIONS

BCM	Baylor College of Medicine
BDM	2,3-butanedione monoxime
ECM	extracellular matrix
ePTFE	expanded polytetrafluoroethylene
GAGs	glycosaminoglycans
IHC	immunohistochemistry
LIPG	endothelial lipase gene
LOX	lysyl oxidase
MMP	matrix metalloproteases
MVICs	mitral valve interstitial cells
PA	pulmonary artery
PBS	phosphate-buffered saline
PET	polyethylene terephthalate
PGA	polyglycolic acid
RVOT	right-ventricular outflow tract
SIS	small-intestinal submucosa
SIS-ECM	Extracellular matrix derived from porcine small-intestinal submucosa
TOF	tetralogy of Fallot

Chapter 1: Introduction, Study Design, and Specific Aims

1.1 Introduction

Congenital cardiovascular defects remain the leading cause of death from congenital malformations.[1] To repair these defects, congenital heart surgeons use patch materials in a plethora of surgeries, including repair of interventricular defects, interatrial defects, reconstruction of the ventricular outflow tracts, repair of heart valves, and repair of the aorta. Currently, no ideal patch material exists that can be used in this population. The materials available for use, including polyethylene terephthalate (PET; Dacron®), expanded polytetrafluoroethylene (ePTFE; GORE-TEX®) and membrane materials such as bovine pericardium, are associated with significant morbidity. These materials can produce significant inflammatory response leading to calcification, can become infected or thrombogenic, and cannot grow with the patient, often necessitating reoperation later in life.[2,3] When used in the repair of the mitral valve, these materials can lead to such complications as recurrent mitral dysfunction and thromboembolic events.[4] There remains a great clinical need for a more optimal biomaterial to use in cardiovascular applications.

Tissue engineering has been used to develop autologous vascular grafts with the potential for repair, remodeling, and growth. Other engineered tissues, such as heart valves, are being developed by seeding appropriate cell types within a suitable scaffold, followed by a period of incubation during which the cells remodel the scaffold and secrete extracellular matrix to form new tissue.[5] The goal of all tissue-engineered materials is to have as many of the ideal features of the tissue they replace as possible. These features include (i) maintaining normal structure and biological function over a

patient's lifetime, (ii) not causing an immunologic response, (iii) being antithrombotic, (iv) having the potential for growth and self-repair, (v) ease of implantation, and (vi) being available in an unlimited supply.[5]

Numerous scaffolds have been developed for the creation of cardiac grafts. Many of the designs have been biodegradable polymeric scaffolds, or grafts in which cells are seeded within a scaffold that degrades slowly, transferring function to the subsequent extracellular matrix produced by these cells. Smooth muscle cell-seeded biodegradable materials have been used in several applications, including repair of the right ventricular outflow tract.[6]

Another approach to the problem of tissue-engineered biomaterials is the application of decellularized scaffolds. In the past decade, decellularized extracellular matrix scaffolds have become increasingly available, originating from a variety of tissue and animal sources.[7–18] The advantages of decellularized scaffolds as opposed to biodegradable ones are that they already contain the requisite strength and contain extracellular matrix in the correct microstructural arrangement.[12,13] In addition, by removing the cells, it is believed that most antigenic elements are eliminated, avoiding an immunological response in the recipient. Collagen is the primary matrix element in these scaffolds, and is considered minimally antigenic.[19]

Once implanted, these scaffolds can be populated by cells coming from two places: adjacent tissue or from the blood. Cells coming from the blood, or circulating progenitor cells, respond to the scaffold environment by excreting extracellular matrix (as would other cell types) and by changing their phenotype.[11]

Small intestinal submucosa (SIS) has proven to be an especially promising

decellularized scaffold. It has been shown to support vascularization, tissue development, and restoration of regional mechanical functionality in numerous tissues in both animals and humans. SIS-ECM is currently being used in patients for musculo-tendinous replacement, bladder reconstruction, dura mater replacement, and body wall repair.[7–10]

While many of the mechanisms responsible for remodeling of SIS-ECM scaffolds remain to be elucidated, several processes have emerged that appear essential for the remodeling process. Degradation by matrix-degrading enzymes, the phenotype of macrophages homing to the scaffold following implantation, the presence or absence of chemical cross-linking of the scaffold, and the subsequent release of growth factors and other cytokines have all been shown to play important roles.[20–25] These growth factors, in turn, promote remodeling processes including angiogenesis, cell migration and cell proliferation.[21,23,25]

There has been growing interest in the use of SIS-ECM to replace, repair, or reconstruct cardiac tissue. SIS-ECM has been used in several cardiac applications with promising results, but remains in the initial phase of testing. When used in the ventricle, it has been shown to be repopulated with myocytes in an adult pig model.[20] In vessels, it has been shown to confer mechanical benefit in the canine model compared to Dacron.[26] In addition, SIS-ECM has been used in valve repair, specifically of the mitral valve, repair of which with non-remodeling materials (such as Dacron or GORE-TEX) can lead to such complications as recurrent mitral dysfunction and thromboembolic events.[4]

Small intestinal submucosa patches offer great promise and new solutions for tissue engineering to meet pediatric needs, and have the potential to transform the care of this population. The clinical applications of an SIS-ECM patch material that remodels into native heart tissue are virtually endless. Documenting the ability of SIS-ECM to remodel

to cardiac tissue would validate and establish a novel graft material with significant implications for a patient population in critical need. The detailed analysis of extracellular matrix components within remodeling cardiac/cardiovascular tissues repaired with a cardiac patch, as presented here, offers significant insight into this remodeling process as well as into the suitability of the juvenile ovine model for these studies, and brings us one step closer to accomplishing the ultimate goal of tissue engineering of cardiac patches: the ability to replace damaged or absent myocardium, heart valves, and blood vessels with functional tissue.

1.2 Study Design

To evaluate whether these SIS-ECM patches remodel to resemble native heart and vascular tissues, this body of work proposes to characterize the SIS-ECM patches by a number of mechanisms. To thoroughly characterize SIS-ECM remodeling potential, both *in vivo* studies, which are the most physiologically accurate but expensive and subject to experimental variability, and *in vitro* studies, which mimic *in vivo* conditions, are less expensive and more easily reproducible, are needed. Therefore we investigated the remodeling potential of an SIS-ECM patch both in an animal model and a splashing bioreactor designed by Barzilla et al.[27] With these experiments, we hope to gain a more complete understanding of this scaffold's remodeling processes.

An *in vivo* study was conducted in which we implanted the SIS-ECM patches atop surgically created defects in the descending aorta, main pulmonary artery, and RVOT of a juvenile ovine model for either five or eight months. Functional tests of the patch placed in the right ventricular outflow tract position were then performed to assess mechanical function; for all three positions, mechanical testing was performed to evaluate elasticity and extensibility, histological stains were used to characterize the structure and

neovascularization of the tissue and potential for calcification, and immunohistochemistry was used to determine the phenotype of the cells and ECM within the explanted repaired tissue/patch and the presence of enzymes involved in extracellular matrix synthesis and turnover.

Our goals for this *in vivo* study were to assess the suitability of the juvenile ovine model for evaluation of the histologic, mechanical, and electrical properties of a commercially available ECM patch following implantation in the aortic, pulmonary artery, and right ventricular outflow tract positions. In order to do this, we investigated whether the ECM patch, after 5-8 months of implantation, acts similarly to native heart and vascular tissue in (i) conduction of an electrical impulse, (ii) microstructure of the extracellular matrix, (iii) neovascularization, (iv) calcification, and (v) cell phenotype and proliferation.

In addition, an *in vitro* study was designed to replicate the remodeling of scaffold materials when used to repair the mitral valve. This study aimed to evaluate the effect of pepsin degradation on the remodeling of SIS-ECM patches that have been seeded with porcine mitral valvular interstitial cells (MVICs) and subjected to mechanical stimulation *in vitro*.

Our goals for this *in vitro* study were to investigate the effect of pre-treatment with matrix-degrading enzymes, cell-seeding with MVICs -- which are key regulators of valve structure and function -- and bioreactor mechanical stimulation on SIS-ECM remodeling *in vitro*, through characterization of (i) mechanical properties, (ii) cell phenotype and proliferation, and (iii) microstructure of the extracellular matrix.

1.3 Specific Aims

1.3.1 Specific Aim 1: Assess the suitability of the juvenile ovine model in evaluating the remodeling of an SIS-ECM patch implanted in the right ventricular outflow tract.

Hypothesis: SIS-ECM patches will have the ability to remodel when placed in the right ventricular outflow tract of a juvenile ovine model.

Approach: Remodeling was characterized using *in vivo* contact echocardiography and electrical mapping, optical mapping on explanted, Langendorff-perfused hearts, and mechanical testing, histology, and immunohistochemistry on explanted tissue.

Significance: SIS-ECM patches were shown to remodel in the RVOT position. With confirmation of these promising results through further evaluation including larger sample sizes and control arms, the potential clinical applications are abundant and would have the potential to transform care of patients needing patched repair of their RVOT such as patients with tetralogy of Fallot.

1.3.2 Specific Aim 2: Assess the suitability of the juvenile ovine model in evaluating the remodeling of an SIS-ECM patch implanted in the descending aorta and main pulmonary artery.

Hypothesis: SIS-ECM patches will have the ability to remodel when placed in the pulmonary artery and aortic positions of a juvenile ovine model.

Approach: Remodeling was characterized using mechanical testing, histology, and immunohistochemistry on explanted tissue.

Significance: SIS-ECM patches were shown to remodel in the aorta and pulmonary artery positions. As in Aim 1, these promising results should inspire further pre-

clinical evaluation, because the potential clinical applications are abundant and would have the potential to transform care of patients needing patched repair of the aorta or pulmonary artery.

1.3.3 Specific Aim 3: Optimize and evaluate the remodeling of an SIS-ECM patch undergoing enzyme degradation, seeding with MVICs, and culture in a mechanical stimulation bioreactor.

Hypothesis: SIS-ECM patches will demonstrate superior remodeling when they are pre-treated with matrix-degrading enzymes, seeded with MVICs, and subjected to mechanical stimulation from a splashing bioreactor.

Approach: Remodeling will be characterized using mechanical testing, histology, and immunohistochemistry on SIS-ECM patches with and without mechanical stimulation.

Significance: Establishing an *in vitro* model that allows further investigation into the importance of enzymatic pretreatment and the crucial role of MVICs in valve remodeling will aid in the translation of this technology to the clinical setting.

Chapter 2: Background

2.1 Congenital Heart Disease and Tissue Engineering Applications

Congenital heart defects occur in close to 1% of live births in the United States, and can impede adequate circulation and threaten the development of multiple organ systems, including the heart and lungs.[28] The goals of surgical repair of congenital heart disease include establishing anatomic continuity and achieving a physiologic circulation.[3] This often requires that congenital heart surgeons use valves, conduits, and a variety of patch materials, which are associated with significant morbidity and mortality secondary to thrombosis, infection, their inability to grow with the patient, and arrhythmias, and can lead to multiple reoperations.[2,3]

Surgical repair of congenital heart disease began in 1939, when Dr. Robert Gross published a report chronicalling the first successful patent ductus ligation.[29] In 1944, at Johns Hopkins Hospital, Dr. Alfred Blalock performed the first surgical palliation of tetralogy of Fallot (TOF), a congenital heart syndrome consisting of four different anomalies: right ventricular hypertrophy, pulmonary stenosis, an overriding aorta, and a ventricular septal defect.[19] Without surgery, 35% of TOF patients die before they reach one year of age, 50% by the age of three, and very few survive into adulthood.

In their landmark paper chronicling their first three operations on cyanotic babies, Helen Taussig and Blalock set forth their argument for surgery: "The operation here reported and the studies leading thereto were undertaken with the conviction that even though the structure of the heart was grossly abnormal, in many instances it might be possible to alter the course of the circulation in such a manner as to lessen the cyanosis

and the resultant disability".[19] Nine years later, Lillehei and his team first completed an intracardiac repair of a tetralogy of Fallot patient, and physicians could begin to surgically address the malformations associated with the syndrome.[30–32] These early operations are considered the dawn of both congenital and adult cardiothoracic surgery.[33] This is particularly relevant to the current study, as TOF patients often require RVOT patch placement following their primary repair. Thus, TOF patients continue to be at the forefront of advancements in the field of congenital heart surgery, as researchers work to create tissue-engineered patches capable of meeting this patient population's needs.

The following decades saw advances in surgical technique, and between 1970 to 1990, the introduction of prostaglandins, advances in infant surgery, and the rise of echocardiography greatly improved outcomes for patients with congenital heart disease.[31] These advances have led to the current 30-day mortality rate of less than three percent for tetralogy of Fallot patients undergoing surgical repair.[34] The mortality rate has similarly dropped for all patients with cardiac defects requiring repair, and over 1 million adults are now living with congenital heart disease.[35]

As the field has advanced, the use of patch material has allowed repair of more and more complicated malformations, enabling surgeons to establish anatomic continuity and physiologic restoration.[3] For example, in patients with tetralogy of Fallot, a prosthetic conduit is often required to restore blood flow from the right side of the heart to the pulmonary system. In this study, we investigated the remodeling of a tissue-engineered cardiac patch implanted in the right ventricular outflow tract, a tissue-engineered application particularly relevant to tetralogy of Fallot patients, many of whom have undergone a transventricular patch repair and often return for pulmonary valve

replacement requiring right ventricular outflow tract patch placement.

2.2 Tissue Engineering of Cardiovascular Patches

No ideal patch material exists for use in the repair of congenital heart defects. The materials available for use include polyethylene terephthalate (PET; Dacron®), expanded polytetrafluoroethylene (ePTFE; GORE-TEX®) and membrane materials such as bovine pericardium. Dacron has been shown to induce a healing response leading to formation of scar tissue and contracture of the implant, thickening and increased stiffness.[36,37] Bovine pericardium has been shown to be associated with graft calcification and contraction.[38,39] All synthetic materials lack the ability to grow, remodel or regenerate. They are not chemotactic and cannot be functionally degraded, and thus cannot grow with the patient, often necessitating reoperation later in life.[3,4] Even native materials such as autologous pericardium, though they do not trigger an immune response, become fibrotic and retracted and can become aneurysmal and arrhythmic.[38,40] In TOF, this can lead to decreased right ventricular output, resulting in right ventricular failure for these patients, who often require multiple reoperations. A clinical need exists for a bioresorbable biomaterial for use in cardiovascular repair applications.

One approach to this problem is the use of cell-seeded biodegradable scaffolds. These scaffolds require that cells be harvested and seeded on the scaffolds prior to implantation. Cardiac patches have been engineered for repair of congenital heart defects by seeding autologous human umbilical cord-derived fibroblasts and endothelial progenitor cells on polyglycolic acid (PGA) scaffolds.[41] Vascular patches have been constructed using autologous cells harvested from peripheral veins seeded onto polymer

scaffolds.[42] Vascular patches have also been constructed by seeding bone marrow-derived cells onto decellularized scaffolds made from dog inferior vena cava.[43]

Another approach to this problem is the use of decellularized extracellular matrix scaffolds.[44] In contrast to synthetic biodegradable meshes, decellularized scaffolds contain extracellular matrix that can remodel, signal surrounding cells, and immediately serve as a load-bearing scaffold.[12,13] Extracellular matrix derived from porcine small-intestinal submucosa (SIS-ECM) in particular has been shown to be chemotactic (Reing et al. 2009[45]) and once implanted can become populated with progenitor cells from adjacent tissues as well as marrow-derived stem cells from the circulation.[46–48] Bone marrow cells can differentiate into smooth muscle cells and endothelial cells, and *in vivo* have been shown to differentiate into cell types that contribute to antiogenesis and vasculogensis.[11] Following migration and attachment, these cells can undergo proliferation, differentiation, and phenotypic maturation, remodeling the implanted scaffold into functional tissue in the process.[49,50] Furthermore, because all of the porcine cells are removed from the scaffold during processing, and because collagen is the primary matrix element remaining, these materials are considered minimally antigenic.[5]

2.3 Small Intestinal Submucosa Scaffolds

In both animals and humans, decellularized, SIS-derived scaffolds have been shown to support vascularization, tissue development, and restoration of regional mechanical functionality in numerous tissues. These materials are currently being used in humans for musculotendinous replacement, bladder reconstruction, dura mater replacement, and body wall repair.[7–10]

A commercial SIS-ECM product (CorMatrix) has also been cleared in the US and Europe for human cardiac tissue repair and pericardial closure as a patch only with no remodeling indication in the US (Fig. 2.1).[51–53] In preclinical models this material has been shown to be repopulated with myocytes[20] and to confer regional mechanical benefit in canine and bovine cardiac-repair models, which has led to its CE approval for cardiac tissue repair in Europe.[26 54]

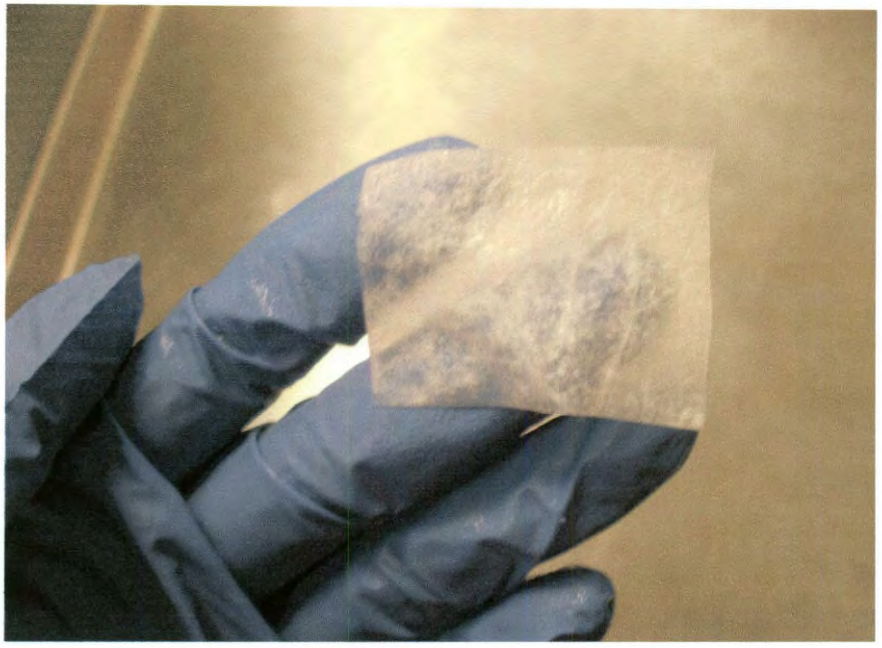

Figure 2.1 The CorMatrix patch prior to implantation. The patch is 4-ply and once rehydrated extremely difficult to tear. Photo taken by the author.

CorMatrix patches are decellularized using detergents and then freeze-dried with core components including proteoglycans and growth factors within the matrix. There appears to be little or no calcification following implantation, making the patch especially useful in pediatric populations. There is also evidence that the CorMatrix patch is replaced by neighboring myocardial or vascular tissue. Therefore, it has the possibility of both restoring tissue functionality and growing along with the child, eliminating the need for multiple repeat surgeries.

2.4 Mitral Valve Disease and Surgical Considerations

Degenerative mitral valve disease is the most common cause of mitral regurgitation in developed countries.[55] Mitral regurgitation is precipitated by leaflet prolapse, which can be caused by chordae elongation or rupture, and is associated with annular dilation. These anatomic changes can lead to clinical symptoms, including atrial fibrillation, pulmonary hypertension, and left ventricular dysfunction.[55]

The mitral valve often must be surgically repaired to address diseases such as myxomatous degeneration, the most common cause of mitral regurgitation in older patients (incidence of 2.4-5%).[56,57] Clinicians prefer repair of the mitral valve over replacement with a bioprosthetic or mechanical valve, due to repair offering superior long-term results and the ability to avoid lifelong anticoagulation treatment.[58] Mitral valve replacement can lead to an increased risk of endocarditis, thrombosis, infection, calcification, and bleeding from chronic anticoagulation.[3] In addition, children have a greater risk of calcification of implanted valves and an accelerated rate of degeneration.[28,59,60] Surgical repair is considered superior to replacement of the mitral valve, with lower operative mortality, improved late survival, preservation of left ventricular function, decreased risk of endocarditis, and avoidance of antiocoagulant-related complications such as hemorrhage.[61,62]

An understanding of mitral valve anatomy and function is necessary for successful repair of the mitral valve.[62] The mitral valve is one of four heart valves, and one of two atrioventricular valves (Fig.2.2).

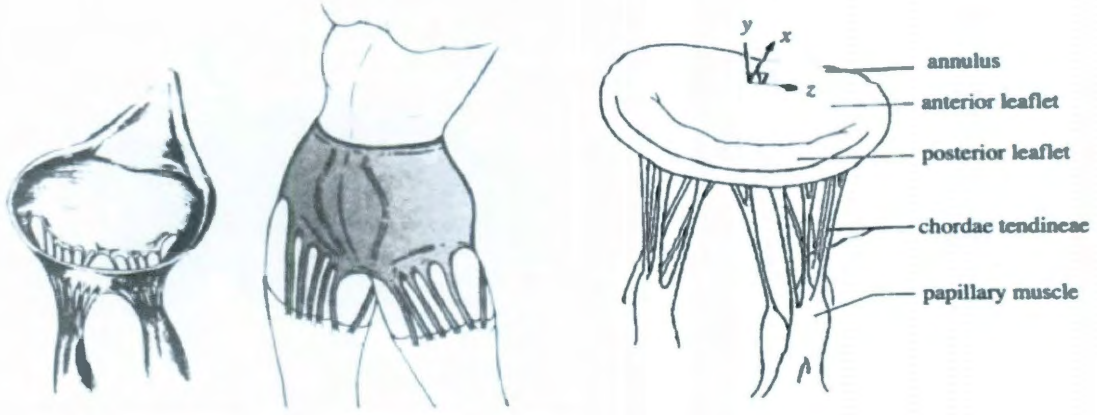

Fig. 2.2: (Left) Bailey's analogy of a mitral valve woman's girdle with garters (unpublished figure prepared for Bailey's manuscript of 1988). http://ats.ctsnetjournals.org/cgi/content/full/65/6/1809/FIG1 (Right) Mitral valve anatomy, showing the mitral valve structure, including the annulus, leaflets, chordae tendinae and papillary muscles Kunzelman KS, Einstein DR, Cochran RP. Fluid-structure interaction models of the mitral valve: function in normal and pathological states. Phil Trans R Soc B 2007;362:1393-1406.

Functional components of the mitral valve include the left atrial wall, the annulus, the anterior and posterior leaflets, chordae tendinae, the papillary muscles and part of the left ventricular myocardium.[62] Abnormal anatomy or dysfunction of any of these components can lead to mitral valve dysfunction.[63] Mitral valve prolapse caused by degenerative disease can range from a simple chordal rupture that involves prolapse of an isolated segment, most commonly in the posterior leaflet, to multi-segment prolapse involving both leaflets in a valve with a large annular size along with significant excess tissue.[58] Surgeons use a variety of surgical techniques to repair the mitral valve, which continue to evolve as new materials become available.

Scaffold material is often used in mitral valve repair, including polyethylene terephthalate (PET; Dacron®), expanded polytetrafluoroethylene (ePTFE; GORE-TEX®) and membrane materials such as bovine pericardium (Figure 2.3).

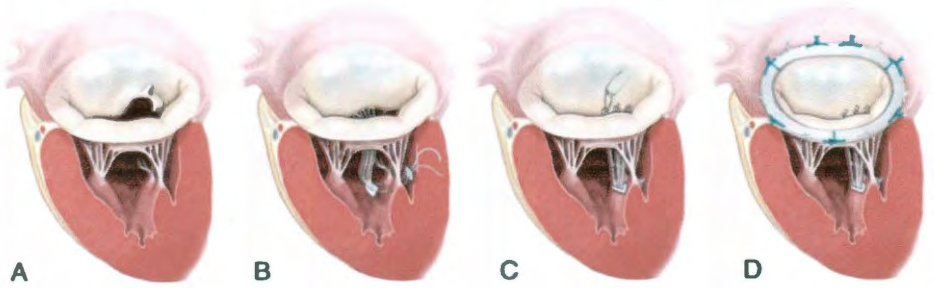

Fig. 2.3: Mitral valve repair in which synthetic materials are currently used: GORE-TEX loop technique and ring annuloplasty. A) Fibroelastic deficiency with anterior lateral scallop prolapse. B) GORE-TEX loops are constructed, and the apparatus is attached to the fibrous tip of the papillary muscle. C) Individual loops are attached to the prolapsing segment margin. D) Completed repair after ring annuloplasty. Adams DH, Rosenhek R, and Falk V. Degenerative mitral valve regurgitation: best practice revolution. Eur Heart J 2010;31:1958-67.

However, when used in the repair of the mitral valve, these materials can lead to such complications as recurrent mitral dysfunction and thromboembolic events.[4] In contrast, a tissue-engineered scaffold with remodeling ability would have the potential to improve the outcomes of mitral valve repair and replacement when patches are used.

In the past decade, decellularized extracellular matrix scaffolds have become increasingly available, originating from a variety of tissue and animal sources.[7–10] These scaffolds contain extracellular matrix that can remodel, be invaded by surrounding progenitor cells in neighboring tissue and marrow-derived stem cells from the circulation, and can bear load immediately upon implantation.[14,18] One such scaffold, SIS-ECM has been shown to remodel in tissues throughout the body, including the cardiovascular system, in myocardium, blood vessels, and in venous valves.[2664] However, its ability to remodel is not fully understood, and its experience in mitral valve repair operations is primarily anecdotal. Further investigation of the remodeling of SIS-ECM when used in mitral valve applications is needed.

2.5 Bioreactors

Although animal models are often used to study tissue-engineered scaffolds (as we have done in our investigation of the remodeling of an SIS-derived cardiac patch in sheep), these models are expensive and require a large number of animals to assess multiple time points.[27] Bioreactor systems, in which investigators create an *in vitro* experimental model, can be used to apply mechanical stimuli to scaffolds seeded with cells from various tissues, as mechanical stimulation has been found to be crucial for maintaining tissue strength and architecture.[65,66]

Interest in replicating aspects of the *in vivo* conditions experienced by the mitral valve led to the creation of several *in vitro* systems that allow dynamic culture of the valve components. These systems apply mechanical forces to the valve components and have demonstrated the ability to maintain the same density and distribution of extracellular matrix and cells as native mitral valve tissue, thus allowing investigation into the effects of drugs and chemicals that have been shown to cause heart valve lesions.[67–70] These systems allow valve cells, including the two major mitral valve cell types, valvular endothelial cells (VECs) and valvular interstitial cells (VICs), to respond to mechanical and chemical stimuli by modulating their production and degradation of proteins, collagen, glycosaminoglycans (GAGs), and DNA.(Barzilla et al. 2010; Weston & A P Yoganathan 2001;[72]) Mitral VICS, which have characteristics of both fibroblasts and smooth muscle cells, are key regulators of valve structure and function in both normal and diseased valves.[73–75]

A wide variety of bioreactor designs for heart valve culture have been developed. These designs have included flow loops,[76,77] cyclic pressure,[71,78] and cyclic flexure,[79,80]

and have tended to be applied to semilunar (aortic and pulmonary) valve applications. In the Grande-Allen lab, two bioreactors have been developed for the study of the mitral valve. One, used for intact mitral valves, is a flow loop organ culture system that can recreate physiologic pressure waveforms up to 150 mmHg and induce pulsatile flow.[70] The other, a splashing bioreactor that applies mechanical stimulation to mitral valve leaflet segments, has been shown to maintain tissue integrity when compared to static culture.[27]

2.6 Matrix Degradation and Its Role in Scaffold Remodeling

While many of the mechanisms responsible for remodeling of SIS-ECM scaffolds remain to be elucidated, degradation by matrix-degrading enzymes appears essential for the remodeling process. For instance, the phenotype of the macrophages that home to the area of scaffold implantation has been shown to greatly influence remodeling outcomes.[24] Chemically cross-linked scaffolds attract pro-inflammatory, cytotoxic macrophage phenotypes (M1), whereas non cross-linked scaffolds attract anti-inflammatory macrophage phenotypes (M2) that promote tissue repair and remodeling.[24] The ability of the host tissue response to degrade the extracellular matrix scaffold, which is impaired with cross-linked scaffolds, has been shown to be an essential factor in remodeling outcomes.[22,79] In addition, macrophage (M2) degradation generates a short protein fragment that acts as a powerful chemoattractant to stem and progenitor cells.[24] Any accurate *in vitro* system of scaffold remodeling must therefore include matrix degradation.

Recent attempts to replicate matrix degradation *in vitro* have shed new light into

how degradation products can affect matrix remodeling. Degradation of the extracellular matrix following implantation has been shown to release component growth factors, which then promote remodeling processes including angiogenesis, cell migration and cell proliferation.[21,23,25] *In vitro* studies have mimicked this degradation by enzymatically degrading the extracellular matrix prior to cell seeding; this enzymatic degradation increases migration and proliferation of cells.[21,25,81] Pepsin digestion should help progenitor like VICs migrate into SIS-ECM. Reing et al showed that decellularized ECM, following degradation by mild enzyme treatment, was active in promoting the migration and proliferation of progenitor cells *in vitro*.[25]

Considering the importance of extracellular matrix degradation and the crucial role of mitral VICs in valve pathogenesis, an *in vitro* experiment was designed to replicate mitral valve scaffold material remodeling. This study aims to evaluate the effect of pepsin degradation on the remodeling of SIS-ECM patches that have been seeded with porcine mitral VICs and subjected to mechanical stimulation *in vitro*, as stated in Aim 3. Establishing an *in vitro* model that allows further investigation into the importance of enzymatic pretreatment and the crucial role of MVICs in valve remodeling will aid in the translation of this technology to the clinical setting.

Chapter 3: Research Designs and Methods: *In Vivo* Study[1]

3.1 Animal study design

3.1.1 Ethical statement and considerations

Before delving into the animal study design, it must first be disclosed that much of this work was industry funded, by CorMatrix, Inc., who also supplied the extracellular matrix patches used in these studies.

In addition, the funding provided allowed for a small sample size of four sheep. Therefore, this study, rather than being a definitive look at the full remodeling potential of these extracellular matrix patches, is an assessment of the juvenile ovine model's suitability for evaluation SIS-ECM remodeling and a development of strategies for this assessment.

Furthermore, due to the fact that there were no patch controls, there was no way of blinding for this data analysis. Therefore, to guard against subjective bias, the histological and immunohistochemical analysis was performed in an automated manner, which we will discuss further.

Finally, it is important to note that we had complete freedom of scientific inquiry for these studies. CorMatrix, Inc. did not participate in the study design, they did not have access to the data as it was being collected nor did they, by contract, influence which data to publish or review any manuscripts prepared for publication.

---

[1] The majority of this and the following chapter are being prepared for submission to *The Journal of Thoracic and Cardiovascular Surgery* and will be published as Scully BB, Fan C, Grigoryan B, Jacot JG, Vick GW, Kim J, Fraser CD, Grande-Allen KJ, and Morales DLS. *In Vivo* Remodeling of an Extracellular Matrix Patch into Functional Myocardium in an Ovine Model.

3.1.2 Choosing an animal model

The juvenile ovine model has been consistently recommended as the most relevant to human cardiovascular performance. Prior studies have demonstrated the efficacy of the ovine model for implantation of extracellular matrix scaffolds.[82] The ovine model has shown similar histopathologic and histochemical changes in allograft heart valves as compared to human allograft valves.[83] In addition, patches implanted in juvenile ovine have been shown to calcify quickly, making them an ideal model to study implanted scaffold calcification.[82] In the present study, a juvenile ovine model was used to evaluate the histologic, mechanical, and electrical properties of a commercially available extracellular matrix patch following implantation in the RVOT, descending aorta, and main pulmonary artery.

3.1.3 Animal protocol

Juvenile male weathers (37-49 kg, less than one year old) were obtained from a vendor and held for a minimum of 14 days of quarantine and acclimation prior to enrollment in the study. Animals were given routine care and feeding during the preoperative period.

Prior to surgery, animals were placed in a stanchion for acclimation and shaved in the left thoracotomy region. 24 hour monitoring was done while the animal was in the stanchion. An IV catheter was placed in the animal's jugular vein for fluid hydration. Food was withheld 18-24 hours prior to surgery and water administered ad libitum. On the morning of surgery a blood sample and an activated clotting time were drawn. Animals were anesthetized with atropine (0.04-0.8 mg/kg IV), xylazine (0.01-0.33 mg/kg

IV), and ketamine (5-20 mg/kg IV) prior to surgery. Cephazolin (15-30 mg/kg IV) prophylaxis was given. In addition, animals were given Buprenorphine (0.01 mg/kg IV/IM q 6 hrs), Banamine (1 mg/kg IV/IM q 8-12 hrs), or other appropriate analgesic at the discretion of the attending veterinarian.

Four juvenile ovine were taken to the operating room in the Michael E. DeBakey animal laboratory at Baylor College of Medicine (BCM). Following transport into the operating room, animals were placed in the right lateral recumbency position. A rumen tube was placed and a rectal temperature monitor was placed. A left thoracotomy was performed and the pericardium was incised from the left ventricle apex to the pulmonary artery. The pulmonary artery, right ventricle, and descending aortic patches were anastomosed using a side clamp and 2 cm-long, full-thickness defects created using a scalpel. A 2 x 2 cm decellularized SIS-ECM patch (CorMatrix ECM®, CorMatrix Cardiovascular Inc, Atlanta, GA) was sewn to the defect using a running 4-0 polydioxanone suture using a running suture technique. While the defect created was a full thickness defect, it was a slit defect (in which the cut edges could potentially re-oppose and heal) rather than a critical size defect (which would be incapable of healing on its own). The patch we sewed in was aneurysmal rather than pulled taut so that the cut edges of the defect would not be re-opposed during the initial surgical repair procedure. The sutures employed were PDS (polydioxanone), a mono-filament synthetic absorbable suture. These sutures cause minimal tissue reaction and degrade completely by 180 days[84]. Native pericardium was not reanastomosed, as it is not routinely anastomosed in children undergoing congenital heart surgery. A chest tube to drain air and fluid was placed prior to closure of the thoracotomy.

A 19G Perineural catheter was placed along the incision line prior to closure for postoperative infusion of Bupivicaine, which was administered for three days. All incisions were then closed using Vicryl in the subcutaneous layers and a skin stapler on the outside skin. All skin sutures or wound clips were removed within 10 days. Extubation was done when the animal was able to swallow and maintain a satisfactory saturated PO2 while breathing room air. A fentanyl patch was placed on the animal at the end of the surgery at a dose of 1 mcg/kg. Banamine and bupivicaine were administered for at least three days.

Following surgery, the sheep were recovered in ICU 414SA within the 4th floor experimental surgery-satellite area and monitored continuously. Once the sheep were standing, they were fed alfalfa pellets and straw and given water ad libitum. Vital signs and urine output were monitored every hour until the sheep was stable enough to remove the chest tube (typically from 6 to 24 hours) and return to the animal facility.

Two sheep were randomly selected for reoperation and euthanasia after 5 months, and the other 2 at 8 months. These time points were chosen based on prior studies showing that decellularized scaffolds implanted in the aorta and pulmonary artery of an ovine model calcify after 20 weeks[82] and that decellularized ECM completely degrades within 3 months.[85]

The ovine was returned to the operating room, where a redo left thoracotomy was undertaken and *in vivo* echocardiography and electrical mapping were performed (as detailed below). Following this, cardioplegia was infused and the hearts explanted and placed on ice for transport. The sheep were humanely euthanized in a manner consistent with the American Veterinary Medicine Association Guidelines on Euthanasia 2007 and

their hearts explanted.[86] This protocol was approved by the IACUC at BCM.

3.2 *In Vivo* Echocardiography

Following repeat thoracotomy under anesthesia with glycopyrrolate (0.01-0.025 mg/kg SQ), epicardial echocardiography was performed on each sheep using a Vivid Q portable echocardiography machine (General Electric, Milwaukee, WI). The RVOT and surrounding structures were visualized and M mode and 2-dimensional echocardiographic evaluation was performed, in collaboration with a pediatric cardiologist specializing in echocardiography.

3.3 *In Vivo* Contact Electrical Mapping

Contact electrical mapping was then performed using a Polaris DX 5575 6-lead catheter (Boston Scientific, San Jose, CA). The electrical activity of the patch and the surrounding right ventricle were assessed by measuring the electrical potential between the leads inside the patch using Vetronics software (BASi, West Lafayette, IN), and data was then transferred from analog printouts through MATLAB software (MathWorks, Natick, MA) to digitized data. The amplitude of the signal was then calculated by measuring the difference between the maximum and minimum of the measured waveform.

3.4 *Ex Vivo* Optical Mapping

3.4.1 Langendorff Perfusion Setup

A Langendorff perfusion system was created using water-jacketed Radnoti

glassware (Radnoti, Monrovia, CA), a Radnoti water bath maintained at 41 degrees Celsius connected to a heater circulating pump (Radnoti, Monrovia, CA), two peristaltic pumps (4-600 mL/min, VWR, Radnor, PA) and 95% O_2 5% CO_2 bubbled in from a wall port. The Tyrode's Solution (made with ultra pure water, 123 mM NaCl, 4.5 mM KCl, 1.8 mM $CaCl_2$, 0.98 mM $MgCl_2$, 20 mM $NaHCO_3$, 1.01 mM NaH_2PO_4, and 11 mM dextrose, with albumin 0.04 g/L added to reduce edema) was pumped into a 2L reservoir, where 95% O_2 5% CO_2 was bubbled in. From there, the solution was pumped into the bubble trap, where it flowed to a heating coil and into the cannulated heart's aorta. After retrograde perfusion of the heart, the Tyrode's solution was collected in the bottom of the heart chamber and pumped back into the reservoir through a paper filter.

Constant pressure was maintained at between 45-60 mm Hg and measured using a Pressure Display 60000 (Medtronic, Minneapolis, MN). Blood gases were drawn on the Tyrode's solution using an Instrumentation Laboratory Blood Gas Machine (Model GEM 3000) and pH, pCO_2, pO_2, Na, K, Ca, Glu, lactate, and hematocrit monitored every 30 minutes. Pacing wires were placed and the heart was paced at 1 Hz. A defibrillator was used to return the cannulated heart to normal sinus rhythm in the case of ventricular fibrillation, beginning at 20 J and increasing to 30 J and then 50 J.

3.4.2 Optical Mapping Study Design

For *ex vivo* whole-heart electrical studies, the SIS-ECM patched hearts were explanted and the animals humanely euthanized. The hearts were infused with cardioplegia, immediately placed on ice, and then subjected within one hour to voltage-sensitive dye mapping, in order to assess the connection to and integration of the patch into the heart wall.[87] Briefly, the explanted hearts were continuously perfused with

Tyrode's solution using the Langendorff method.[88] On resumption of beating, they were infused with a dual-emission, voltage-sensitive, ratiometric fluorescent dye (di-4-ANEPPS, 1 μM; Molecular Probes, Portland, OR). 2,3-butanedione (BDM) was added to delay tissue swelling. The conduction of electrical impulses in the implanted patches was compared to that of native heart tissue by pacing the heart at 1 Hz with a voltage of 1.5 V and then illuminating the heart with a light-emitting diode array at a frequency near 502 nm. Light emissions near 540 nm and 610 nm were captured simultaneously using a 560 nm dichroic mirror to send the emitted light into separate digital cameras (Pike P-032B; Allied Vision Technologies, Stadtroda, Germany) fitted with optical filters (Omega Optical, Brattleboro, VT) at approximately 982 frames per second.

Images from both cameras were recorded simultaneously using Streampix 5 Multicamera software (Norpix, Inc. Montreal, Quebec, Canada) and analyzed using MATLAB. The ratio of the emission intensities was used to calculate the voltage potential across the cell membrane. Fast Fourier analysis of each pixel utilizing MATLAB was conducted to isolate primary frequencies present. Pacing occurred at 1 Hz; therefore, frequency at 1 Hz was isolated and visible peaks were seen on the epicardium of the heart. From the Fourier analysis, we calculated the phase of the 1 Hz waveform. From the phase analysis, we converted the phase to a time-shift depolarization, in which the depolarization time of the right ventricular face and the speed and direction of the depolarization wave across the SIS-ECM patch were visualized.[88,89] The Optical Mapping MATLAB Code used, developed by Chris Fan, can be found in Appendix 1.

3.5 Tissue Preparation

Following optical mapping, the harvested tissue was dissected, reserving 2 mm-wide sections of patched and native tissue for mechanical testing. Additional 2 mm-wide sections were fixed in 10% neutral buffered formalin and dehydrated using a series of graded flex and xylene (VWR, Radnor, PA). They were then embedded in paraffin and cut into 5-micron thick sections using a rotary microtome and affixed to glass slides for histological and immunohistochemical evaluation (described in sections 3.8 and 3.11).

3.6 Mechanical Testing

Mechanical testing was performed to compare the elastic modulus (stiffness) and extensibility of native and patched tissue. The width and thickness of each tissue section (1 section from each patch and 2 from the surrounding myocardium of each heart) was measured in 3 positions and averaged. The ends of each length of tissue were affixed to balsa wood mounts with cyanoacrylate (Loctite 435, Henkel, Rocky Hill, CT). The wooden mounts were clamped into an Enduratec 3200 mechanical tester (Bose Corporation, Eden Prairie, MN) and the sample was extended to a taut length, bearing 0 N load. This "gauge length" of the tissue was recorded and preconditioning was performed using 10 stretch-unstretch cycles of increasing stretch magnitude. The sample was then pulled to tension at a rate of 0.4 mm/sec until reaching a final length of 155% of the original length in order to ensure a greater than 150% extension ratio. Load and deformation values were converted to stress and strain by dividing by the sample cross-sectional area (width x thickness) and gauge length, respectively. The elastic modulus

was obtained for each tissue section by calculating the slope of the linear portion of the stress-strain curve and its x-intercept represented the tissue extensibility.

3.7 Strain Mapping

For the aorta and pulmonary artery patches, a grid was applied to the each SIS-ECM sample using a mesh sheet dipped in charcoal and impressed onto the tissue. A Pike032B CCD (FPS) camera was used to record the deformation of the tissue. Digital image correlation code originally written by Christopher Eberl and adapted by Christopher Durst was used to track the displacement of the charcoal dots in each frame of the video.[90,91] MATLAB code was used to analyze the resulting displacement and generate maps that illustrate regional tissue strain; this code can be found in Appendix 2.

3.8 Histology

3.8.1 Histology Background

The remodeled SIS-ECM patch was compared to two controls, the segment of the native heart tissue previously mentioned, and a negative control, SIS-ECM that had not been implanted in the ovine model. Several types of stains were performed to determine the extent to which vascular tissue had replaced the SIS-ECM, in the case of the SIS-ECM patches in the pulmonary artery position and the aorta, and myocardial tissue in the case of the SIS patches placed in the right ventricular outflow tract.

To evaluate the overall microstructure of extracellular matrix within the tissue as well as the extent of formation of new blood vessels in the SIS-ECM patch, general multicolor histological stains were used to demonstrate the normal layered structure of

the vessel (specifically, looking for the presence of intima, media, and adventitia) for SIS-ECM patches in the aorta and pulmonary arteries, and to quantify the diameter of the cardiac fibers in the SIS-ECM patches placed in the right ventricular outflow tract.

3.8.2 Movat Pentachrome

Movat pentachrome staining allowed visualization of several extracellular matrix components, including collagen (yellow), elastin (black), glycosaminoglycans (blue), muscle and fibrin (red), and nuclei (dark purple). These stains were performed by using serial baths of Alcian Blue (1% w/v Alcian Blue and 0.09% v/v acetic acid in ddiH_2O, Acros Organics, Geel, BE), alkaline alcohol (10% ammonium hydroxide, 4.5% ddiH_2O, 85.5% ethanol), Voerhoff's Hemotoxylin (5% w/v hemotoxylin in ethanol; 2% w/v iodine, 4% potassium iodide in ddiH_2O; 10% w/v ferric chloride hexahydrate in ddiH_2O; mixed 2:1:1 volumetrically, respectively), ferric chloride (2% w/v in ddiH_2O), aqueous sodium thiosulfate (5% w/v in ddiH_2O), Crocein Scarlet (0.1% w/v Brilliant Crocein MOO and 0.5% v/v acetic acid in ddiH_2O; 0.1% w/v acid fuschin and 0.5% v/v acetic acid in ddiH_2O; mixed 1:1 volumetrically; Acros Organics), 0.5% acetic acid, two changes of phosphotungstentic acid (5% w/v in ddiH_2O), pure ethanol, and Safran (6% w/v in ethanol, Poly Scientific, Bay Shore, NY).

3.8.3 Masson's Trichrome

Masson's trichrome (adapted from Kiernan's Histological and Histochemical Methods[92]) staining allowed excellent visualization of collagen fibers (blue), muscle fibers (red) and cell nuclei (dark purple). These stains were performed using serial baths

of Lillie's iron-hematoxylin (1.1% alcoholic hematoxylin: 1.0 g of hematoxylin dissolved in 100 ml of 95% ethanol and an iron salts solution of 12.5 g ferric chloride and 24.5g ferrous sulphate in 3298 mL of distilled water and 42.0 mL of concentrated hydrochloric acid), 1% Biebrich scarlet (5 g Biebrich scarlet, 495 ml distilled water, 5 ml glacial acetic acid), PMA-PTA solution (5 g phosphomolybdic acid, 5 g phosphotungstic acid, in 200 ml distilled water), 2.5% Fast green FCF (50 g Fast Green FCF in 195 ml water and 5.0 ml glacial acetic acid) and acidified water (1 ml glacial acetic acid added per 200 ml distilled water).

3.8.4 Alizarin Red

To ensure that the SIS-ECM patch had not calcified in the pulmonary artery and aorta positions, sections were stained with alizarin red (alizarin red solution in distilled water, adjusted to pH 4.1-4.3 with 10% ammonium hydroxide) and compared to a calcified control (bone from a rabbit skull).

3.9 Cardiac Fiber Diameter Quantification

Masson's trichrome stained slides were used to quantify cardiac muscle fiber diameter for the RVOT patches and surrounding native tissue. Slides were scanned and analyzed in ImageJ (NIH, Bethesda, MD) after calibrating the scale for 3.5 microns per pixel. Five areas of interest were chosen and a line drawn perpendicular to several muscle fibers, and the line tool used to determine the length of the line in the scale already set. Muscle fibers were counted and the line length divided by number of fibers to determine the average fiber diameter.

3.10 Quantification of Neovascularization

Masson's trichrome stained slides were also used to quantify patch neovascularization for all three patch locations. In Adobe Photoshop (Adobe, San Jose, CA) the counting tool was used to manually count each blood vessel. Following this, ImageJ was used to select the total area of interest for both patch and native tissue and the area was divided by the number of vessels to determine blood vessel density in vessels per area. All patch area and native tissue area was analyzed for each slide.

3.11 Immunohistochemistry

3.11.1 Immunohistochemical stains

Several immunohistochemical stains were used to demonstrate markers for specific types of extracellular matrix components, including collagen, elastin, and proteoglycans, and markers related to the basement membrane, matrix degradation, and cell proliferation.

To determine the phenotype of the cells within the SIS-ECM patch, additional immunohistochemistry was performed. For the SIS-ECM patches in the pulmonary artery and aortic positions, stains were performed for several characteristic markers of vascular smooth muscle cells (these cells should be located in the media), vascular endothelial cells (intima), and vascular fibroblasts (adventitia), as shown in Table 3.1.

Table 3.1 Aorta and PA Patch IHC Markers and Their Function

IHC Marker	Function
Lysyl Oxidase	Cross-linking enzyme in collagen synthesis
Calponin h1	Stabilizes the actin network in vascular smooth muscle cells. It can regulate actin contraction and hence is a marker of the contractile ability of mature smooth muscle cells.
Smooth muscle alpha actin	Expressed by smooth muscle cells (an early stage marker of this phenotype).
Matrix metalloprotease I	Enzyme involved in matrix degradation.
LIPG	Expressed in coronary artery endothelial cells, has phospholipase and triglyceride lipase activity and binds heparin

For the SIS-ECM patches in the right ventricular outflow tract position, stains for characteristic markers of cardiac muscle cells, endothelial cells, and cardiac fibroblasts were performed, as seen in Table 3.2. For all patches, cell proliferation was demonstrated by antibodies against proliferating cell nuclear antigen. Blood cells invading the tissue were identified by antibodies against CD45 (leukocyte common antigen).

Table 3.2 RVOT Patch IHC Markers and Their Function

IHC Marker	Function	Vendor	Dilution
Sarcomeric alpha-actinin	Cardiac-specific marker that attaches actin thin filaments to the z-line of the sarcomere contractile complex	Abcam	1:25
CD45	Membrane protein indicating differentiated hematopoetic cells	Abcam	1:50
Cardiac troponin I	Cardiac-specific marker that binds to actin in the contractile complex	Abcam	1:50
Cardiac Troponin T	Cardiac-specific marker that binds to actin in the contractile complex	Abcam	1:50

3.11.2 IHC Analysis

After staining, samples were analyzed for staining intensity using ImageJ Software. Slides were scanned with a Pathscan Enabler IV (Meter Instruments, Houston, TX) at 7200 DPI in RGB color space. ImageJ was used to quantify staining intensity on a scale of 0-255; the m-file developed by Bagrat Grigoryan can be found in Appendix 3. Briefly, areas of each image containing overlapped tissue and tissue that was not adhered to the slide were removed for all analyses. For each slide, native tissue and patch areas were analyzed separately. Background subtraction and color correction were used with the rolling ball method (pixel radius 150 mm, light background, sliding paraboloid). An

algorithm developed by Ruifrok and Johnston was used to deconvolute the image, and a built-in vector for hematoxylin and DAB (H DAB) was used to separate the image into respective vector colors.[93] Using the red color vector, the lower threshold was set to 0 and the upper threshold was set to the value obtained when either the native tissue or the patch area from the negative control image became undetectable. The image was converted into a binary mask, and small holes were filled. Parameters were set to analyze regions of interest within a specified range (size 40-infinity, circularity 0.00-1.00), and the results containing the mean and area of each region of interest were exported to Microsoft Excel for further analysis.

The total intensity stained was calculated using the equation

$$\frac{\Sigma(m_i * a_i)}{\Sigma a_i}$$

where m_i is the mean region of interest stained and a_i is the area stained.

3.12 Statistics

All statistical analyses were conducted using SigmaPlot 12.0 (Systat Software Inc, San Jose, CA). Data are presented as mean and standard deviation. Two-way multi-factorial analysis of variance (ANOVA, nonparametric) was used to compare native versus patch sections at 5 and 8 months for all IHC, extensibility, and muscle fiber diameter comparisons. One-way ANOVA testing was also used to compare neovascularization of the patch at 5 months versus 8 months, and native versus patch elastic modulus at 5 and 8 months. Post-hoc testing was used for sub-group comparisons. The level of significance was set at α=0.05

Chapter 4: Results of an RVOT Patch Implanted in a Juvenile Ovine Model[2]

4.1 Animals and surgical procedure

All 4 animals survived the surgical procedures and follow-up period, and were included in the study. Study animals were sacrificed at postoperative days 143, 174, 237, and 244.

4.2 In vivo epicardial echocardiography

Epicardial echocardiography was performed in all 4 study animals. This technique showed that the patch region contracted with the native myocardium, with thickening of the patch region seen during systole (Fig 4.1).

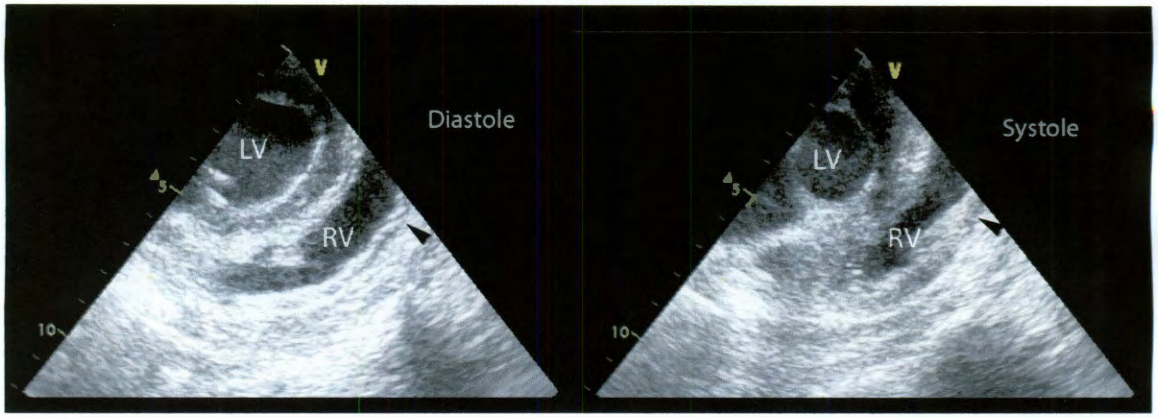

Figure 4.1 Epicardial echocardiogram of SIS-ECM implanted sheep hearts (still). Note thickening of region of patch (arrowhead) during systole. LV = left ventricle. RV = right ventricle.

---

[2] The majority of this and the previous chapter are being prepared for submission to *The Journal of Thoracic and Cardiovascular Surgery* and will be published as Scully BB, Fan C, Grigoryan B, Jacot JG, Vick GW, Kim J, Fraser CD, Grande-Allen KJ, and Morales DLS. *In Vivo* Remodeling of an Extracellular Matrix Patch into Functional Myocardium in an Ovine Model.

4.3 *In Vivo* Contact Electrical Mapping

Contact electrical mapping showed a coordinated electrical signal across the SIS-ECM patch at both 5 and 8 months (Fig 4.2). The amplitude of the signal averaged from the patch at 5 and at 8 months was not significantly different than the signal from the native neighboring ventricular tissue (4.38 ± 0.373 mV vs. 4.834 ± 0.617 mV, p = 0.639 at 5 months and 1.54 ± 0.167 mV vs. 1.34 ± 0.168, p = 0.052 at 8 months).

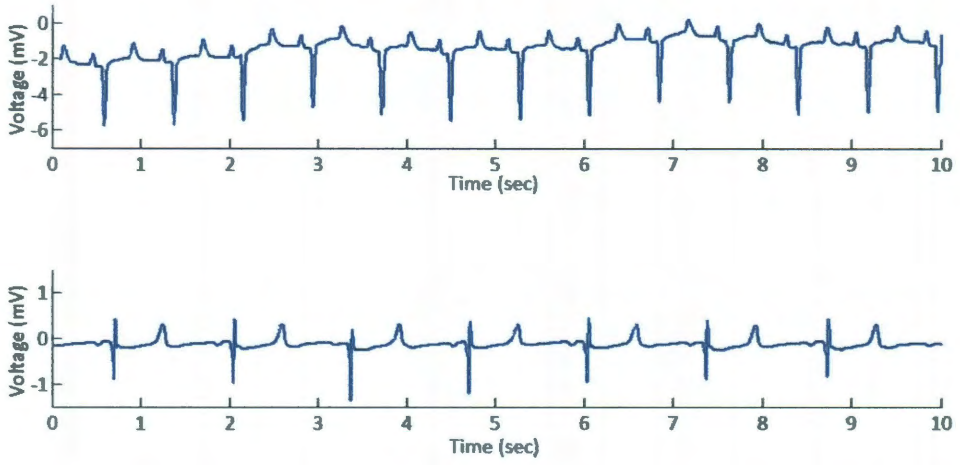

Fig 4.2: In vivo electrical contact mapping of SIS-ECM implanted in sheep right ventricle. (Above) Trace at 5 months. (Below) Trace at 8 months.

4.4 Optical mapping

Of the 4 hearts studied, Langendorff perfusion with subsequent paced beating was successful in one heart from each time point. Optical mapping showed that the electrical signal was being conducted across the patch, both at 5 and 8 months. Fourier-transform analysis revealed a peak frequency at 1 Hz in the middle of the patch at both time points, corresponding to the stimulating frequency. Time-shift activation maps showed continuity of electrical signal across the RVOT, including the patch region, at both time

points (Fig. 4.3).

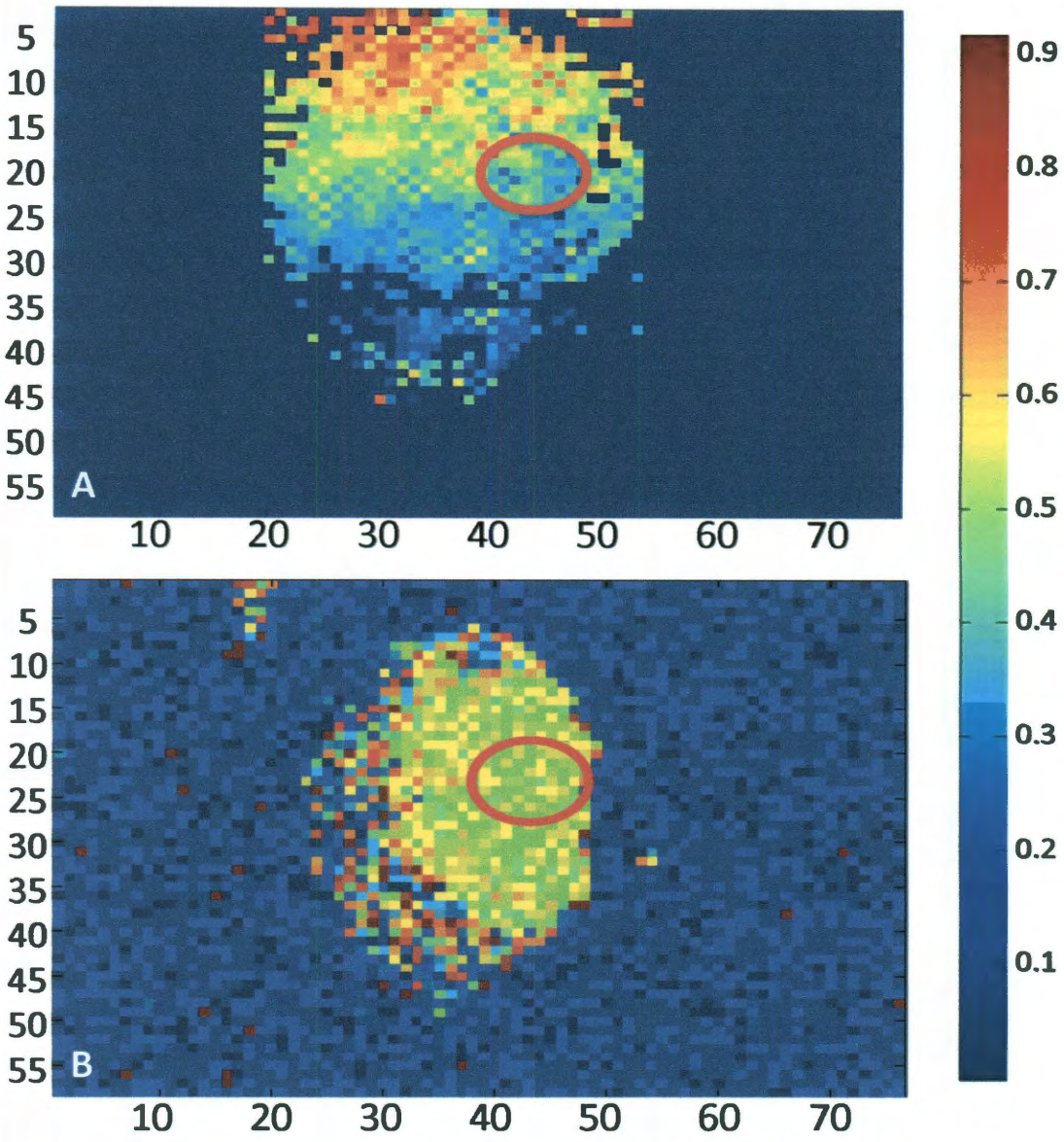

Fig 4.3: Optical mapping analysis. The temporal activation of the heart is shown at 5 months (A) and 8 months (B) post-implantation, with similar conduction to that of native tissue along the epicardial layer of the SIS-ECM patch. Color scale is identical in both images and shows the difference in temporal activation measured from the apex calculated after Fourier analysis. Circles indicate location of the SIS-ECM patch. Scale on righthand side is in seconds.

4.5 Mechanical testing

Prior to implantation, the SIS-ECM patch material had an elastic modulus of 42.9

± 11.6 MPa, which decreased to 1.28 MPa ± 0.9 at 5 months, and to 0.976 ± 0.3 MPa at 8 months (Fig. 4.4). There was no statistical difference between the stiffness of the SIS-ECM measured at 8 months and the neighboring native right ventricle tissue (0.976 ± 0.3 vs. 0.614 ± 0.2 MPa, p=0.333). The extensibility of SIS-ECM and native ventricular tissue was not significantly different at either 5 or 8 months (23.1 ± 7.7% for native tissue versus 24.3 ± 12.6% (p=0.928) at 5 months and 21.6 ± 3.1% (p=0.384) at 8 months for patch).

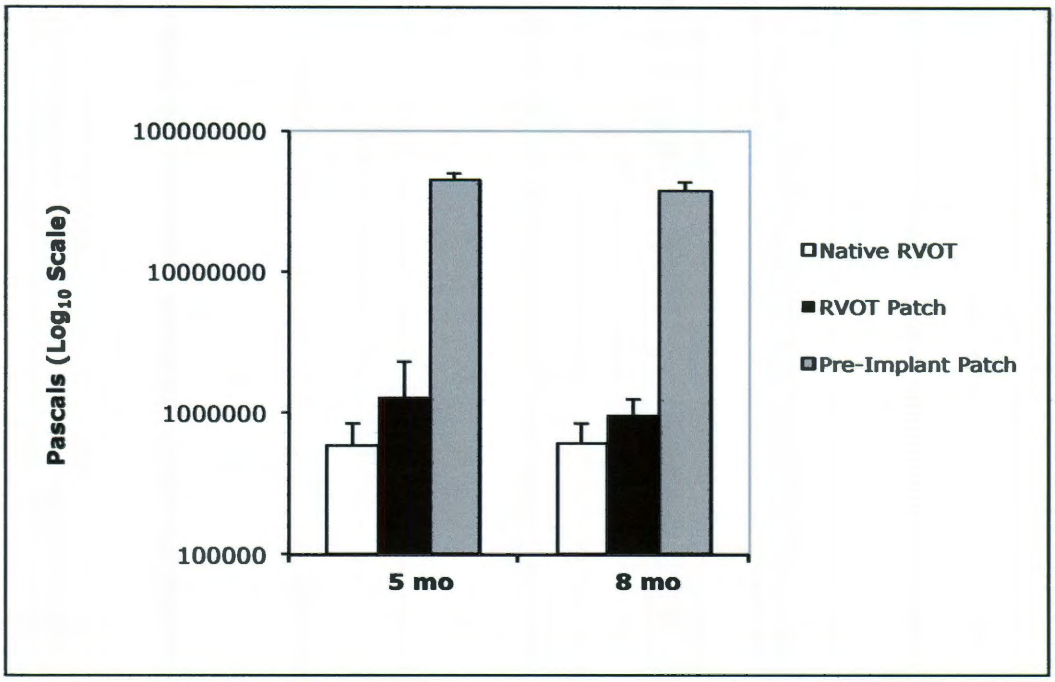

Fig 4.4: Comparison of Young's modulus in SIS-ECM implanted hearts versus native myocardium. Logarithmic scale used to report elastic modulus.

4.6 Strain Mapping

Strain mapping was performed concurrently with mechanical testing. Strain mapping was challenging in this application due to the difficulty of applying the charcoal grid and the variation in color of the tissue. In addition, the points at the edges of the

tissue were easily distorted as the tissue was pulled to tension, which can be explained in part by Saint Venant's Principle, which states that the stresses, strains and displacements far from the ends of a rod or beam subjected to end loading depend only on the resultant forces and moments acting on its ends. The material heterogeneity was thus not captured as well as we had hoped; however the results do show a less uniform strain throughout the patch when compared to native tissue, suggesting that remodeling is occurring at different rates in the transition regions compared to the center. Heterogeneity of strain is suggested by the strain maps obtained, however with a larger sample size clearer links may emerge between strain patterns and material remodeling.

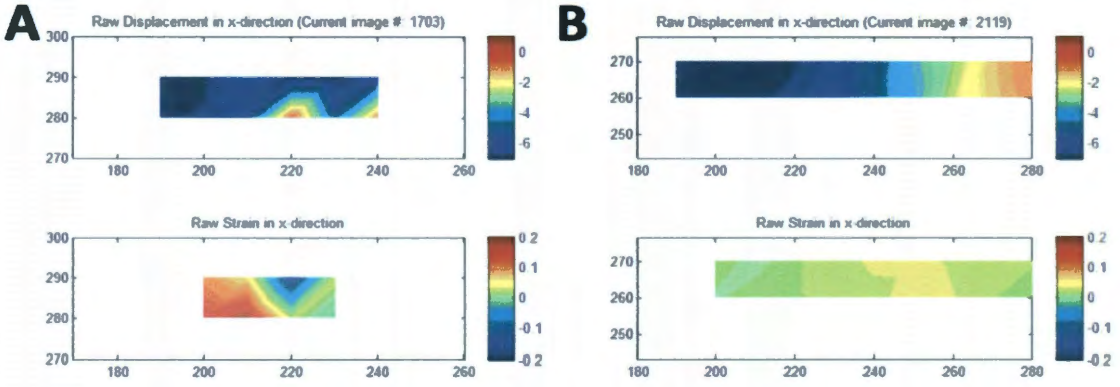

Figure 4.5 Strain Mapping was performed concurrently with mechanical testing, and demonstrated greater anisotropy in the patch when compared to the native tissue. Representative images are shown. A) Patch placed in the RVOT at 5 months. B) Native RVOT.

4.7 Histology and IHC

Gross visual assessment of the patched hearts at 5 months was suggestive of bioresorption (Fig. 4.6, A-B). At 8 months, the patch thickness approached that of the native tissue (Fig. 4.6, C). By 8 months, gross muscle was visible inside the suture line (Fig. 4.6, C-D). It was also observed that the healed regions at both time points were in

the circular shape of the original patch, as opposed to a straight line, which was the shape of the slit incision in the RVOT.

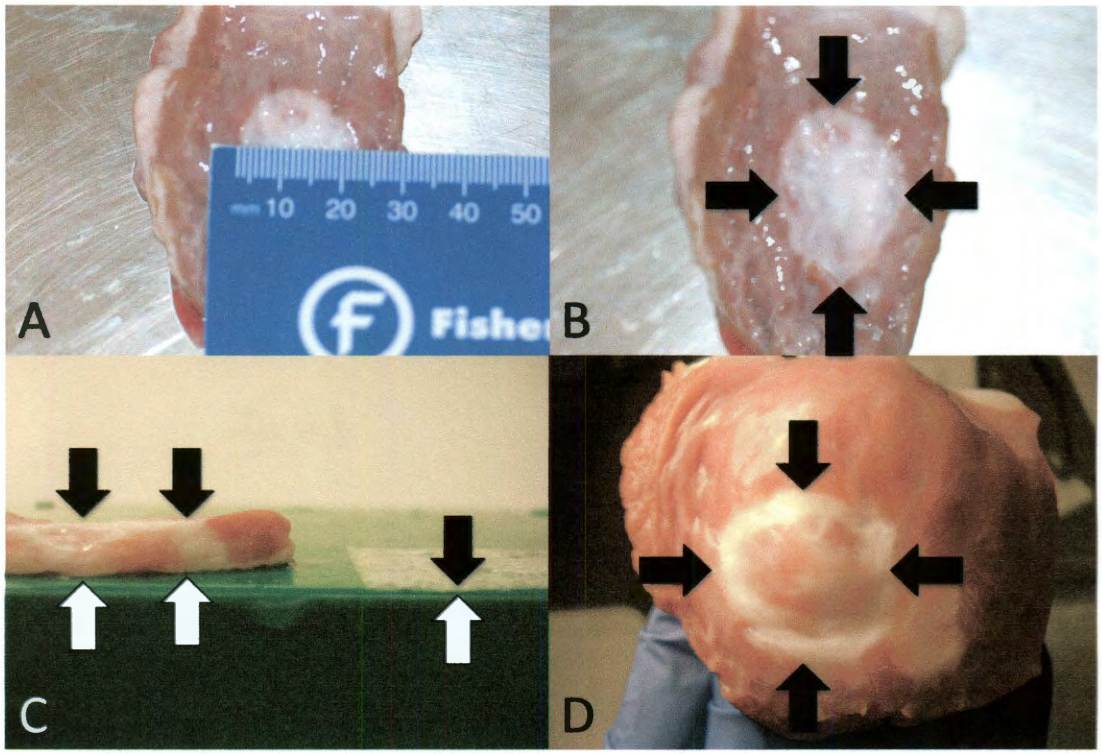

Fig 4.6: Gross visual assessment of implanted SIS-ECM patch material. A) 5-month sample with ruler for size reference. B) 5-month sample with black arrows pointing to perimeter of patch. C) Side view of patch thickness. Arrows point to top and bottom of patch pre (right) and post-implant (left). D) 8-month sample with black arrows point to scarring at patch circumference. Gross muscle can be seen inside patch. Photos taken by author.

Histological analysis of tissue samples at 5 and 8 months revealed evidence of neovascularization and formation of organized muscle cell islands within the SIS-ECM patch (Fig. 4.7, A, B), with cells seen throughout the patch area (Fig. 4.7, C). Furthermore, degrading sutures were easily identifiable at both 5 and 8 months. Degrading PDS material could be seen in circular areas underneath the microscope (Fig. 4.7 A and C).

Neovascularization was 3.5 times greater at 5 months compared to 8 months (Fig.

4.7, D) as measured by number of vessels per area (3.08 ± 1.2 vessels/mm^2 versus 0.88 ± 0.3 vessels/mm^2, respectively, p = 0.004). By 8 months, muscle fibers inside the patch stained positive for cardiac muscle markers, such as Troponin I (Fig. 4.7, E). Muscle fiber organization appeared to have increased at 8 months as compared with 5 months, with the corresponding appearance of fascicle-like structures (Fig. 4.7, F-H). At 8 months, muscle fiber diameter between patch and native tissue was not statistically different (12.5 ± 2.6 vs. 9.7 ± 2.4 μm, p = 0.059). No evidence of calcification was observed at 5 or 8 months, as apparent from the absence of alizarin red staining (Fig. 4.8, F).

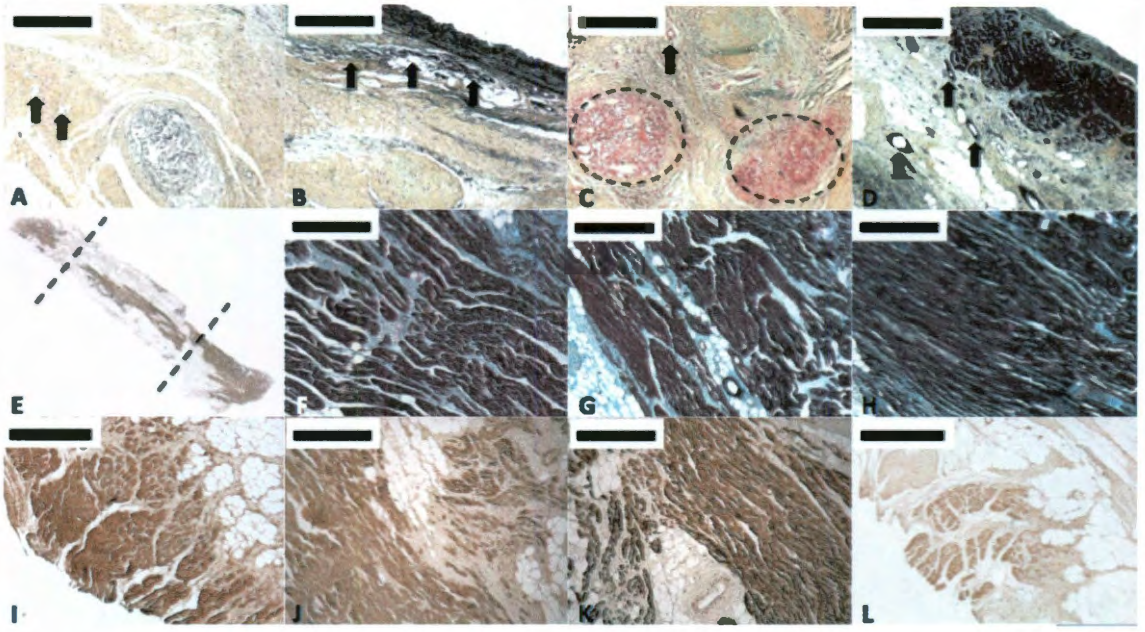

Fig 4.7: Histological analysis of SIS-ECM patch implanted in RVOT. Movat's Pentachrome stains (A-D): A) neovascularization in 5-month tissue samples (black arrows). B) muscle-cell islands in 5-month sample (black arrows). C) cell infiltration into center of patch at 5 months. Circular dotted lines show degrading PDS suture material. D) neovascularization (black arrows) and muscle fiber organization at 8 months. E) gross muscle remodeling inside suture lines (dotted lines) at 8 months with Troponin I stain. Masson's Trichrome stain (F-H): F) native ventricle muscle fibers at 8 months. G) patch muscle fibers at 8 months. H) patch muscle fibers demonstrating alignment at 8 months. IHC stains (I-L): I) sarcomeric alpha actinin stain at 8 months. J) Cardiac troponin T stain at 8 months. K) Cardiac troponin I stain at 8 months. L) CD45 stain at 8 months. Black bars: 400 microns.

IHC staining with antibodies against sarcomeric alpha actinin, troponin T, and troponin I revealed intense staining in the patch area (Fig. 4.7, I-K and Fig. 4.8 C-E) confirming that the cells demonstrated a cardiac myocyte phenotype. Similar results were obtained with antibodies against CD45 (Fig. 4.7, L and Fig. 4.8, B), indicating the hematopoietic origin of these muscle cells. There was no staining in the negative-control slides (Fig. 4.8, G-J). For sarcomeric alpha actinin, CD45, troponin I and troponin T, the difference in staining intensity between the native tissue and patch decreased from 5 months to 8 months (Fig 4.8; A-D, refer to Table 4.1 for results of significance testing). The staining intensity of sarcomeric alpha actinin was significantly higher in the patch compared to the native ventricle at 5 months ($p=0.003$), but not at 8 months ($p=0.789$). Similarly, the staining intensities of troponin I and troponin T were significantly higher in the patch at 5 months ($p=0.004$ and 0.022 respectively), but not at 8 months ($p=0.186$ and 0.666, respectively). There was no significant difference between the staining intensities of CD45 between the patch and the native ventricle at either 5 months or 8 months.

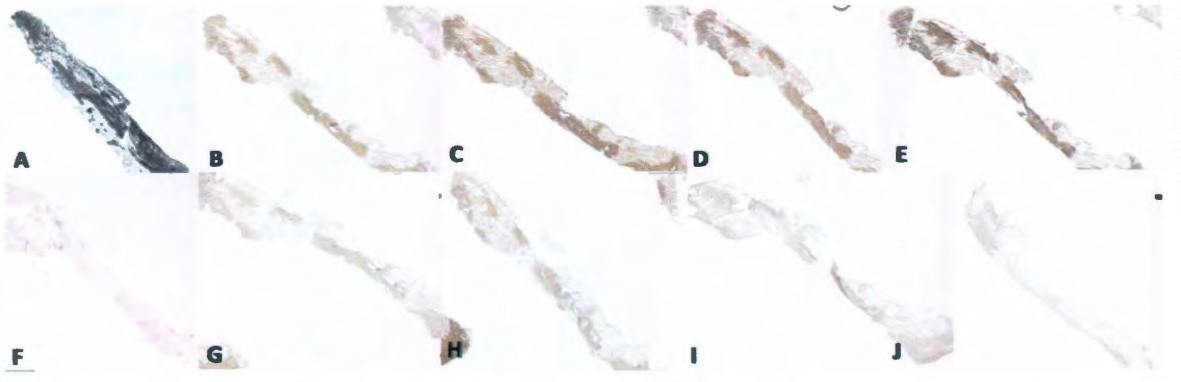

Fig 4.8: IHC images of SIS-ECM patch implanted in RVOT at 8 months. A) Movat's pentachrome stain of RVOT patch at 8 months for comparison. B) CD45. C) Sarcomeric alpha actinin. D) Cardiac Troponin I. E) Cardiac Troponin T. F) Alizarin red stain. G)-J) corresponding negative controls beneath antibody-stained slides B)-E).

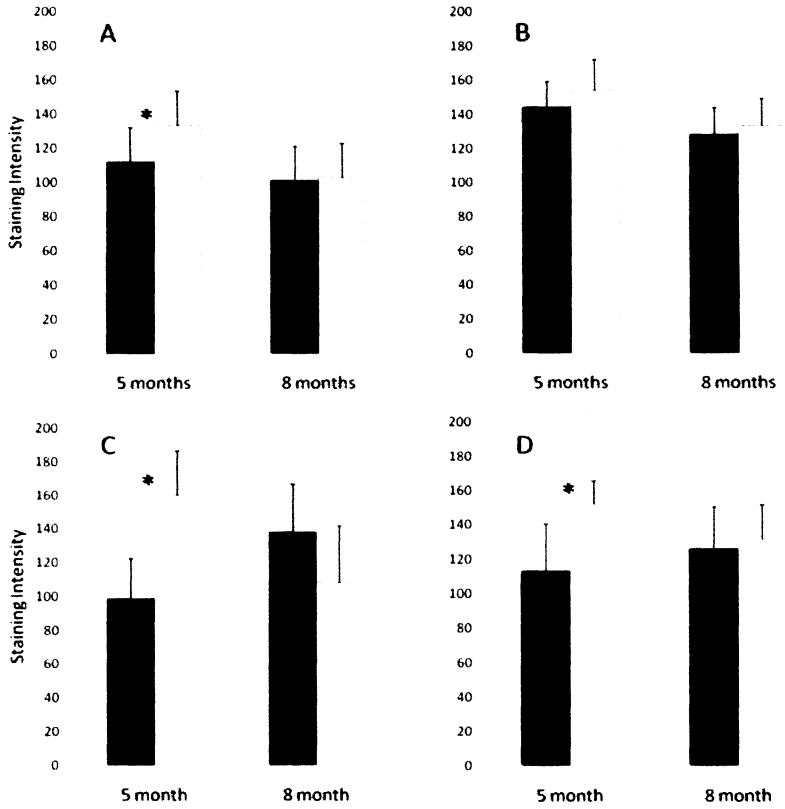

Fig. 4.9. IHC analysis: Graphs of staining intensity (area of interest, normalized to background staining). Black columns represent native tissue and white columns represent patch tissue. Asterisks denote statistical significance between columns ($p < 0.05$). P-values from 2-way ANOVA analysis are shown in Table 1. A) Sarcomeric alpha actinin. B) CD45. C) Troponin I. D) Troponin T.

Table 4.1: Immunohistochemistry comparisons in staining intensity of patch material and native myocardium at 5 months and 8 months. P values in bold indicate a significant difference.

	Patch at 5 mo	Native at 5 mo	P values*	Patch at 8 mo	Native at 8 mo	P values**
Sarcomeric alpha actinin	132.4±21.37	111.3±12.3	**p = 0.003**	103.1±15.2	100.0±21.0	p = 0.789
CD45	152.5±17.8	142.9±14.9	p = 0.181	133.0±16.0	124.1±15.9	p = 0.328
Troponin I	159.8±26.5	98.6±23.6	**p = 0.004**	108.2±33.2	137.8±28.7	p = 0.186
Troponin T	151.9±13.5	112.8±27.4	**p = 0.022**	131.2±20.2	125.8±24.2	p = 0.666

- Comparison is patch versus native tissue at 5 months

** Comparison is patch versus native tissue at 8 months

4.8 Discussion

4.8.1 Histologic evidence of constructive myocardial remodeling

The goal of this study was to evaluate, by multiple approaches, the utility of the juvenile ovine model for the assessment of remodeling of SIS-ECM implanted in the RVOT, and to compare the remodeled SIS to functional myocardium. The ovine model proved highly suitable for this study with all animals surviving the surgery, thriving post-operatively for 5-8 months, and demonstrating well-defined regions of remodeling where the patch was implanted. The histological analysis of explanted tissue showed evidence of progressive, time-dependent tissue remodeling, with neovascularization, muscle-cell

island formation, and organization of muscle fibers, with eventual resorption of the patch and formation of fascicles (Fig. 4.5). Interestingly, vessel density was 3.5 times greater at 5 months compared to 8 months. It is possible that more immature blood vessels were followed by fewer but more mature ones, or that as the cells became more differentiated, nutrient demand and therefore blood vessel requirement decreased, as more efficient metabolism has been reported necessary for cardiac differentiation of stem cells.[94] In addition, comparison of muscle fiber diameter in the patch versus native tissue showed no difference at 8 months. Prior studies have shown significant differences between right ventricle muscle fiber diameter in hearts under different remodeling conditions, suggesting that muscle fibers in the patch are responding to similar loading conditions as those in the native ventricle.[95]

IHC staining for sarcomeric alpha-actinin, troponin I, and troponin T was consistent with a cardiac muscle phenotype for the cells found within the patch (Fig 4.6, I-L). In addition, staining intensity increased between 5 and 8 months, with statistical differences between patched and native tissue observed at 5 months for sarcomeric alpha actinin, cardiac troponin I and T markers but no statistical difference seen at 8 months, demonstrating further remodeling with increasing time from implant. Importantly, the formation of islands of muscle cells occurred in the interior of the patch, and not just at the periphery. This is particularly interesting because the patch size used, 2 x 2 cm, had a very large surface area. It has been previously reported that the maximum distance for cellular ingrowth from surrounding tissue into unseeded matrix scaffolding is approximately 0.5 cm.[96] The presence of viable islands of differentiated muscle cells in the SIS-ECM patch and positive staining with CD45, a marker of hematopoietic origin,

suggests that some of the cells populating the SIS-ECM were derived from sources other than local myocardial progenitor cells. Other studies have shown that SIS-ECM degradation products are not only chemotactic,[25,45] but attract c-kit positive cells,[46] and it is therefore possible that the cells found within the borders of the patch are marrow-derived. In addition, the muscle island was circular, more resembling the patch, as opposed to elongated as might be expected from a healed straight line slit.

Also of interest in the histologic analysis was the absence of calcification, even at 8 months. This finding is notable in that synthetic and bioprosthetic materials are notoriously prone to calcification in juvenile sheep, which usually occurs within 4 weeks of implantation.[97]

4.8.2 Improvement in material elasticity

Implanted surgical materials, such as Dacron, are known to maintain their high stiffness compared to native tissue over time.[98] In contrast, the mechanical stiffness of the SIS-ECM decreased over the course of the study, as measured by Young's modulus. By the 8-month time point, the material behavior of SIS-ECM had become statistically indistinguishable from that of the surrounding native tissue, having become less stiff and more extensible. This mechanical testing data provides evidence suggesting that the SIS has remodeled to resemble myocardium. An alternative explanation could be that there was no contribution of the SIS-ECM patch to the mechanical properties and that the native RVOT had healed on its own, but that there was some fibrosis of the myocardial tissue. The fibrosis would lead to increased stiffness and decreased extensibility of the myocardial tissue, such as is seen in heart failure[99]. However, due to the circular shape of

the remodeled region of RVOT, it seems unlikely that there was no mechanical contribution from the SIS-ECM patch. Thus, the similarity between the patch and native tissue mechanical characteristics demonstrates a significant and functional remodeling process.

4.8.3 Evidence of electrical conductivity

The SIS-ECM showed unique and favorable bioelectrical properties consistent with significant cellular and functional remodeling. At 5 and 8 months, contact electrical mapping and optical voltage mapping both showed evidence that the implanted SIS-ECM patch was capable of transducing coordinated electrical signals. Furthermore, Fourier transform analysis identified the dominant and principal frequency in the middle of the patch to be 1 Hz, which was the frequency at which the heart was being paced. These findings are remarkable, given that other patch materials, such as native pericardium, bovine pericardium, PET, and ePTFE are electrically inert.[100]

This functional data is also interesting in light of the fact that although cells staining positively for muscle markers such as sarcomeric alpha actinin, troponin I and troponin T were seen throughout the patch at both 5 and 8 months, mature muscle cell phenotypes were seen in islands rather than in a continuous stretch from one suture line to the other. The presence of islands supports invading cells differentiating; if the native myocardium had simply healed together, muscle cell phenotypes would be more continuous surrounding a middle straight line healed scar. The ECM has been shown to play a central role in transmitting mechanical forces, mediated by ECM-integrin-cytoskeleton coupling.[101] The electrical signals conducted across the patch in this study

suggest that SIS-ECM is capable of providing a suitable environment for the invasion and differentiation of cardiomyocytes. Further investigation will need to be done to further characterize the electrical signals transmitted over a remodeling patch, and to ensure that arrhythmias do not develop.

4.8.4 Limitations and future directions

A significant limitation of this study is the small sample size, confounded by the fact that only 2 of the 4 hearts were successfully reperfused for the optical mapping experiment. There was also no comparator patch material (such as Dacron or pericardium) used in the study. Although the Dacron patches would be incapable of remodeling, they would have provided an important comparison for the deposition of pannus on the patch material.

Although the slit defect that we created allowed cell invasion and subsequent remodeling to take place, a critical size defect model, in which a portion of the native tissue would be removed prior to sewing in the ECM patch, may be a better choice for evaluating the remodeling of the patch in the future. A critical size defect model would have avoided the potential for the proximal tissue to re-anastomose, and allowed more initial tension to be placed on the implanted patch. While we do not believe that the tissue on either side of the slit defect re-anastomosed, based on the circular suture lines visible at both 5 and 8 months, a patch model that eliminates this possibility would considerably strengthen the results of related future studies.

In addition, although this was not possible in this initial study due to the small numbers of animals, in future studies we would like to include both an earlier and a later

time point. The earlier time point would be used to study the inflammatory process, which is completed within 3 weeks in cardiac tissue and results in the formation of scar tissue by four weeks.[102] A later time point of one year would allow for further investigation into the patches' mechanical properties and contractility following a longer remodeling period.

Nevertheless, these preliminary results showing functional electrical activity within the implanted patch are remarkable and, to our knowledge, unprecedented. This degree of remodeling has not been reported for any other patch material currently used for human cardiac repair. In the future, we intend to continue this line of investigation using a larger number of animals, a comparator arm (using native pericardium as control material), a 3D activation propagation map of the RV electrical activity, as well as advanced imaging to document the change in viability and functionality of the patch over time.

4.8.5 The ECM and constructive remodeling: Build it and they will come[3]

The field of tissue engineering has experienced a paradigm shift over the last decade as new evidence about the importance of the extracellular matrix in tissue remodeling and regeneration has become available.[103] Where it was once thought that provision of sufficient numbers of pluripotent stem cells was the key to tissue regeneration, this idea has not met with success in practice. It is increasingly accepted that stem cells can only perform their regenerative function within a conducive microenvironment provided by a biochemically functional extracellular matrix.[41] Indeed,

---

[3] This analogy is the brainchild of DLS Morales, and was presented by him at BCM's Surgery Grand Rounds in February 2011.

adult tissues, such as mature myocardium, that were once thought to be mitotically senescent have been shown to contain tissue-specific progenitor cells that are capable of proliferation, maturation, and regeneration, given the proper environment. This phenomenon can be likened to a productive office building; even a large number of skilled office workers would be hard-pressed to act productively if housed in a building that lacked basic utilities, furnishings, telephones, and computers. Furnished with the appropriate tools, environment, and direction, however, just a few of these same workers could be capable of supporting a productive, growing and self-sustaining business. In this analogy, the extracellular matrix provides the proper environment, and the body provides stem cells – the "workers" - that repopulate the matrix and transform it into healthy, functional tissue. This repopulation is likely to be particularly robust in children, who have a greater pool of pluripotent cells.

4.8.6 Conclusion

In summary, the SIS-ECM patch, when surgically implanted in the juvenile ovine RVOT, demonstrates constructive remodeling into functional myocardium as evidenced by histological, mechanical, and electrical properties. Juvenile ovine appear a suitable model for evaluating the remodeling of an SIS-ECM patch implanted in the right ventricular outflow tract, allowing evaluation of conduction of an electrical signal, cell infiltration and phenotype, and remodeling extracellular matrix properties. Should future studies support these findings, this material may present an exciting new solution for cardiac grafting and tissue repair, especially in the pediatric population.

Chapter 5: Results of an Aorta and Pulmonary Artery Patch Implanted in a Juvenile Ovine Model[4]

5.1 Mechanical Testing

Prior to implantation, the SIS-ECM patch material had an elastic modulus of 42.9 ± 11.6 MPa. In the descending aorta, this decreased to 2.88 ± 2.89 MPa at 5 months, and to 3.185 ± 0.836 MPa at 8 months (Fig. 5.1). Native aorta had an elastic modulus of 0.335 ± 0.019 MPa.

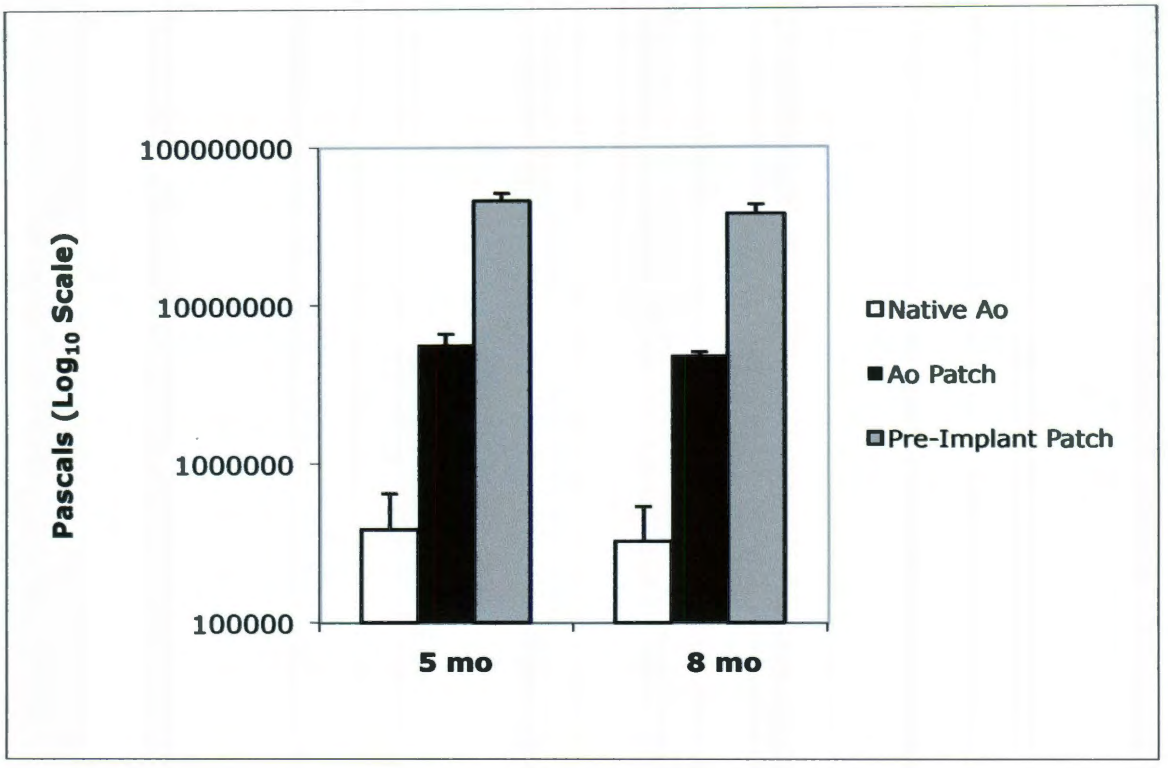

Figure 5.1 Comparison of Young's modulus in SIS-ECM implanted in the descending aorta versus native aorta. Logarithmic scale used to report elastic modulus.

[4] The majority of this chapter is being prepared for submission and will be published as Scully BB, Grigoryan B, Fan C, Fraser CD, Grande-Allen KJ, and Morales DLS: *In Vivo* Remodeling of an Extracellular Matrix Patch in the Aorta and Pulmonary Artery Positions in an Ovine Model.

In the main pulmonary artery, the elastic modulus decreased to 5.627 ± 4.234 MPa at 5 months, and to 4.833 ± 0.243 MPa at 8 months (Fig. 5.2).

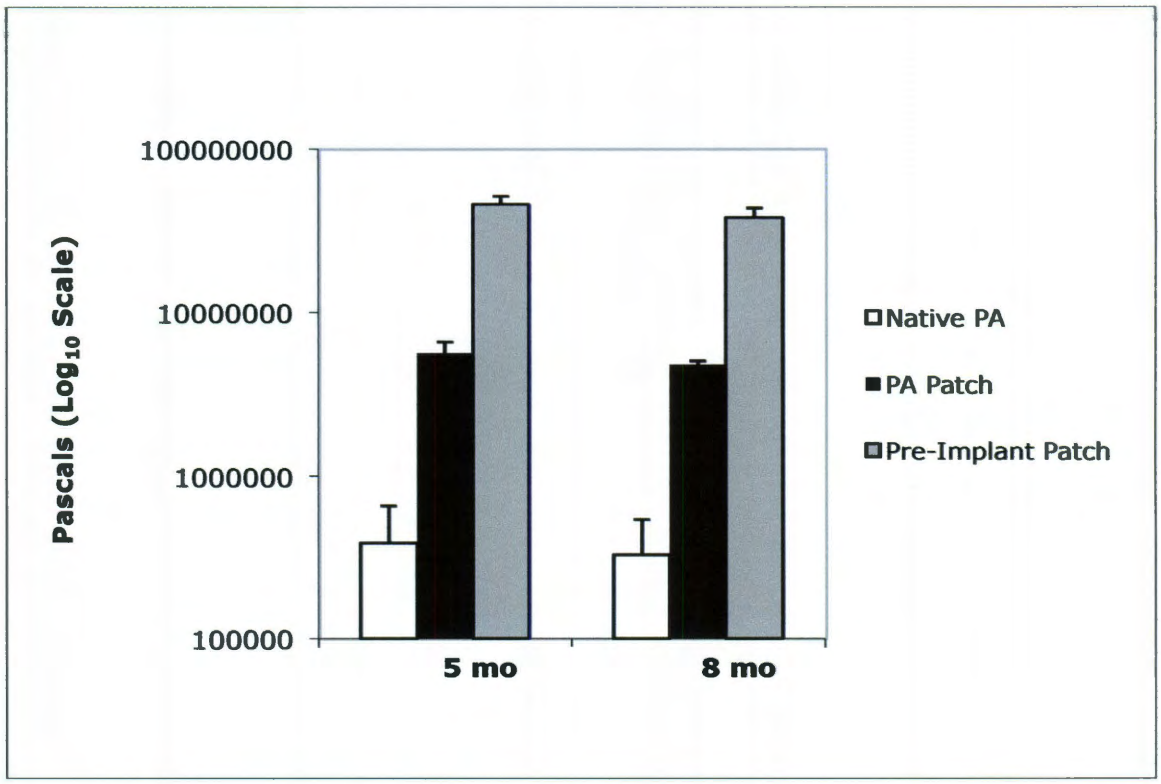

Figure 5.2 Comparison of Young's modulus in SIS-ECM implanted in the main PA versus native PA. Logarithmic scale used to report elastic modulus.

5.2 Strain Mapping

Strain mapping was performed concurrently with mechanical testing. Many of the same challenges that prevented a sufficiently precise analysis of the material heterogeneity in the RVOT patch samples were faced with the vascular tissues as well. In the aorta, as with the RVOT, strain appeared more heterogeneous in the patch (Fig. 5.3 A,C) when compared to native tissue (Fig. 5.3 B,D), and this heterogeneity was observed for both time points. In the PA, there was less difference observed between the patch (Fig. 5.3 E) and the native tissue (Fig. 5.3 F).

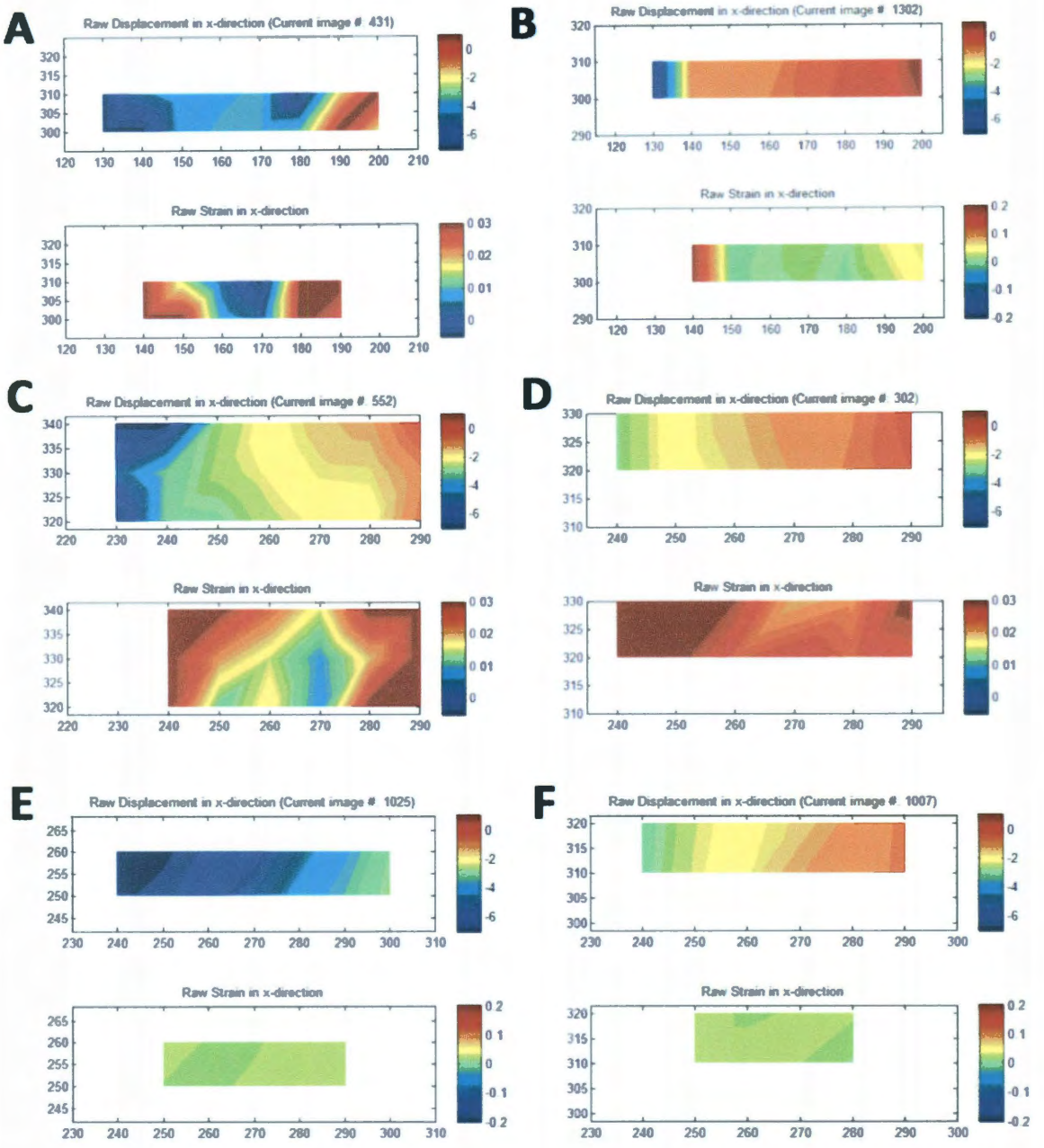

Figure 5.3 Representative Strain Mapping images from the Aorta and PA patch positions. A) Taken from aorta patch at 5 months. B) Native aorta at 5 months. C) Aorta patch at 8 months. D) Native aorta at 8 months. E) PA patch at 5 months. F) Native PA at 8 months.

5.3 Histology

At both 5 and 8 months, the patch had integrated well into the surrounding tissue in both the aortic and pulmonary artery positions. Figure 5.4 shows the gross dissection of

the patch and surrounding tissue in both locations. The patch was aneurysmal at both the aortic and pulmonary artery locations.

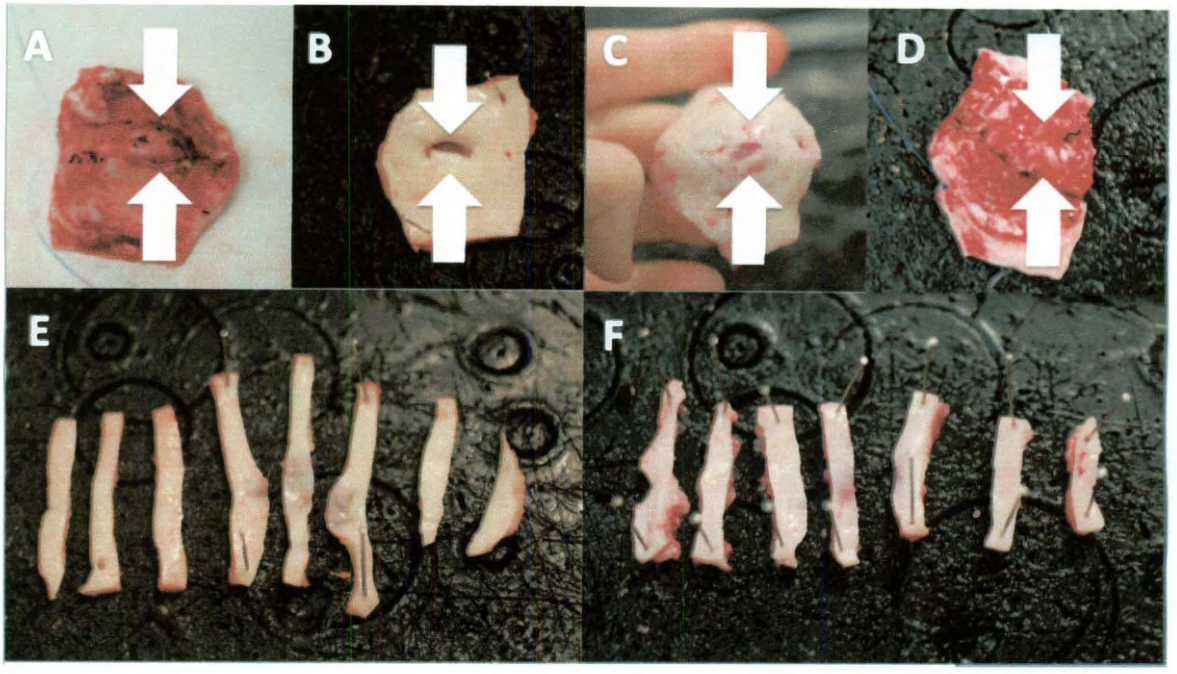

Figure 5.4 Gross dissection of aorta and PA patches at eight months. White arrows mark patch edges. A) Descending aorta patch, adventitia side. B) Descending aorta patch, intima side. C) Main pulmonary artery patch, intima side. D) Main pulmonary artery patch, adventitia side. E) Descending aorta dissected into 2-mm wide strips for mechanical testing and tissue fixation. Sections containing patch are 4th, 5th, and 6th from the left. F) Main pulmonary artery dissected into 2-mm wide strips. Sections containing patch are 3rd, 4th, and 5th from the left. Photos taken by author.

Histologic analysis of both the aortic and PA patches showed significant remodeling by 5 months. In the aorta at 5 months, cells could be seen throughout the patch, neovascularization has begun, and staining for elastin and glycosaminoglycans (GAGs), matrix components that were not found in the pre-implanation patch, was evident (Fig. 5.5 A-B and D-E). By 8 months, vessel layers were more defined, the transition regions (the tissue immediately adjacent to the suture line) had become less distinct, and the vessels had more elastin and muscle staining (Fig. 5.5 C, F).

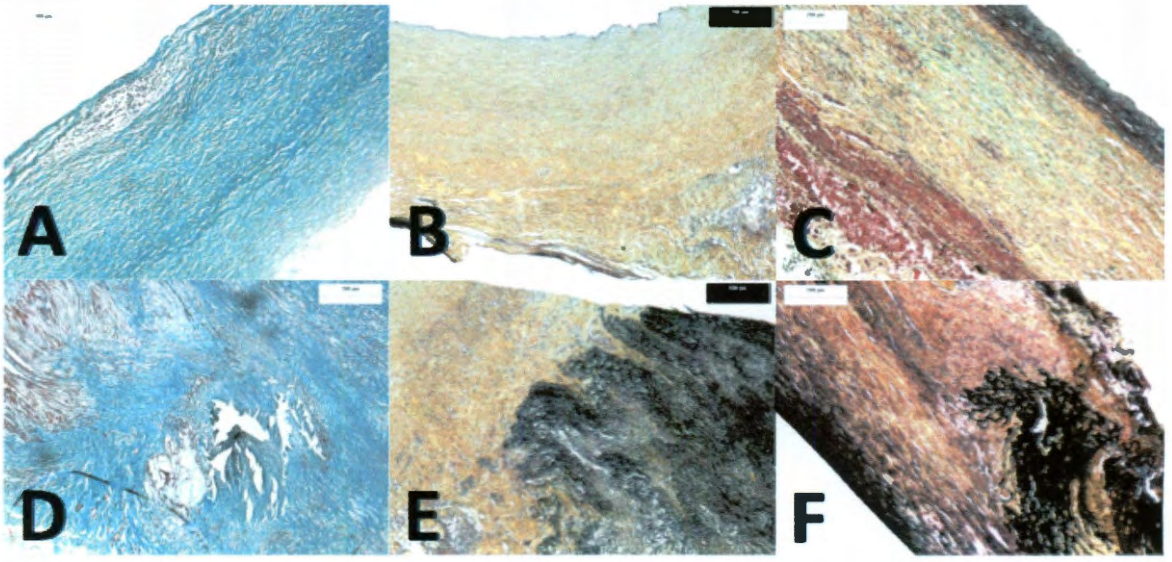

Figure 5.5 Histologic evaluation of the SIS-ECM patch placed in the descending aorta. Patch only sections are shown with transition regions of patch and native tissue directly below. A) Masson's trichrome stain of the patch placed in the aortic position at 5 months. Cells can be seen throughout as well as heavy staining of collagen (blue). B) Movat's pentachrome stain of aortic patch at 5 months. Layering is beginning to be seen with stronger collagen staining of the adventitia side (yellow). C) Movat's pentachrome of aortic patch at 8 months. More well-defined layers have formed, with an elastin-staining layer (black), collagen layer (yellow), and muscle staining layer (red). D) Masson's of transition region between native tissue and patch (degrading suture can be seen in the middle). Native tissue (on left) shows greater muscle staining (red). E) Movat's pentachrome stain of transition region at 5 months. Elastin stain (black) clearly differentiates the native tissue from the patch. F) By 8 months, the tissue directly adjacent to the suture line is less defined, as more elastin staining can be seen inside the patch.

In the pulmonary artery at 5 months, neovascularization was already apparent and cells could be seen throughout the patch (Fig. 5.6 B,C, F,G). The patch stained for not only collagen, but also elastin (black) and glycosaminoglycans (blue-green) (Fig. 5.6 C,G). In contrast, prior to implantation, the patch was almost completely collagen staining (yellow) and could clearly be differentiated from the native tissue (Fig. 5.6 A,E). By 8 months, patch (Fig. 5.6, H) resembled native tissue (Fig. 5.6, D), with both staining well for muscle (reddish purple) and elastin (black).

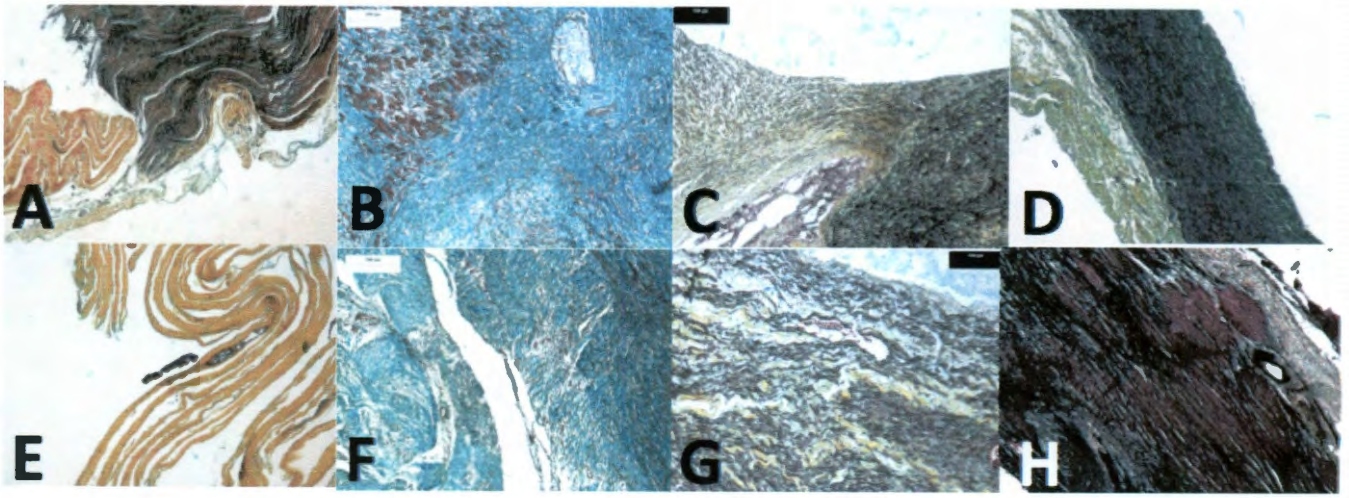

Figure 5.6 Histologic evaluation of the SIS-ECM patch placed in the main PA. Transition regions where the patch and native tissue meet are shown at the top with patch only sections below. A) and E) Movat's pentachrome stain of patch and native tissue prior to implantation. B) and F) Masson's trichrome staining of transition region and patch, respectively at 5 months. C) and G) Movat's pentachrome stain of transition region and patch at 5 months. D) Movat's pentachrome stain of native PA compared to H) patch.

5.4 Immunohistochemistry

IHC staining for endothelial lipase gene (LIPG), lysyl oxidase (LOX), smooth muscle alpha actin, matrix metalloprotease (MMP) 1, and calponin h1 was performed, and revealed strong staining of the patch in both the aortic and PA positions at 5 and 8 months. There was no staining in the negative-control slides. The difference in staining intensity between the patch and native tissue at both 5 and 8 months was measured and 2-way ANOVA performed (see tables 5.1 and 5.2 for results of significance testing). Interestingly, no statistically significant difference was found between patch and native tissue in either the aorta or PA at both 5 and 8 months.

Table 5.1 Immunohistochemistry comparisons in staining intensity of patch material and native PA at 5 months and 8 months.

	Patch at 5 mo	Native at 5 mo	P values*	Patch at 8 mo	Native at 8 mo	P values**
LIPG	110.6±51.88	110.6±57.19	p = 0.5	126.88±38.46	123.9±34.0	p = 0.55
LOX	122.5±40.8	129.6±13.3	p = 0.676	109.9±17.7	122.5±26.4	p = 0.627
Smooth muscle alpha actin	141.8±51.5	109.0±51.3	p = 0.854	141.9±27.2	138.6±22.5	p = 0.565
MMP 1	130.7±49.4	140.7±49.4	p = 0.363	136.9±43.9	117.3±51.6	p = 0.740
Calponin h1	118.0±24.6	113.0±29.5	p = 0.642	106.0±15.3	112.1±9.25	p = 0.325

Table 5.2 Immunohistochemistry comparisons of staining intensity of patch material and native aorta at 5 months and 8 months.

	Patch at 5 mo	Native at 5 mo	P values*	Patch at 8 mo	Native at 8 mo	P values**
LIPG	87.3±28.5	85.3±21.6	p = 0.537	98.1±34.0	99.3±27.3	p = 0.482
LOX	141.3±23.7	147.1±17.5	p = 0.342	119.2±11.1	101.6±25.0	p = 0.927
Smooth muscle alpha actin	146.0±29.8	130.8±42.6	p = 0.786	134.2±11.2	139.5±8.19	p = 0.364
MMP 1	157.8±45.1	127.4±46.2	p = 0.834	117.7±37.9	120.3±34.4	p = 0.456
Calponin h1	156.2±22.5	137.1±31.4	p = 0.731	109.6±4.67	115.2±23.7	p = 0.376

These immunostaining results suggest that several cell migration/differentiation and matrix production processes were well underway in the remodeling patch. LIPG has phospholipase and triglyceride lipase activity and binds heparin; it is expressed in coronary artery endothelial cells. Its presence in both the patch and native tissue in the aortic and PA positions suggests that the patch had remodeled to have an endothelial tissue component such as a neo-intima or vasa vasorum.

Lysyl oxidase is a cross-linking enzyme in collagen and elastin synthesis. Its presence in both the patch and native tissue in both the aortic and PA positions suggests that new collagen and elastic fibers are being synthesized by cells that have invaded the patch.

Smooth muscle alpha actin is expressed by smooth muscle cells, and staining for this smooth muscle cell marker was found in both patch and native tissue in the aorta and PA. This suggests that cells within the remodeled matrix had a smooth muscle phenotype, a result further supported by staining for calponin h1, which stabilizes the actin network in vascular smooth muscle cells and is a maker of their contractile ability.

Finally, matrix metalloprotease-1 (MMP-1) is an enzyme important in matrix degradation. Staining for this enzyme suggests that active extracellular matrix turnover was taking place in the patch in both the aorta and PA.

5.5 Discussion

5.5.1 Improvement in material elasticity

Many types of implanted surgical materials, such as Dacron, are known to maintain their high stiffness compared to native tissue over time.[98] In contrast, the mechanical stiffness of the SIS-ECM implanted in the aorta and PA decreased significantly over the course of the study, as measured by Young's modulus. While the elastic moduli of both the aortic and PA patches did not decrease as much as that seen in the RVOT patch, they did approach the elastic moduli of the surrounding native tissue. The lower magnitude change in the vascular patches compared to the RVOT patch may have been due to the inherently higher collagen content and elastic moduli of blood vessels compared to the RVOT. If the SIS-ECM had been explanted at longer time points, the elastic modulus of patch in the aortic and PA positions may have become even closer to that of native tissue.

Interestingly, the aorta patch appeared to have greater heterogeneity of strain

compared to the PA patch; this heterogeneity may have been due to the increased systemic pressures experienced by the patch in the aortic position. As with the RVOT patch, heterogeneity of strain was suggested by the strain maps, however with a larger sample size clearer links may emerge between strain patterns and material remodeling.

5.5.2 Histologic evidence of vessel remodeling

The goal of this study was to evaluate the suitability of the juvenile ovine model for a multi-faceted analysis of the ability of SIS-ECM implanted in the aorta and pulmonary artery positions to remodel into functional vasculature. The histological analysis of tissue explanted from these ovine models showed evidence of progressive, time-dependent tissue remodeling, with neovascularization, cell invasion, increased staining of elastin and smooth muscle, and eventual resorption of the patch (Fig. 5.5 and 5.6). Interestingly, distinct layers could be seen at 5 months and became more defined by 8 months, particularly in the aortic position. This layered structure was particularly interesting in light of the three-layer structure of the native vessel (adventitia, media, and intima). The increase in staining for elastin and smooth muscle at 8 months suggests that the implanted patches are remodeling in response to the physiological loading environment as well as in response to the surrounding vasculature. Remarkably, the remodeled patches in the aortic and PA positions have remodeled to resemble the surrounding tissue, and at both 5 and 8 months look significantly different than their RVOT patch counterparts. The greater degree of remodeling at 8 months suggests that further remodeling to resemble functional vasculature would take place if the patches were explanted at a later time point.

At 5 and 8 months, the patch was found to be aneurysmal at both the aortic and pulmonary artery locations; this shape was likely due to a combination of the thinness of the tissue and the high magnitudes of pressure experienced in the vessels..Given that the 2x2 cm patch was sewn into the vessel following a full thickness linear cut without any of the tissue being removed, the aneurysmal nature of the remodeled patch was a clear demonstration that the wound did not simply re-oppose.

Also of interest in the histologic analysis was the absence of calcification for both aortic and PA patches (as in the RVOT), even at 8 months. This finding is notable in that synthetic and bioprosthetic materials implanted in juvenile sheep are notoriously prone to calcification, which can occur within 4 weeks of implantation.[97]

5.5.3 Limitations and future directions

As described in detail in the RVOT chapter, a significant limitation of this study is the very small sample size. Nevertheless, these preliminary results show an impressive and time-dependent remodeling of an SIS-ECM patch implanted in both the aortic and PA positions. Larger sample sizes and control groups are needed to further investigate the potential of this novel cardiovascular patch.

5.5.4 Conclusions

In summary, we have found that an SIS-ECM patch, when surgically implanted in the ovine aorta and PA, is capable of constructive remodeling into functional vascular tissue as evidenced by histological and mechanical properties. Juvenile ovine appear a suitable model for evaluating the remodeling of an SIS-ECM patch implanted in the aorta

and PA, allowing evaluation of cell infiltration and phenotype and remodeling extracellular matrix properties. Should future studies support these findings, this material may present an exciting new solution for cardiac grafting and tissue repair, especially in the pediatric population.

Chapter 6: Research Design and Methods: *In Vitro* Study[5]

6. 1 Scaffold preparation

Decellularized porcine SIS-ECM (CorMatrix©) was cut into strips measuring 3.18x0.64 cm (length x width). Pepsin-treated SIS-ECM strips were digested using 2 mg/mL pepsin solution (50 mg pepsin from porcine gastric mucosa and 0.25 mL 1 N hydrochloric acid in 24.75 mL dI water) for four hours under agitating conditions. Untreated SIS-ECM strips were soaked in DMEM medium containing 1% antibiotic solution for four hours. Cell seeded samples were statically seeded with third passage porcine mitral VICs at a cell density of 1.5×10^6 cells/cm^2 and incubated for five days at 37°C in a rubber mold, cut to hold four SIS-ECM strips in a glass petri dish; each SIS-ECM strip was covered with 0.6 mL of cell suspension. Mitral VICs were harvested as described by Gupta et al[104]. Media was changed every 1-2 days. Unseeded samples were incubated in medium for five days at 37°C in the same type of mold. Using 4-0 Prolene suture, dynamic samples were then sewn into the middle module of the "splashing" mechanical stimulation bioreactor system previously described by Barzilla et al (see section 6.2)[27]. A volume of 4.5 mL medium was added and the bioreactor was placed in a 37°C incubator for seven days with media being changed every 1-2 days. Samples without mechanical stimulation were floated in medium in sterile, plastic petri dishes and incubated at 37°C for seven days.

---

[5] The majority of this and the following chapter are being prepared for submission to *The Annals of Biomedical Engineering* and will be published as Scully BB, Grigoryan B, Erskine K, Fan C, Durst C, Kwak M, Barzilla J, Morales DLS, and Grande-Allen KJ. Evaluation of Matrix Degradation of a Small Intestinal Submucosa Patch Seeded with Mitral Valvular Interstitial Cells: An *In Vitro* Study.

6.2 Pepsin Optimization

In order to optimize the pepsin concentration used for enzymatic pretreatment of SIS-ECM, mechanical testing was performed on SIS-ECM treated with pepsin solution with a range of concentrations from 0.015-0.1 wt % and shaken in pepsin solution for varying time points of 1, 2, 4, 8, 12, 24, and 32 hours.

6.3 Bioreactor Setup

A splashing bioreactor designed by Barzilla et al was used to provide gentle cyclic stretch and perfusion to the SIS-ECM.[27] Used medium was plated on agar to verify maintenance of sterile conditions in the rotating system. In this system, the SIS-ECM is mounted diagonally across the middle of the three modular segments, and the entire chamber is assembled then rotated through 360 degrees continuously for the culture duration, forcing the cell culture media to splash around the SIS-ECM on both sides [see Figure 6.1]. Because an excess length of the SIS-ECM is sewn into the bioreactor, the majority of the tissue section hangs loosely and is thus subjected to periodic flexure and stretch-induced perfusion with every rotation of the system. Oxygen delivery to the cells is maintained via a tissue flask cap with a thin porous membrane in its center that allows permeation of outside air, while protecting against contamination.

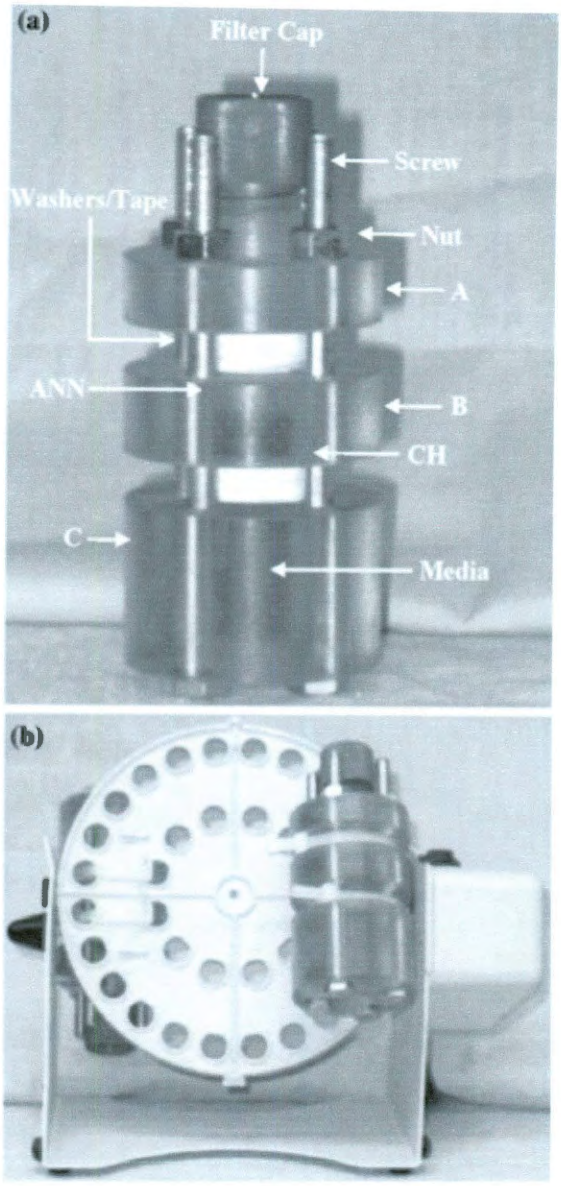

Fig. 6.1 From Barzilla et al. a) Splashing bioreactor chamber comprised of three hollow segments into which the scaffold is mounted (at ANN and CH). Media inside the chamber provides nutrients for the cells seeded on the scaffold. b) The chamber is rotated 360 degrees at 0.33 revolutions per second, allowing media to splash over the scaffold surfaces.

6.4 Mechanical Testing

After incubation and with or without dynamic treatment, the SIS samples were cut in half widthwise; half of the sample was used for mechanical testing and the other half

was analyzed with histology and immunohistochemistry. For mechanical testing, the SIS-ECM sample was blotted with bibulous paper to remove excess moisture from medium. The sample's width and thickness were measured in three positions and each was averaged. The ends of each length of sample were then super glued into a balsa wood mount, cut specifically for the sample. The balsa wood mounts were screwed into the clamps of the Enduratec 3200 mechanical tester (Bose Corporation, Eden Prairie, MN), and the sample was pulled to a taut length, bearing 0 N load. The length between clamps (gauge length) was measured. Mechanical testing was initiated by first preconditioning the sample, which included 10 cycles of increasing stretch and relaxation. The sample was then pulled to 55% of gauge length at a rate of 0.15 mm/sec. The Young's elastic modulus and extensibility were calculated from the load and displacement data by calculating the slope of the linear portion of the stress-strain curve and its x-intercept, respectively.

6.5 Strain Mapping

Strain mapping was performed on pepsin treated and cell seeded samples as described previously, using charcoal markers and digital image correlation code.

6.6 Histology

Histology was performed to determine the overall microstructure of extracellular matrix within the SIS-ECM samples, as well as the occurrence of cell remodeling. Hematoxylin and eosin, Movat's pentachrome, Masson's trichrome, and a hematoxylin and saffron stain (to look specifically at cell nuclei and collagen alignment) were

performed to demonstrate SIS-ECM structure and the location of extracellular matrix components including collagen type I, highly hydrated glycosaminoglycans and proteoglycans, elastic fibers, and smooth muscle.

6.7 Immunohistochemistry

Immunohistochemical analysis was performed to identify markers associated with valvular interstitial cell activation (smooth muscle alpha actin), cell proliferation -- specifically the early G1 phase and S phase of the cell cycle (PCNA), and cell adhesion and migration processes (fibronectin), as shown in Table 6.1. Slides were rehydrated and antigen retrieval performed (AR in PBS, 80°C for 30 min), then sections were blocked with 10% goat serum buffer (Sigma, St. Louis, MO) and incubated for 1 hour at 37°C with primary antibodies against the markers in table 6.1. After rinsing in phosphate-buffered saline, biotinylated secondary antibodies (Jackson Immunoresearch, West Grove, PA) were applied for 1 hour at room temperature. Positive staining was then demonstrated by a chromogen reaction using Vectastain Elite ABC and diaminobenzidine kits (Vector Laboratories, Burlingame, CA). All samples were counterstained with hematoxylin. Eliminating administration of the primary antibody created negative control samples for all markers.

Analysis of staining intensity was performed as previously outlined using ImageJ.

Table 6.1 SIS-ECM Patch IHC Markers and Their Function

IHC Marker	Function	Vendor	Dilution
Smooth muscle alpha actin	Expressed by smooth muscle cells (early stage marker for this phenotype)	Abcam	1:1000
PCNA	An auxiliary protein of DNA polymerase delta involved in the control of eukaryotic DNA replication.	Abcam	1:2000
Fibronectin	Binds cell surfaces, involved in cell adhesion and motility	Abcam	1:100

Chapter 7: Results of Matrix Degradation of a Small Intestinal Submucosa Patch Seeded with Mitral Valvular Interstitial Cells and Cultured in a Bioreactor[6]

7.1 Pepsin Optimization

Mechanical testing of SIS-ECM treated with pepsin solution with a concentration ranging from 0.015-0.1 weight % and time points of 1, 2, 4, 8, 12, 24, and 32 hours demonstrated a substantial loss of stiffness after 4 hours in all of the tested concentrations (Figure 7.1). By 32 hours, the SIS-ECM separated into 4 distinct layers and became overly difficult to handle.

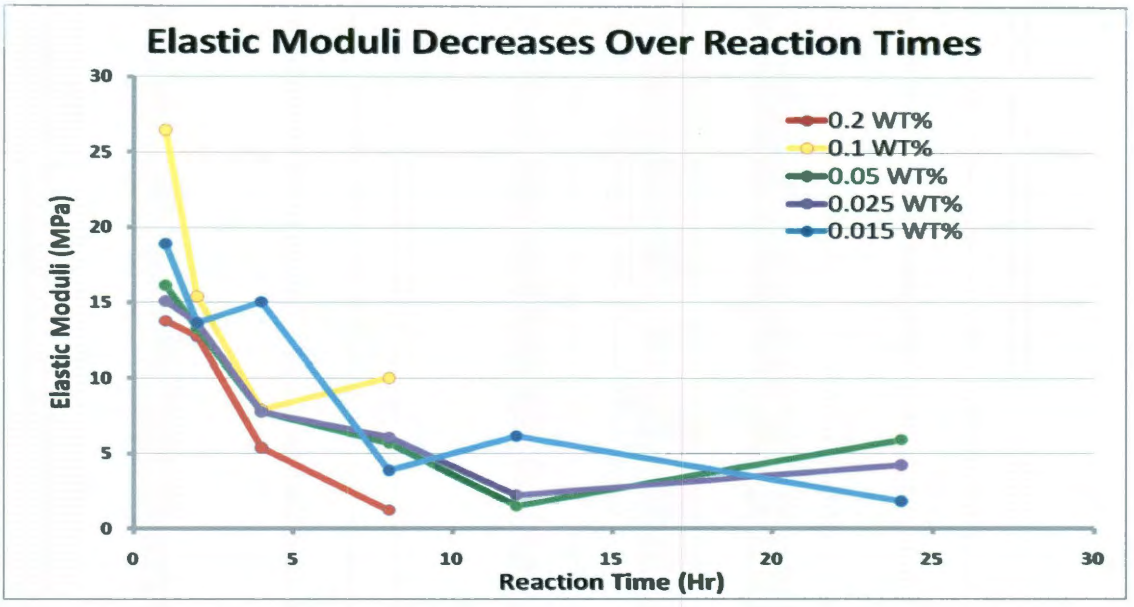

Figure 7.1: The elastic modulus of the SIS-ECM decreased over time, with the majority of stiffness lost after 4 hours. Graph created and pepsin optimization conducted by Minsuk Kwak, B.S.

[6] The majority of this and the preceding chapter are being prepared for submission to *The Annals of Biomedical Engineering* and will be published as Scully BB, Grigoryan B, Erskine K, Fan C, Durst C, Kwak M, Barzilla J, Morales DLS, and Grande-Allen KJ. Evaluation of Matrix Degradation of a Small Intestinal Submucosa Patch Seeded with Mitral Valvular Interstitial Cells: An *In Vitro* Study.

7.2 Cell Seeding

Seeding of the SIS-ECM was verified using hematoxylin and eosin staining (Figure 7.2). In the pepsin-treated SIS-ECM, cells were seen both forming a layer on the surface of the SIS-ECM as well as invading into the deeper layers of the tissue.

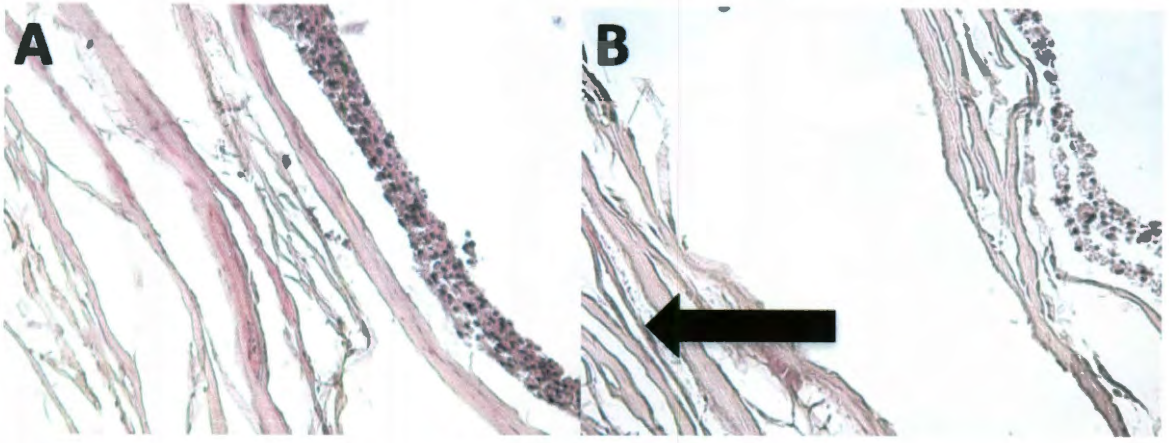

Figure 7.2: H&E stain demonstrating successful cell seeding of SIS-ECM scaffold after five days of seeding. A) MVICs formed a neolayer on the surface of the scaffold and B) could be seen having infiltrated several layers into the tissue (black arrow)

7.3 Mechanical Testing

Untreated SIS-ECM had an elastic modulus of 42.9 ± 11.6 MPa. When comparing pepsin digested, cell seeded groups with and without mechanical stimulation after one week, there was a statistical difference between groups (11.8 ± 5.1 MPa vs. 38.5 ± 10.9 MPa, respectively) (Fig. 7.2). However, there was no statistical difference between the stiffness of the acellular pepsin-digested groups with and without mechanical stimulation (23.5 ± 18.5 vs. 34.7 ± 13.7 MPa, respectively). Likewise, the cell-seeded undigested group did not demonstrate statistical difference between groups with and without mechanical stimulation (38.7 ± 25.6 MPa vs. 26.0 ± 10.7 MPa, respectively). When comparing all of the groups without mechanical stimulation, the pepsin digested, cell

seeded scaffolds were significantly less stiff than the other 2 groups. However, there was no difference between the mechanically stimulated groups.

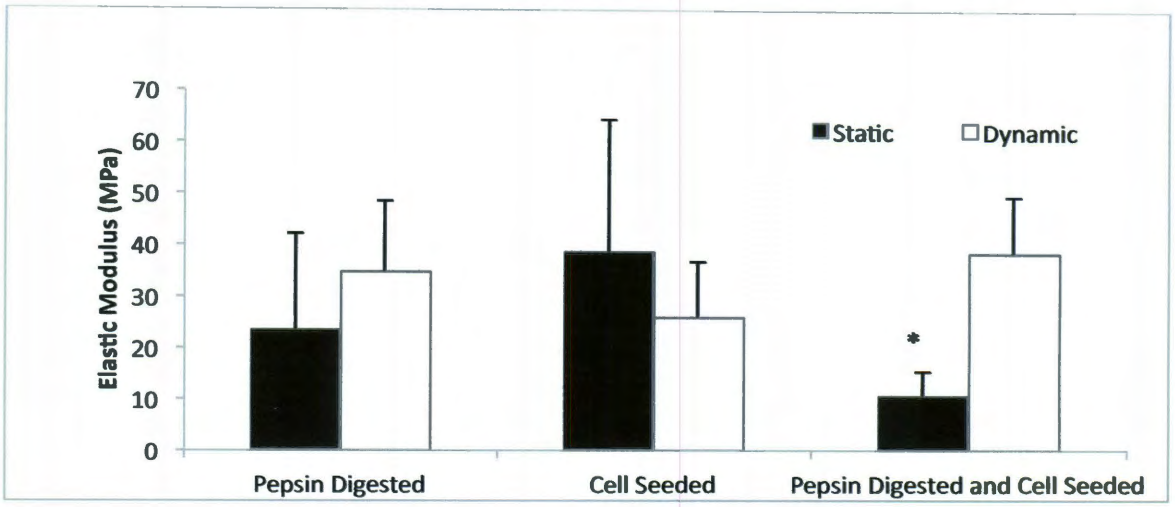

Fig. 7.3 Comparison of Young's modulus in static (without mechanical stimulation) versus dynamic (with mechanical stimulation) groups. The asterisk denotes statistical significance for the pepsin digested, cell seeded group without mechanical stimulation.

The extensibility was generally higher in the statically cultured groups (without mechanical stimulation) when compared to the dynamic groups. For pepsin digested and cell-seeded SIS-ECM, the group without mechanical stimulation had an extensibility of 9.62 ± 13.01% versus 4.82 ± 4.93% for the dynamic group. For SIS-ECM that was pepsin digested only, the group without mechanical stimulation had an extensibility of 15.48 ± 10.69% versus 10.71 ± 13.87% for the dynamic group. For SIS-ECM that was cell seeded only, the group without mechanical stimulation had an extensibility of 14.45 ± 9.23%, versus 13.17 ± 9.91% for the dynamic group. None of these differences were found to be statistically significant.

7.4 Strain mapping

Strain mapping was performed on pepsin-treated and cell seeded dynamic SIS, cell-seeded only dynamic SIS, and pepsin-treated floating controls. Tissue in the pepsin-treated and cell seeded dynamic group appeared more homogenous than expected when compared to cell-seeded alone; it is possible that the pepsin treatment leads to decreased heterogeneity, as the pepsin-treated control group also appears to have largely homogeneous strain. As found in the *in vivo* strain mapping, material heterogeneity was not captured as well as might be expected with a denser charcoal grid or a larger sample size.

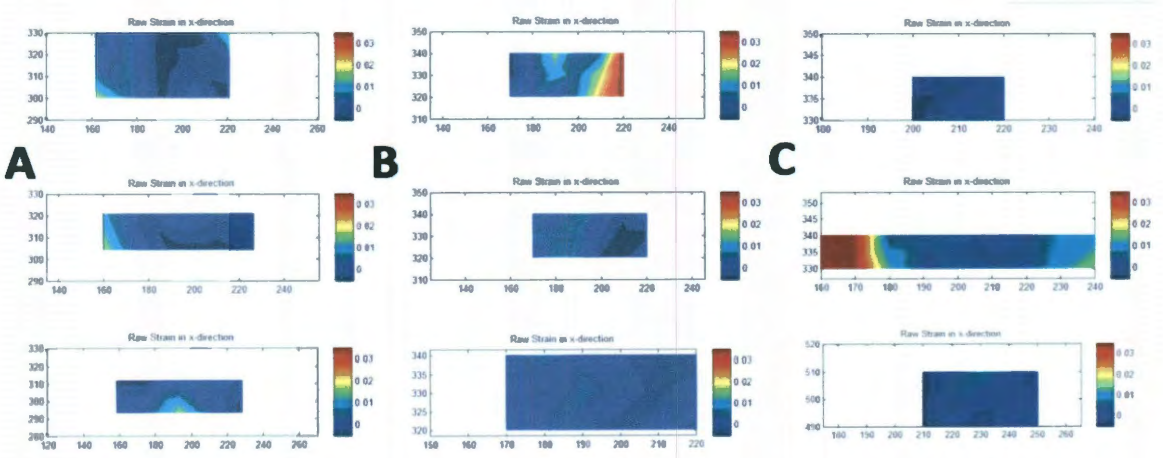

Fig. 7.4 Strain mapping results for A) pepsin-treated and cell seeded dynamic SIS-ECM, B) cell-seeded only dynamic SIS-ECM, and C) pepsin-treated floating controls.

7.5 Histology

Untreated SIS-ECM patches stained mostly for collagen (yellow) with some GAGs (blue-green) by Movat's pentachrome stain (Fig. 7.5 E) and space between distinct layers was visible. Pepsin pretreatment and mechanical stimulation led to greater tissue cohesiveness as seen by hematoxylin and saffron stain (Fig. 7.5 B & F). Without pepsin

pretreatment, the cell-seeded mechanically stimulated group showed less tissue cohesiveness, although cells were able to invade the first few layers of the SIS-ECM patch (Fig. 7.5 C & G). Pepsin pretreatment and cell-seeding prior to mechanical stimulation resulted in SIS-ECM patches that demonstrated the most tissue cohesiveness as well as the deepest penetration of the MVICs into the middle of the patch (Fig. 7.5 D &H).

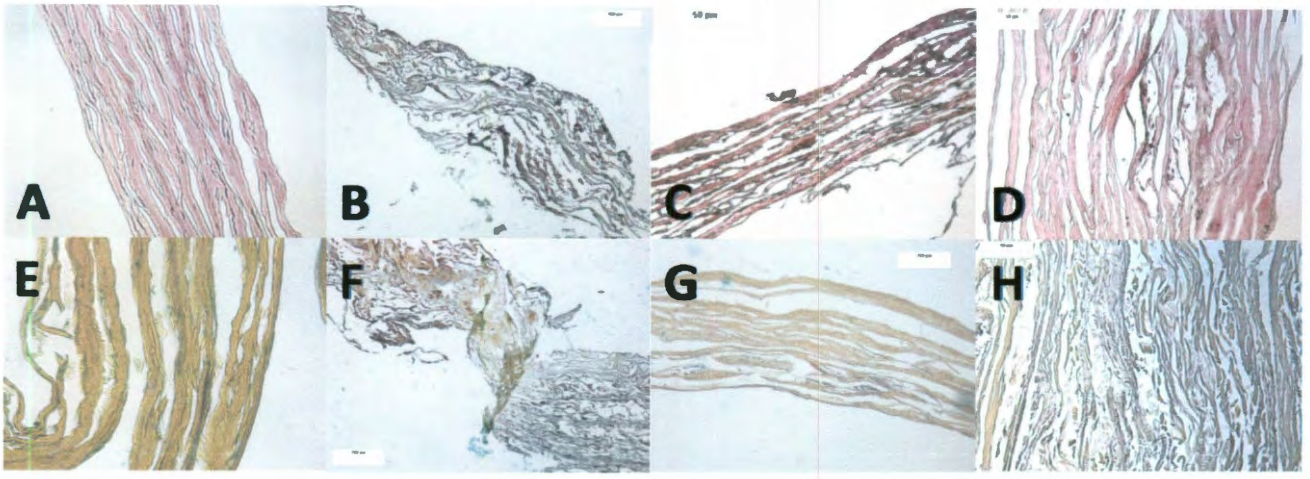

Fig. 7.5 Histologic evaluation of SIS-ECM patches undergoing mechanical stimulation. A) H&E stain and E) Movat's pentachrome stain (collagen stains yellow) for comparison. B) and F) Movat's pentachrome stains of pepsin pretreated SIS-ECM undergoing mechanical stimulation. C) H&E and G) Hematoxylin and saffron stains of cell-seeded SIS-ECM undergoing mechanical stimulation. D) H&E and H) Hematoxylin and saffron stains of pepsin pretreated and cell-seeded SIS-ECM undergoing mechanical stimulation.

7.6 Immunohistochemistry

The only IHC stain in the *in vitro* study that showed any statistical difference between groups was the fibronectin stain. More specifically, the cell seeded, pepsin digestion group demonstrated less intensity of fibronectin staining compared to the samples only digested with pepsin (Fig. 7.6, A-C versus D-F and Fig. 7.7). Staining for smooth muscle alpha actin and for PCNA was not statistically different between groups.

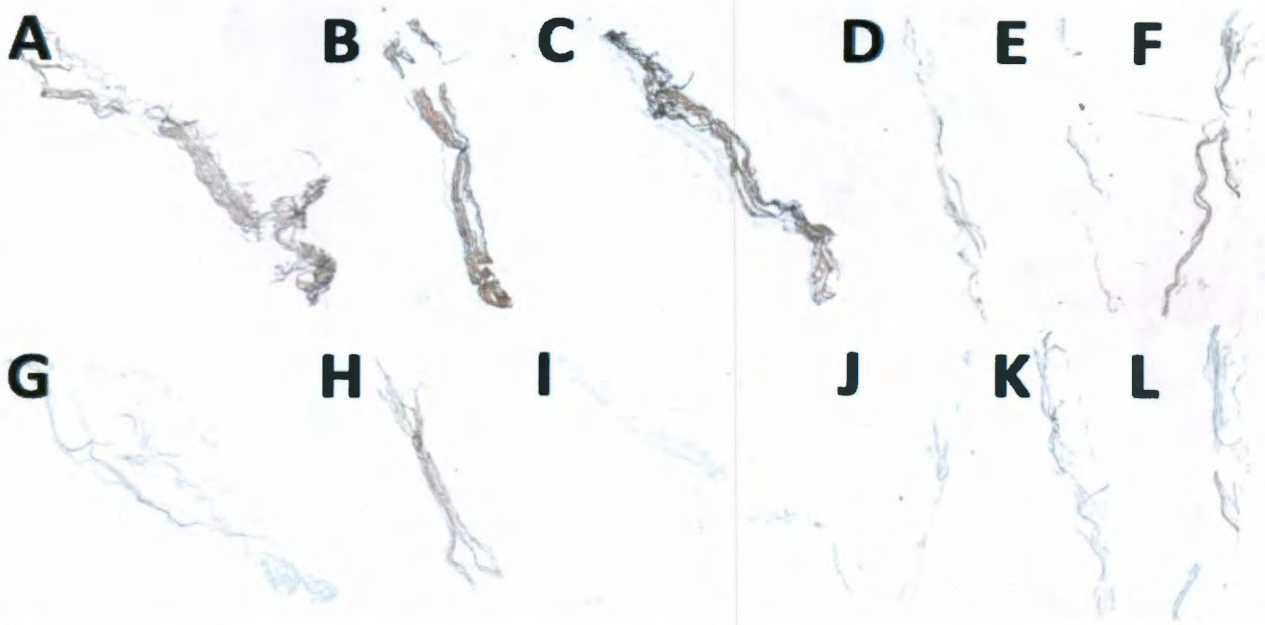

Fig. 7.6 IHC stain for fibronectin. Antibody stain on top row with controls below. A) Cell-seeded only SIS-ECM patch undergoing mechanical stimulation B) Pepsin pretreated and cell-seeded SIS-ECM patch undergoing mechanical stimulation C) Pepsin pretreated only SIS-ECM patch undergoing mechanical stimulation. D) Floating cell-seeded only SIS-ECM patch E) Floating pepsin pretreated and cell-seeded SIS-ECM patch. F) Floating pepsin pretreated only SIS-ECM patch. G)-L) Corresponding controls below primary antibody stained tissue.

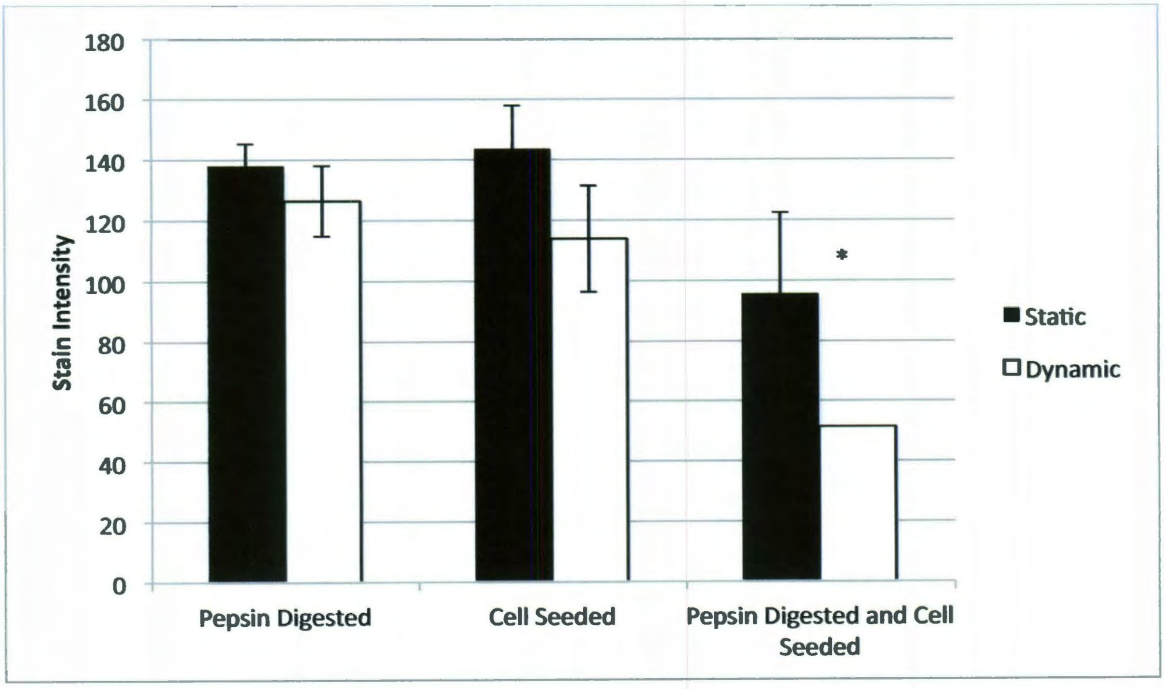

Fig. 7.7 Staining intensity for fibronectin comparing the pepsin digested, cell seeded, and pepsin digested and cell seeded groups. Asterisk indicates statistical significance.

7.7 Discussion

7.1.1 Overall Trends

In this series of experiments, we used the elastic modulus of the ECM material as a surrogate indicator of matrix remodeling. We postulated the following outcomes: 1) proteolytic pre-digestion of the ECM material with pepsin would result in a decrease in elastic modulus that could not be regained in the absence of living cells; 2) given the appropriate growth conditions, seeding the ECM material with cells would provide the potential for matrix remodeling, as evidenced by a corresponding increase in elastic modulus; 3) the dynamic mechanical environment of the bioreactor would influence the VICs' ability to remodel the ECM material.

With respect to the first outcome, we found that pepsin digestion of the ECM resulted in a significant decrease in elastic modulus compared to untreated material, as shown in Figure 7.1. In the cultured samples, in spite of the relatively short time point of 1 week in culture, SIS-ECM patches exposed to mechanical stimulation showed clear differences compared to their floating counterparts. SIS-ECM patches pretreated with pepsin and then cultured in the bioreactor became stiffer, yet the groups kept floating for 7 days had the largest decrease in elastic modulus. Interestingly, the SIS-ECM patches that were seeded with MVICs but did not undergo pepsin pretreatment had lower elastic modulus following mechanical stimulation than either pepsin pre-treated group, but the highest elastic modulus of the floating controls. Mechanical stimulation and enzymatic degradation may be symbiotic processes in remodeling of SIS-ECM patches. However, none of these observational differences were found to be statistically significant. Further studies are needed to confirm the effects of mechanical stimulation and enzymatic

degradation.

Interestingly, pepsin-digested, cell-seeded samples showed a significant and noteworthy response to mechanical stress: Under static conditions, pepsin-digested, cell-seeded ECM samples lost further stiffness compared to the samples digested with pepsin alone, or to those seeded without prior pepsin digestion. However, when similar samples were subjected to the mechanical forces encountered in the splashing bioreactor, no such loss occurred, suggesting that the lack of mechanical stress either fails to induce a pro-remodeling response in the seeded VICs, or actively induces an anti-remodeling response in these cells.

Enzymatic degradation likely plays a key role in cell behavior *in vitro*, as has been shown *in vivo*. MVICs also stained for smooth muscle alpha actin, suggesting cell activation. The greatest infiltration of MVICs into the SIS-ECM patch was seen in those patches that were pre-treated with pepsin before seeding with cells. This is echoed in the strong fibronectin stain, a marker for cell invasion. In addition, the SIS-ECM patches undergoing both pepsin pre-treatment and cell seeding demonstrated greater tissue cohesiveness, with less distinct layers visible by microscopy.

7.7.2 Limitations

The present study has several notable limitations. In particular, the number of tests that could be run in parallel was limited practically by the size of the bioreactor. Small sample size may have confounded statistical interpretation of the data. Furthermore, while we used elastic modulus as a surrogate for evidence of matrix remodeling, there may be other material characteristics that would give us a more

accurate understanding of the matrix dynamics within the ECM material. Finally, although our bioreactor has been previously validated, it is a simplified system and does not completely encompass all of the many variable encountered *in vivo* in the mitral valve.

7.7.3 Future Directions

While significant changes were seen following one week of dynamic culture, longer culture times in the splashing bioreactor would likely continue many of the trends observed and allow greater cell integration and proliferation. Strong staining for fibronectin was seen in the groups undergoing mechanical stimulation at one week, suggesting that MVICs were actively invading the SIS-ECM patch. A longer culture duration may give these cells the opportunity to further remodel the SIS-ECM patch by proliferating and laying down new ECM.

Due to their high cost and lesser ease of experimentation, large animal validation studies of this SIS-ECM patch material should not be its only method of testing. Bioreactor culture has the potential to greatly add to knowledge of the SIS-ECM remodeling process and can be used to create good models of matrix degradation and invading cell behavior.

7.7.4 Conclusions

Pre-digestion with pepsin, and the presence or absence of mechanical stress, appears to play a role in the ability of VICs to remodel ECM material in a dynamic *in vitro* model of mitral valve repair. SIS-ECM pretreated with pepsin and mechanically

stimulated demonstrated superior remodeling compared to non-pepsin degraded SIS-ECM and floating controls. These results will contribute to the goal of creating an *in vitro* model of SIS-ECM remodeling.

Chapter 8: Responsibly Managing the Clinical Application of Tissue-Engineered Scaffolds: How Ontology May Dictate Ethics[7]

8.1 Introduction

Although tissue engineering has been described as a field "still in its infancy,"[105] the impact it has already had on patient care and the public consciousness has been significant. In the past decade, increasing numbers of tissue engineered-scaffolds have become available to repair or replace a myriad of patient tissue. In addition, a paradigm shift has occurred; while pluripotent stem cells were once considered the key to tissue regeneration, the microenvironment within which cells carry out their function has proved equally critical.[103,106] Investigators have therefore focused effort on decellularized scaffolds that, once implanted, can remodel, bear load, and become populated with invading progenitor cells from surrounding tissue.[25,45,48] One such promising scaffold, SIS-ECM, used in the studies previously detailed, has been used successfully for such varied applications as musculotendinous and dura mater replacement, bladder reconstruction, body wall, and myocardium repair.[7–10,20]

The complexity of these scaffolds has led the European Association for Bioindustries (EuropaBio) to call for a distinct definition. EuropaBio argues that "it is necessary that the definition of human tissue engineered product is differentiated from the definition of medicinal product, as well as that for a somatic cell therapy medicinal product and gene therapy medicinal product".[107] Defining these tissue-engineered products is important, the Association notes, because "existing guidelines are specific for

---

[7] The majority of this chapter has been submitted to *The Lancet* and will be published as Scully BB, Morales DLS, and Grande-Allen KJ and McCullough LB. Responsibly Managing the Clinical Application of Tissue-Engineered Scaffolds: How Ontology May Dictate Ethics

pharmaceutical development and those are not suitable" for tissue-engineered products.[107] Investigators and IRBs are also in need of ethically justified guidelines for responsibly managing the clinical innovation of tissue-engineered products. The purposes of this paper are to clarify the nature of tissue-engineered scaffolds as undergoing ontologic metamorphosis, a concept to be explained, and to identify ethical challenges of this metamorphosis.

8.2 Methods

EuropaBio is correct: the central issue is ontological. What kind of clinical entity are tissue-engineered scaffolds? Clarity about what exactly these scaffolds are, and what they are not, is essential for addressing ethical issues. We will use Sulmasy et al.'s criteria to distinguish these scaffolds from other available biomaterials, and explore in what instances the resulting conceptualization may help to construct the necessary ethical framework for approaching these scaffolds.[108] We believe that ontology should drive the ethical framework that, in turn, should guide clinical application of tissue-engineered decellularized scaffolds.

8.3 Findings

8.3.1 Ontology

Paola and Walker describe the example of an implantable cardioverter-defibrillator (ICD) becoming a part of the patient and introduce the concept of biofixtures to explore whether or not a DNR consent authorizes its inactivation. In doing so, they introduce but do not fully develop the concept of an "ontologic metamorphosis", where

one thing becomes "a part of something theretofore disjoint."[109] Although a tissue-engineered scaffold can be said to become a part of the patient, it is not like an ICD. We submit that a tissue-engineered scaffold goes a step further than an implantable device such as an ICD, in that it both becomes part of the patient's physiology, like a device would, and additionally stimulates a process of replacement that leads to the original scaffold's disappearance and replacement with normal tissue (whereas machines replace but remain distinguishable from surrounding anatomy). In this way, the matrix truly does undergo an ontological metamorphosis from a separate entity (for example, the decellularized matrix that can be derived from porcine small-intestinal submucosa) into being replaced by the patient's own cells, with an identical structure and function to the surrounding tissue.

Sulmasy et al.'s criteria for a replacement therapy can be used to demonstrate scaffolds' uniqueness. These criteria are (i) the intervention's responsiveness to changes in the organism or its environment; (ii) properties such as growth and self-repair; (iii) independence from an external energy source or supplies; (iv) independence from external control by an expert; (v) immunologic compatibility; and (vi) physical integration into the patient's body.[108]

8.3.2. The intervention's responsiveness to changes in the organism or its environment

Decellularized tissue-engineered scaffolds begin to respond to changes in the organism immediately upon implantation. Extracellular matrix (ECM), once thought to be biologically inert and referred to as the "ground matrix," is now known to be constantly adapting in response to its environment and the cells that inhabit it. Matrix

metalloproteases break down the existing extracellular matrix and are balanced out by the secretion of additional ECM by its inhabiting cells. De Vries et al. note that these scaffolds, once populated by the host organisms' cells, contain metabolically active cells in a dynamic environment, which mediate an ongoing interaction between the product and the recipient's body.[105] This dynamism produces variability; as Trommelmans et al note, a scaffold "is a dynamic, physiologically active entity and is thus intrinsically variable."[110] Because each recipient contains her own unique physiology, no two implanted scaffolds are alike.

In the case of decellularized tissue-engineered scaffolds not seeded with cells prior to implantation, as opposed to scaffolds containing stem cells or other non-autologous cells, each recipient provides the cells that populate the scaffold after implantation. For scaffolds in contact with blood, such as cardiac patches, cells coming from the blood, or circulating progenitor cells, respond to the scaffold environment by excreting ECM (as would other cell types) and by changing their phenotype.[5] This newly excreted matrix eventually replaces the original scaffolding, which continues to be broken down. Perhaps more than any implant, tissue-engineered scaffolds respond to their environment.

8.3.3 Properties such as growth and self-repair

The ability of implanted decellularized scaffolds to grow with the patient and repair themselves is considered to be a fundamental characteristic.[5] The entire field of tissue engineering, according to de Vries et al, is claimed to be part of a new medical paradigm, namely, that of regenerative medicine".[105] EuropaBio argues: "the emphasis

for hTEPs should be their tissue regenerative properties".[107] This ability to grow and self-repair is thought to be one of the great advantages of these scaffolds and has potential to transform the treatment of patients with disease processes necessitating tissue replacement, particularly those in children and fetuses, where the inability of currently available patch materials to grow with the patient has often necessitated frequent reoperations until they reach maturity. As seen in Table 1, this ability to grow and self-repair is one of the distinguishing characteristics of tissue-engineered decellularized scaffolds separating them from any implantable biomaterial that has come before. Prostheses, synthetic patches, devices, and homograft materials: none of these can grow with the patient or repair themselves when damaged. The unprecedented ability of tissue-engineered scaffolds to grow and repair themselves creates unique ethical challenges, as we shall see.

8.3.4 Independence from external energy sources or supplies

Once implanted, decellularized scaffolds are completely independent from any external energy sources or supplies. This differentiates them from machines, which require continuous monitoring and upkeep. Deplazes et al. note that bioengineering products "should functionally be like a machine but [their] origin and development are still very close to that of traditional organisms".[111] While they argue that "the definition of an entity as machine seems to allow bypassing the discussion about the assignment and evaluation of instrumental and intrinsic values", these values "can be raised in the case of organisms".[111] However, their independence from external energy sources or supplies does not quite make these scaffolds organisms, either. As seen in Table 1, an

independence from external energy sources or supplies is not a new feature of implanted biomaterials, as it is shared by technologies as varied as orthopedic hardware, prostheses, patch materials, cadaveric tissue, and human tissue and organ transplants (Table 1).

8.3.5 Independence from external control by an expert

Once implanted these scaffolds function independently of any external control. Although implanted tissue engineered scaffolds may potentially be monitored by an expert, for instance with serial MRIs, such an expert could exert minimal if any control over the scaffold. Unlike a transplanted organ, whose effect on the surrounding tissue is modulated by an expert-controlled regimen of medication according to imaging and other studies, or an implanted device that can be manipulated, these scaffolds operate completely independently of the experts who implant them. Sulmasy et al. note: "the most important feature of a replacement therapy is that it provides the function that has been pathologically lost."[108] Although a substitute therapy, such as peritoneal dialysis, requires external control by an expert or team of experts, a replacement therapy does not.

Their independence from external control by an expert makes these scaffolds similar to cadaveric and human tissue transplants, which share this characteristic with orthopedic hardware and prostheses and patch material. In contrast, implanted drug delivery systems, devices, and human organ transplants require extensive outside control. While Sulmasy et al. argue that a transplanted organ constitutes a replacement therapy by this definition, here we can see a further distinction for decellularized scaffolds: unlike a transplanted organ, which does in fact require the control of a specialized team of experts, and whose effects on a patient's body can be modified, for instance by

immunosuppressants, once implanted a scaffold is truly independent of outside expert control, suggesting that these scaffolds are more of a replacement than transplanted organs. Because of this distinction, we propose the phrase "autonomous replacement therapy," which emphasizes tissue-engineered scaffolds' unique independence from external control by an expert.

8.3.6 Immunologic compatibility

Like the ability to grow and self-repair, the immunogenicity of decellularized scaffolds is key to their identification as such. By removing cells, it is believed that most antigenic elements are eliminated, avoiding an immunological response in the recipient. In addition, collagen is the primary matrix element in these scaffolds, and is considered minimally antigenic.[5] This limited immunogenicity removes the need for tissue typing, which plagues organ transplantation, or the addition of a synthetic or drug-releasing barrier, such as that found in implanted devices like coronary artery stents. Because the high immunologic compatibility of these scaffolds contributes to their independence from any outside control (in the form of physicians prescribing immunosuppressants, for instance), it is a critical characteristic making them autonomous replacement therapies.

8.3.7 Physical integration into the patient's body

This integration again separates these scaffolds from the majority of other implantable biomaterials, suggesting that the way we view them should differ as well. Because of their immediate remodeling upon implantation, decellularized scaffolds are rapidly integrated into the patient's body. De Vries et al. therefore note that implanting a

tissue-engineered product is an "irreversible process," one that additionally suggests that these are replacement therapies. Researchers have combined decellularized scaffolds with autologous cells, for instance in the development of tissue-engineered valve stents, a technology that is theoretically reversible.[112] However, it is the astonishing potential extent of their integration that has made these scaffolds a source of great hope for clinicians. This integration also makes them more of a replacement therapy than other patch materials, which can ultimately be rejected by the body and become calcified or thrombotic.[2,3]

Unlike all other implantable biomaterials including organ transplantation, these scaffolds meet every one of Sulmasy's criteria for replacement therapies. As such, we must view them as novel entities in that they uniquely undergo a complete ontologic metamorphosis into autonomous replacement therapies. Any adequate ethical framework must take account of this novelty.

Table 8.1 Characteristics of Implantable Biomaterials

Implanted biomaterial	Examples	Responds to change in organism or environment	Can grow and self-repair	Independence from external energy sources or supplies	Independence from external control by an expert	Immunologic compatibility	Physical Integration into the patient's body	Irrevers-ible process	Off-the-shelf availa-bility
Orthopedic hardware	Stabilizing pin, plate	-	-	+	+	-	+	-	+
Prostheses	Hip, knee replacement, PMMA for chest wall repair	-	-	+	+	-	+	-	+
Synthetic meshes	Hernia repair, pelvic floor repair, urologic slings	-	-	+	+	-	+	-	+
Synthetic patch	Dacron, Gortex	+	-	+	+	-	+	-	+
Drug-eluting implants	Stents	-	-	-	-	-	+	-	+
Implantable drug delivery systems	Insulin pumps, birth control	-	-	-	-	-	-	-	+
Short-term devices	VADs	+	-	-	-	-	-	-	+
Destination devices	VADs, ICDs, pacemakers	+	-	-	-	-	+	-	+
Cadeveric tissue	Heart valves, corneas	+	-	+	+	-	+	-	+
Human tisue transplants	Blood, bone marrow, veins for coronary artery bypass grafts	+	-	+	+	+/-	+	+	-
Human organ transplants	Heart, lungs, kidney, liver	+	-	+	-	-	+	-	-
Human cell-seeded scaffolds	**Bone scaffolds, skin grafts**	+	+	+	+	+*	+	+	-
Decellularized extracellular matrix scaffolds	**SIS-ECM, UBM (urinary bladder matrix), decellularized organs**	+	+	+	+	+	+	+	+

8.4 Ethical Challenges

In order to distinguish these scaffolds from other implantable biomaterials, we have created a table that maps out their characteristics (Table 8.1). As is shown here, decellularized scaffolds differ from destination devices such as ICDs in five characteristics, four of which together represent two-thirds of Sulmasy's criteria: unlike ICDs, decllularized scaffolds can grow and self-repair, are independent from external energy sources or supplies and control by an expert, and are immunologically compatible with the host organism. In addition to these characteristics, the implantation of these scaffolds is a largely irreversible process. Just as it is impossible to remove blood infused into a patient from a donor, because it becomes so integrated with the patient's existing blood, once a tissue-engineered scaffold is implanted its integration into the existing tissue is so extensive that it becomes impossible to distinguish the implanted tissue from the native. The extent of implanted decellularized tissue-engineered patches' response to changes between organisms and environments suggests that they are a true replacement therapy.

Tissue engineering scaffolds are unique, because as we have seen with their unique fulfillment of Sulmasy's criteria, they undergo a complete ontologic metamorphosis from implantable patch to functioning part of the patient's anatomy. In the case of decellularized tissue-engineered scaffolds, as seen in Table 8.1, they are also unique in being available "off the shelf," making them available for immediate use in patients. As the ontological investigation of tissue-engineered scaffolds has shown, the main advantages of these technologies constitute their greatest ethical challenges.

First, the unprecedented ability of these scaffolds to grow and self-repair may prove clinically risky. Trommelmans et al note: "against an enormous benefit stand potential large risks, probably even emergent risks due to the process of regeneration that have never before been encountered."[110] As a true replacement therapy, scaffolds will be irreversible and clinical risks, especially long-term ones, may be unavoidable. Because of this, there has been a growing interest in how to manage emerging biotechnologies' risks without limiting their potential benefits. Gutmann et al. recently identified the ideals of public beneficence, which requires vigilance "about risks and harms, standing ready to revise policies that pursue potential benefits with insufficient caution," and intellectual freedom, which argues "when new technologies intended for good may be used to cause harm—these risks alone are generally insufficient to justify limits on intellectual freedom." [113] The risks posed by matrix scaffolds have not been proven to outweigh their potential benefits, making their continued use ethically justifiable.

Here we must also be cognizant of the biasing potential of investigator enthusiasm, defined as the detachment of clinical judgment from the discipline of evidence-based reasoning. The promise of these scaffolds is certainly tantalizing, but the need for an optimal biomaterial for patient applications may obscure their flaws, and lead to premature implementation in human subjects, particularly in children, and even fetuses, whose current lack of implantable tissues that can grow with them often necessitates multiple reoperations that contribute to increased morbidity. Investigators have already begun to explore extracellular matrices' potential for intrauterine repair of congenital disorders, such as spina bifida.[115] Investigation needs to identify short-term

and long-term risks, so that patients can be as well-informed as possible, presuming long-term risks do not outweigh benefits.

Second, unlike other implantable biomaterials, and even distinct from transplanted human tissues such as blood or bone marrow, these scaffolds are minimally immunogenic; however, the risk of an immune response is greater due to the extent of their integration into the host organism. In addition, this greater immunologic compatibility may make the removal of these scaffolds less permissible than other implantable biomaterials. Whereas an implanted organ, when it evokes an overtly strong immune response, may be taken out and replaced, these scaffolds behave more like human tissue transplants, such as blood and bone marrow, which can be typed to avoid immunologic cross-reactivity but can be especially dangerous when they do induce an immune response (such as in transfusion reactions in the case of an incorrect blood type or graft versus host disease following bone marrow transplantation). The increased risk posed by their extensive integration requires the informed consent process for these scaffolds to be more rigorous if being used for the purpose of tissue remodeling. Perhaps the greatest challenge of all will be the problem of enthusiasm, which may undermine such rigorous investigation, considering the great need that exists for such patch materials. Like cloning, which has been called the "holy grail of medicine"[116] for its potential regenerative properties, there will be risks to the technology of tissue-engineered scaffolds, some of which may not be discovered for years. In addition, for many of these scaffolds, FDA approval may only require proof that they are "as good as" other available patch materials, negating the need for a more costly investigation of all of the scaffolds' properties and mechanisms. Such patches should only be used for the

existing FDA indications. If a material is being used for a FDA approved function such as replacement of bladder wall or dura, then consent can be similar as when a nonspecific patch material is used. However, if it is being used for remodeling purposes and is not FDA approved for this purpose, then patients should specifically consent to the use of a matrix scaffold. Physicians should ensure they understand these scaffolds' unique benefits and risk, in order for them to make a truly informed decision.

The FDA cannot, however, regulate what is said to patients and their families. Without an FDA approved indication for tissue remodeling, a clinician should in no way say or indicate to a patient or their family that a patch is being used for this indication unless they are performing a study and have an IRB approved consent form. Physicians must be careful to use clinically accurate, non-exaggerating language when describing these technologies to patients and keep in mind that these potential risks must be considered in the context of the overall benefits. However, if physicians use these new technologies for their FDA approved indications, they on firm ethical ground.

8.5 Conclusions

As tissue-engineered scaffolds are used in more and more tissues and gain acceptance for a host of new applications, the ethical framework with which physicians use them will be influenced by how they are defined. As we have seen, these scaffolds fulfill all of Sulmasy's criteria for replacement therapies, making them distinct from other available implantable biomaterials. Tissue-engineered scaffolds are unique in their complete ontologic metamorphosis and pose distinctive ethical challenges that must be responsibly managed. In particular, enthusiasm in the media and lay public, fed by the

medical community, must be carefully controlled. Clinical use should be only for FDA approved indications unless an IRB-approved study is underway. Physicians, IRBs and other regulatory bodies will need to take these distinctions into account when constructing ethical frameworks with which to view this technology. However, this responsibility should not detract from the exciting potential that tissue-engineered scaffolds may have in treating and potentially curing many human illnesses.

Chapter 9: Implications and Future Directions

9.1 Implications

9.1.1 Clinical Significance

A cardiovascular patch with the ability to remodel and grow with the patient would transform the care of children and adults with congenital heart diseases such as tetralogy of Fallot, as well as be applicable to countless other cardiovascular applications. This body of work evaluated the potential of the juvenile ovine model for investigations of the remodeling of a newly available SIS-ECM patch via a large variety of experimental modalities. The novelty of this work lies in the use of a larger SIS-ECM patch than has been previously described for repair of vessels,[96] its placement in the RVOT, and in the use of a novel bioreactor to further investigate its remodeling processes. This work is the basis for a larger study soon to be underway, and has attempted to apply an exhaustive panel of characterizations towards assessing the remodeling potential of an extremely promising tissue-engineered cardiac patch.

9.1.2 Ethical Considerations

As tissue-engineered scaffolds are used in more and more tissues and gain acceptance for a host of new applications, the ethical framework with which physicians use them will be influenced by how they are defined. Tissue-engineered scaffolds are unique in their complete ontologic metamorphosis (going from scaffold material to a part of the patient's own tissue) and pose distinctive ethical challenges that must be responsibly managed. In particular, enthusiasm in the media and lay public, fed by the medical community, must be carefully controlled. Contract studies, such as the research

presented in chapters 3-5, that are funded by the medical device industry require close scrutiny and extra precautions to avoid conflicts of interest. Clinical use should be only for FDA approved indications unless an IRB-approved study is underway. Physicians, IRBs and other regulatory bodies will need to take these distinctions into account when constructing ethical frameworks with which to view this technology. However, this responsibility should not detract from the exciting potential that tissue-engineered scaffolds may have in treating and potentially curing many human illnesses.

9.2 Future Directions

A significant limitation of the *in vivo* study is the very small sample size, confounded by the fact that only 2 of the 4 hearts were successfully reperfused for the optical mapping experiment. There was also no comparator patch material used to serve as a negative control or to provide a comparison with the closest alternative patch. Nevertheless, these preliminary results showing functional electrical activity within the implanted patch are remarkable and, to our knowledge, unprecedented for any patch material currently used for human cardiac repair. In the future, we plan to extend this line of investigation using a larger number of animals, and including a comparator arm, most likely using bovine pericardium as control material. In addition to the experiments already performed, we intend to perform gadolinium-enhanced magnetic resonance imaging to assess wall motion and muscle-tissue viability and motility using a 3T whole-body MR system using a phased-array receiver coil and vector electrocardiogram for R-wave triggering. In addition, 3-D electrical mapping using a 3-D electrophysiological mapping system will be used to create an anatomic voltage map and a 3D activation/propagation map of the RV. Sonomicrometry will also be used to compare

contractility in the patch materials versus myocardial tissue, and additional histology and mechanical testing will be used to confirm and extend the results of this study.

A significant addition to this work would be a continued *in vitro* investigation using the splashing bioreactor described in chapters 6-7, with longer time points and perhaps using other enzymes, such as papain, to degrade the matrix. In addition, more precise strain mapping analysis would contribute to a greater knowledge of the material properties of the remodeling tissue.

Human validation of the patch material would be an important next step in serving our pediatric population. One patient population in particular that would be a potential candidate for such research would be patients with tetralogy of Fallot who undergo reoperation for pulmonary valve replacement requiring reconstruction of their right ventricular outflow tracts necessitating new patch material. To determine whether the patch has remodeled we could follow up with a variety of imaging techniques, including magnetic resonance imaging (MRI) with gadollinium for viability imaging, echocardiography to measure tissue strain, and positron emission tomography (PET) scan with glucose uptake for metabolic imaging.

9.3 Conclusions

In conclusion, we have found that an SIS-ECM patch, when surgically implanted in the ovine RVOT, aorta and PA, is capable of constructive remodeling as evidenced by electrical, histological and mechanical properties. The juvenile ovine model appears suitable for assessing this novel patch's remodeling potential, allowing evaluation of cell infiltration, cell phenotype, and remodeling extracellular matrix properties, including

change in elastic modulus, collagen composition and calcification. Additionally, in the RVOT the juvenile ovine model proves suitable for assessing conduction of an electrical signal. In addition, a splashing bioreactor has proved to be an excellent culture environment for the investigation of the SIS-ECM patch's remodeling. Based on the limitations with this study, the promise of remodeling associated with SIS merits further investigation in further studies. As tissue-engineered scaffolds are used in more and more tissues and gain acceptance for a host of new applications, the ethical framework with which physicians use them will be influenced by how they are defined. However, while further studies are needed for validation of this patch, these series of studies have shed important light on the remodeling ability of a novel cardiovascular patch, which has the potential to transform the care of a needy patient population.

Chapter 10: Bibliography

1. Roger VL, Go AS, Lloyd-Jones DM, et al. Heart disease and stroke statistics--2011 update: a report from the American Heart Association. *Circulation*. 2011;123(4):e18-e209. Available at: http://www.ncbi.nlm.nih.gov/pubmed/21160056. Accessed March 4, 2012.

2. Oechslin EN, Harrison DA, Harris L, et al. Reoperation in adults with repair of tetralogy of fallot: indications and outcomes. *The Journal of thoracic and cardiovascular surgery*. 1999;118(2):245-51. Available at: http://www.ncbi.nlm.nih.gov/pubmed/10424997. Accessed April 8, 2012.

3. Mirensky TL, Breuer CK. The development of tissue-engineered grafts for reconstructive cardiothoracic surgical applications. *Pediatric research*. 2008;63(5):559-68. Available at: http://www.ncbi.nlm.nih.gov/pubmed/18427302. Accessed April 8, 2012.

4. Kim JB, Kim HJ, Moon DH, et al. Long-term outcomes after surgery for rheumatic mitral valve disease: valve repair versus mechanical valve replacement. *European journal of cardio-thoracic surgery : official journal of the European Association for Cardio-thoracic Surgery*. 2010;37(5):1039-46. Available at: http://www.ncbi.nlm.nih.gov/pubmed/20036134. Accessed April 8, 2012.

5. Bronzino JD. *The biomedical engineering handbook, third edition - 3 volume set: tissue engineering and artificial organs (Google eBook)*. CRC Press; 2006:1304. Available at: http://books.google.com/books?id=k13DWbq_pxoC&pgis=1. Accessed April 8, 2012.

6. Ozawa T, Mickle DAG, Weisel RD, et al. Optimal biomaterial for creation of autologous cardiac grafts. *Circulation*. 2002;106(12 Suppl 1):I176-82. Available at: http://www.ncbi.nlm.nih.gov/pubmed/12354729. Accessed April 8, 2012.

7. Probst M, Dahiya R, Carrier S, Tanagho EA. Reproduction of functional smooth muscle tissue and partial bladder replacement. *British journal of urology*. 1997;79(4):505-15. Available at: http://www.ncbi.nlm.nih.gov/pubmed/9126077. Accessed April 8, 2012.

8. Calvano CJ, Moran ME, Parekh A, Desai PJ, Cisek LJ. Laparoscopic augmentation cystoplasty using the novel biomaterial Surgisis: small-intestinal submucosa. *Journal of endourology / Endourological Society*. 2000;14(2):213-7. Available at: http://www.ncbi.nlm.nih.gov/pubmed/10772517. Accessed April 8, 2012.

9. Lopes MF, Cabrita A, Ilharco J, et al. Esophageal replacement in rat using porcine intestinal submucosa as a patch or a tube-shaped graft. *Diseases of the esophagus : official journal of the International Society for Diseases of the Esophagus / I.S.D.E.*

2006;19(4):254-9. Available at: http://www.ncbi.nlm.nih.gov/pubmed/16866856. Accessed April 8, 2012.

10. Chen F, Yoo JJ, Atala A. Acellular collagen matrix as a possible "off the shelf" biomaterial for urethral repair. *Urology*. 1999;54(3):407-10. Available at: http://www.ncbi.nlm.nih.gov/pubmed/10475343. Accessed April 8, 2012.

11. McKay R. Stem cells--hype and hope. *Nature*. 2000;406(6794):361-4. Available at: http://www.ncbi.nlm.nih.gov/pubmed/10935622. Accessed April 8, 2012.

12. Cebotari S, Mertsching H, Kallenbach K, et al. Construction of autologous human heart valves based on an acellular allograft matrix. *Circulation*. 2002;106(12 Suppl 1):I63-I68. Available at: http://www.ncbi.nlm.nih.gov/pubmed/12354711. Accessed April 8, 2012.

13. Wilson GJ, Courtman DW, Klement P, Lee JM, Yeger H. Acellular matrix: a biomaterials approach for coronary artery bypass and heart valve replacement. *The Annals of thoracic surgery*. 1995;60(2 Suppl):S353-8. Available at: http://www.ncbi.nlm.nih.gov/pubmed/7646187. Accessed April 8, 2012.

14. Cobb MA, Badylak SF, Janas W, Simmons-Byrd A, Boop FA. Porcine small intestinal submucosa as a dural substitute. *Surgical neurology*. 1999;51(1):99-104. Available at: http://www.ncbi.nlm.nih.gov/pubmed/9952131. Accessed April 8, 2012.

15. Zhang F, Zhang J, Lin S, et al. Small intestinal submucosa in abdominal wall repair after TRAM flap harvesting in a rat model. *Plastic and reconstructive surgery*. 2003;112(2):565-70. Available at: http://www.ncbi.nlm.nih.gov/pubmed/12900615. Accessed April 8, 2012.

16. Suckow MA, Voytik-Harbin SL, Terril LA, Badylak SF. Enhanced bone regeneration using porcine small intestinal submucosa. *Journal of investigative surgery : the official journal of the Academy of Surgical Research*. 12(5):277-87. Available at: http://www.ncbi.nlm.nih.gov/pubmed/10599003. Accessed April 8, 2012.

17. Badylak SF, Tullius R, Kokini K, et al. The use of xenogeneic small intestinal submucosa as a biomaterial for Achilles tendon repair in a dog model. *Journal of biomedical materials research*. 1995;29(8):977-85. Available at: http://www.ncbi.nlm.nih.gov/pubmed/7593041. Accessed April 8, 2012.

18. Bell E. *Tissue Engineering: Current Perspectives*. Birkhäuser; 1993:241. Available at: http://books.google.com/books?id=fAF-QgAACAAJ&pgis=1. Accessed April 8, 2012.

19. Blalock A, Taussig HB. Landmark article May 19, 1945: The surgical treatment of malformations of the heart in which there is pulmonary stenosis or pulmonary atresia. By Alfred Blalock and Helen B. Taussig. *JAMA : the journal of the American Medical*

Association. 1984;251(16):2123-38. Available at: http://www.ncbi.nlm.nih.gov/pubmed/6368878. Accessed April 8, 2012.

20. Badylak S, Obermiller J, Geddes L, Matheny R. Extracellular matrix for myocardial repair. *The heart surgery forum*. 2003;6(2):E20-6. Available at: http://www.ncbi.nlm.nih.gov/pubmed/12716647. Accessed April 8, 2012.

21. Vorotnikova E, McIntosh D, Dewilde A, et al. Extracellular matrix-derived products modulate endothelial and progenitor cell migration and proliferation in vitro and stimulate regenerative healing in vivo. *Matrix biology : journal of the International Society for Matrix Biology*. 2010;29(8):690-700. Available at: http://www.ncbi.nlm.nih.gov/pubmed/20797438. Accessed March 22, 2012.

22. Courtman DW, Errett BF, Wilson GJ. The role of crosslinking in modification of the immune response elicited against xenogenic vascular acellular matrices. *Journal of biomedical materials research*. 2001;55(4):576-86. Available at: http://www.ncbi.nlm.nih.gov/pubmed/11288086. Accessed April 8, 2012.

23. Badylak SF. The extracellular matrix as a biologic scaffold material. *Biomaterials*. 2007;28(25):3587-93. Available at: http://www.ncbi.nlm.nih.gov/pubmed/17524477. Accessed March 7, 2012.

24. Badylak SF, Valentin JE, Ravindra AK, McCabe GP, Stewart-Akers AM. Macrophage phenotype as a determinant of biologic scaffold remodeling. *Tissue engineering. Part A*. 2008;14(11):1835-42. Available at: http://www.ncbi.nlm.nih.gov/pubmed/18950271. Accessed April 4, 2012.

25. Reing JE, Zhang L, Myers-Irvin J, et al. Degradation products of extracellular matrix affect cell migration and proliferation. *Tissue engineering. Part A*. 2009;15(3):605-14. Available at: http://www.ncbi.nlm.nih.gov/pubmed/18652541. Accessed April 8, 2012.

26. Kochupura PV, Azeloglu EU, Kelly DJ, et al. Tissue-engineered myocardial patch derived from extracellular matrix provides regional mechanical function. *Circulation*. 2005;112(9 Suppl):I144-9. Available at: http://www.ncbi.nlm.nih.gov/pubmed/16159807. Accessed March 18, 2012.

27. Barzilla JE, McKenney AS, Cowan AE, Durst CA, Grande-Allen KJ. Design and validation of a novel splashing bioreactor system for use in mitral valve organ culture. *Annals of biomedical engineering*. 2010;38(11):3280-94. Available at: http://www.ncbi.nlm.nih.gov/pubmed/20661646. Accessed April 7, 2012.

28. Mayer JE, Shin'oka T, Shum-Tim D. Tissue engineering of cardiovascular structures. *Current opinion in cardiology*. 1997;12(6):528-32. Available at: http://www.ncbi.nlm.nih.gov/pubmed/9429823. Accessed April 8, 2012.

29. Gross RE, Hubbard JP. Landmark article Feb 25, 1939: Surgical ligation of a patent ductus arteriosus. Report of first successful case. By Robert E. Gross and John P. Hubbard. *JAMA : the journal of the American Medical Association*. 1984;251(9):1201-2. Available at: http://www.ncbi.nlm.nih.gov/pubmed/6363741. Accessed April 8, 2012.

30. LILLEHEI CW, COHEN M, WARDEN HE, VARCO RL. The direct-vision intracardiac correction of congenital anomalies by controlled cross circulation; results in thirty-two patients with ventricular septal defects, tetralogy of Fallot, and atrioventricularis communis defects. *Surgery*. 1955;38(1):11-29. Available at: http://www.ncbi.nlm.nih.gov/pubmed/14396676. Accessed April 8, 2012.

31. Neill CA, Clark EB. Tetralogy of Fallot. The first 300 years. *Texas Heart Institute journal / from the Texas Heart Institute of St. Luke's Episcopal Hospital, Texas Children's Hospital*. 1994;21(4):272-9. Available at: http://www.pubmedcentral.nih.gov/articlerender.fcgi?artid=325189&tool=pmcentrez&rendertype=abstract. Accessed April 8, 2012.

32. CAMPBELL M, DEUCHAR DC, BROCK R. Results of pulmonary valvotomy and infundibular resection in 100 cases of Fallot's tetralogy. *British medical journal*. 1954;2(4880):111-22. Available at: http://www.pubmedcentral.nih.gov/articlerender.fcgi?artid=2079269&tool=pmcentrez&rendertype=abstract. Accessed April 8, 2012.

33. Ruhlman M. *Walk on Water: The Miracle of Saving Children's Lives*. Penguin Books; 2004:352. Available at: http://books.google.com/books?id=5DaC5NnqyuAC&pgis=1. Accessed April 8, 2012.

34. van Doorn C. The unnatural history of tetralogy of Fallot: surgical repair is not as definitive as previously thought. *Heart (British Cardiac Society)*. 2002;88(5):447-8. Available at: http://www.pubmedcentral.nih.gov/articlerender.fcgi?artid=1767405&tool=pmcentrez&rendertype=abstract. Accessed April 8, 2012.

35. Brickner ME, Hillis LD, Lange RA. Congenital heart disease in adults. First of two parts. *The New England journal of medicine*. 2000;342(4):256-63. Available at: http://www.ncbi.nlm.nih.gov/pubmed/10648769. Accessed April 8, 2012.

36. Rittenhouse EA, Sauvage LR, Stamm SJ, et al. Radical enlargement of the aortic root and outflow tract to allow valve replacement. *The Annals of thoracic surgery*. 1979;27(4):367-73. Available at: http://www.ncbi.nlm.nih.gov/pubmed/378151. Accessed April 8, 2012.

37. Barros D'Sa AA, Berger K, Di Benedetto G, et al. A healable filamentous Dacron surgical fabric. Experimental studies and clinical experience. *Annals of surgery*. 1980;192(5):645-57. Available at:

http://www.pubmedcentral.nih.gov/articlerender.fcgi?artid=1344947&tool=pmcentrez&rendertype=abstract. Accessed April 8, 2012.

38. Pires AC, Saporito WF, Cardoso SH, Ramaciotti O. Bovine pericardium used as a cardiovascular patch. *The heart surgery forum*. 1999;2(1):60-9. Available at: http://www.ncbi.nlm.nih.gov/pubmed/11276462. Accessed April 8, 2012.

39. Di Eusanio M, Schepens MAAM. Left atrial thrombus on a Teflon patch for ASD closure. *European journal of cardio-thoracic surgery : official journal of the European Association for Cardio-thoracic Surgery*. 2002;21(3):542. Available at: http://www.ncbi.nlm.nih.gov/pubmed/11888778. Accessed April 8, 2012.

40. Kumar SP, Prabhakar G, Kumar M, et al. Comparison of fresh and glutaraldehyde-treated autologous stented pericardium as pulmonary valve replacement. *Journal of cardiac surgery*. 1995;10(5):545-51. Available at: http://www.ncbi.nlm.nih.gov/pubmed/7488776. Accessed April 8, 2012.

41. Schmidt D, Mol A, Neuenschwander S, et al. Living patches engineered from human umbilical cord derived fibroblasts and endothelial progenitor cells. *European journal of cardio-thoracic surgery : official journal of the European Association for Cardio-thoracic Surgery*. 2005;27(5):795-800. Available at: http://www.ncbi.nlm.nih.gov/pubmed/15848316. Accessed April 8, 2012.

42. Shin'oka T, Imai Y, Ikada Y. Transplantation of a tissue-engineered pulmonary artery. *The New England journal of medicine*. 2001;344(7):532-3. Available at: http://www.ncbi.nlm.nih.gov/pubmed/11221621. Accessed March 28, 2012.

43. Cho S-W, Park HJ, Ryu JH, et al. Vascular patches tissue-engineered with autologous bone marrow-derived cells and decellularized tissue matrices. *Biomaterials*. 2005;26(14):1915-24. Available at: http://www.ncbi.nlm.nih.gov/pubmed/15576165. Accessed April 8, 2012.

44. Badylak SF, Freytes DO, Gilbert TW. Extracellular matrix as a biological scaffold material: Structure and function. *Acta biomaterialia*. 2009;5(1):1-13. Available at: http://www.ncbi.nlm.nih.gov/pubmed/18938117. Accessed March 1, 2012.

45. Beattie AJ, Gilbert TW, Guyot JP, Yates AJ, Badylak SF. Chemoattraction of progenitor cells by remodeling extracellular matrix scaffolds. *Tissue engineering. Part A*. 2009;15(5):1119-25. Available at: http://www.pubmedcentral.nih.gov/articlerender.fcgi?artid=2789572&tool=pmcentrez&rendertype=abstract. Accessed April 8, 2012.

46. Zhao Z-Q, Puskas JD, Xu D, et al. Improvement in cardiac function with small intestine extracellular matrix is associated with recruitment of C-kit cells, myofibroblasts, and macrophages after myocardial infarction. *Journal of the American College of*

Cardiology. 2010;55(12):1250-61. Available at: http://www.ncbi.nlm.nih.gov/pubmed/20298933. Accessed April 8, 2012.

47. Zantop T, Gilbert TW, Yoder MC, Badylak SF. Extracellular matrix scaffolds are repopulated by bone marrow-derived cells in a mouse model of achilles tendon reconstruction. *Journal of orthopaedic research : official publication of the Orthopaedic Research Society*. 2006;24(6):1299-309. Available at: http://www.ncbi.nlm.nih.gov/pubmed/16649228. Accessed April 8, 2012.

48. Badylak SF, Park K, Peppas N, McCabe G, Yoder M. Marrow-derived cells populate scaffolds composed of xenogeneic extracellular matrix. *Experimental hematology*. 2001;29(11):1310-8. Available at: http://www.ncbi.nlm.nih.gov/pubmed/11698127. Accessed April 8, 2012.

49. Badylak SF. The extracellular matrix as a scaffold for tissue reconstruction. *Seminars in cell & developmental biology*. 2002;13(5):377-83. Available at: http://www.ncbi.nlm.nih.gov/pubmed/12324220. Accessed April 8, 2012.

50. Badylak SF. Xenogeneic extracellular matrix as a scaffold for tissue reconstruction. *Transplant immunology*. 2004;12(3-4):367-77. Available at: http://www.ncbi.nlm.nih.gov/pubmed/15157928. Accessed March 15, 2012.

51. Scholl FG, Boucek MM, Chan KC, Valdes-Cruz L, Perryman R. Preliminary Experience With Cardiac Reconstruction Using Decellularized Porcine Extracellular Matrix Scaffold: Human Applications in Congenital Heart Disease. *World Journal for Pediatric and Congenital Heart Surgery*. 2010;1(1):132-136. Available at: http://pch.sagepub.com/content/1/1/132.full. Accessed April 8, 2012.

52. Gerdisch MW, Akinwande AO, Matheny RG. Use of a novel acellular xenograft as a patch for aortic annular enlargement during aortic valve replacement. *Innovations (Philadelphia, Pa.)*. 2010;5(1):60-2. Available at: http://www.ncbi.nlm.nih.gov/pubmed/22437278. Accessed April 8, 2012.

53. Boyd WD, Johnson WE, Sultan PK, Deering TF, Matheny RG. Pericardial reconstruction using an extracellular matrix implant correlates with reduced risk of postoperative atrial fibrillation in coronary artery bypass surgery patients. *The heart surgery forum*. 2010;13(5):E311-6. Available at: http://www.ncbi.nlm.nih.gov/pubmed/20961831. Accessed April 8, 2012.

54. Rosen M, Roselli EE, Faber C, et al. Small intestinal submucosa intracardiac patch: an experimental study. *Surgical innovation*. 2005;12(3):227-31. Available at: http://www.ncbi.nlm.nih.gov/pubmed/16224643. Accessed April 8, 2012.

55. Filsoufi F, Carpentier A. Principles of reconstructive surgery in degenerative mitral valve disease. *Seminars in thoracic and cardiovascular surgery*. 2007;19(2):103-10. Available at: http://www.ncbi.nlm.nih.gov/pubmed/17870003. Accessed April 8, 2012.

56. Collins P, Cotton RE, Duff RS. Symptomatic mitral myxomatous transformation in the elderly. *Thorax*. 1976;31(6):765-70. Available at: http://www.pubmedcentral.nih.gov/articlerender.fcgi?artid=470508&tool=pmcentrez&rendertype=abstract. Accessed April 8, 2012.

57. Freed LA, Acierno JS, Dai D, et al. A locus for autosomal dominant mitral valve prolapse on chromosome 11p15.4. *American journal of human genetics*. 2003;72(6):1551-9. Available at: http://www.pubmedcentral.nih.gov/articlerender.fcgi?artid=1180315&tool=pmcentrez&rendertype=abstract. Accessed April 8, 2012.

58. Adams DH, Rosenhek R, Falk V. Degenerative mitral valve regurgitation: best practice revolution. *European heart journal*. 2010;31(16):1958-66. Available at: http://www.pubmedcentral.nih.gov/articlerender.fcgi?artid=2921508&tool=pmcentrez&rendertype=abstract. Accessed April 8, 2012.

59. Baskett RJ, Ross DB, Nanton MA, Murphy DA. Factors in the early failure of cryopreserved homograft pulmonary valves in children: preserved immunogenicity? *The Journal of thoracic and cardiovascular surgery*. 1996;112(5):1170-8; discussion 1178-9. Available at: http://www.ncbi.nlm.nih.gov/pubmed/8911313. Accessed April 8, 2012.

60. Albert JD, Bishop DA, Fullerton DA, Campbell DN, Clarke DR. Conduit reconstruction of the right ventricular outflow tract. Lessons learned in a twelve-year experience. *The Journal of thoracic and cardiovascular surgery*. 1993;106(2):228-35; discussion 235-6. Available at: http://www.ncbi.nlm.nih.gov/pubmed/8341063. Accessed April 8, 2012.

61. Gillinov AM, Blackstone EH, Nowicki ER, et al. Valve repair versus valve replacement for degenerative mitral valve disease. *The Journal of thoracic and cardiovascular surgery*. 2008;135(4):885-93, 893.e1-2. Available at: http://www.ncbi.nlm.nih.gov/pubmed/18374775. Accessed April 8, 2012.

62. Kunzelman KS, Einstein DR, Cochran RP. Fluid-structure interaction models of the mitral valve: function in normal and pathological states. *Philosophical transactions of the Royal Society of London. Series B, Biological sciences*. 2007;362(1484):1393-406. Available at: http://www.pubmedcentral.nih.gov/articlerender.fcgi?artid=2440403&tool=pmcentrez&rendertype=abstract. Accessed March 29, 2012.

63. Perloff JK, Roberts WC. The mitral apparatus. Functional anatomy of mitral regurgitation. *Circulation*. 1972;46(2):227-39. Available at: http://www.ncbi.nlm.nih.gov/pubmed/5046018. Accessed April 8, 2012.

64. Lantz GC, Badylak SF, Hiles MC, et al. Small intestinal submucosa as a vascular graft: a review. *Journal of investigative surgery : the official journal of the Academy of*

Surgical Research. 6(3):297-310. Available at: http://www.ncbi.nlm.nih.gov/pubmed/8399001. Accessed April 8, 2012.

65. Nguyen TD, Liang R, Woo SL-Y, et al. Effects of cell seeding and cyclic stretch on the fiber remodeling in an extracellular matrix-derived bioscaffold. *Tissue engineering. Part A*. 2009;15(4):957-63. Available at: http://www.pubmedcentral.nih.gov/articlerender.fcgi?artid=2787449&tool=pmcentrez&rendertype=abstract. Accessed April 8, 2012.

66. Brountzos E, Pavcnik D, Timmermans HA, et al. Remodeling of suspended small intestinal submucosa venous valve: an experimental study in sheep to assess the host cells' origin. *Journal of vascular and interventional radiology : JVIR*. 2003;14(3):349-56. Available at: http://www.ncbi.nlm.nih.gov/pubmed/12631640. Accessed April 8, 2012.

67. Weston MW, Yoganathan AP. Biosynthetic activity in heart valve leaflets in response to in vitro flow environments. *Annals of biomedical engineering*. 2001;29(9):752-63. Available at: http://www.ncbi.nlm.nih.gov/pubmed/11599583. Accessed April 8, 2012.

68. Lefebvre XP, He S, Levine RA, Yoganathan AP. Systolic anterior motion of the mitral valve in hypertrophic cardiomyopathy: an in vitro pulsatile flow study. *The Journal of heart valve disease*. 1995;4(4):422-38. Available at: http://www.ncbi.nlm.nih.gov/pubmed/7582155. Accessed April 8, 2012.

69. Jimenez JH, Soerensen DD, He Z, He S, Yoganathan AP. Effects of a saddle shaped annulus on mitral valve function and chordal force distribution: an in vitro study. *Annals of biomedical engineering*. 2003;31(10):1171-81. Available at: http://www.ncbi.nlm.nih.gov/pubmed/14649491. Accessed April 8, 2012.

70. Gheewala N, Grande-Allen KJ. Design and Mechanical Evaluation of a Physiological Mitral Valve Organ Culture System. *Cardiovascular Engineering and Technology*. 2010;1(2):123-131. Available at: http://www.springerlink.com/content/l26v7221m3574676/. Accessed April 8, 2012.

71. Platt MO, Xing Y, Jo H, Yoganathan AP. Cyclic pressure and shear stress regulate matrix metalloproteinases and cathepsin activity in porcine aortic valves. *The Journal of heart valve disease*. 2006;15(5):622-9. Available at: http://www.ncbi.nlm.nih.gov/pubmed/17044366. Accessed April 8, 2012.

72. Xing Y, Warnock JN, He Z, Hilbert SL, Yoganathan AP. Cyclic pressure affects the biological properties of porcine aortic valve leaflets in a magnitude and frequency dependent manner. *Annals of biomedical engineering*. 2004;32(11):1461-70. Available at: http://www.ncbi.nlm.nih.gov/pubmed/15636107. Accessed April 8, 2012.

73. Mulholland DL, Gotlieb AI. Cell biology of valvular interstitial cells. *The Canadian journal of cardiology*. 1996;12(3):231-6. Available at: http://www.ncbi.nlm.nih.gov/pubmed/8624972. Accessed April 8, 2012.

74. Anon. Cardiac Valve Interstitial Cells: Regulator of Valve Structure and Function. *Cardiovascular Pathology*. 1997;6(3):167-174. Available at: http://www.cardiovascularpathology.com/article/S1054-8807(96)00115-9/abstract. Accessed April 8, 2012.

75. Lester W, Rosenthal A, Granton B, Gotlieb AI. Porcine mitral valve interstitial cells in culture. *Laboratory investigation; a journal of technical methods and pathology*. 1988;59(5):710-9. Available at: http://www.ncbi.nlm.nih.gov/pubmed/3054314. Accessed April 8, 2012.

76. Konduri S, Xing Y, Warnock JN, He Z, Yoganathan AP. Normal physiological conditions maintain the biological characteristics of porcine aortic heart valves: an ex vivo organ culture study. *Annals of biomedical engineering*. 2005;33(9):1158-66. Available at: http://www.ncbi.nlm.nih.gov/pubmed/16133923. Accessed April 7, 2012.

77. Hildebrand DK, Wu ZJ, Mayer JE, Sacks MS. Design and hydrodynamic evaluation of a novel pulsatile bioreactor for biologically active heart valves. *Annals of biomedical engineering*. 2004;32(8):1039-49. Available at: http://www.ncbi.nlm.nih.gov/pubmed/15446500. Accessed April 8, 2012.

78. Engelmayr GC, Hildebrand DK, Sutherland FWH, Mayer JE, Sacks MS. A novel bioreactor for the dynamic flexural stimulation of tissue engineered heart valve biomaterials. *Biomaterials*. 2003;24(14):2523-32. Available at: http://www.ncbi.nlm.nih.gov/pubmed/12695079. Accessed April 8, 2012.

79. Liang H-C, Chang Y, Hsu C-K, Lee M-H, Sung H-W. Effects of crosslinking degree of an acellular biological tissue on its tissue regeneration pattern. *Biomaterials*. 2004;25(17):3541-52. Available at: http://www.ncbi.nlm.nih.gov/pubmed/15020128. Accessed March 15, 2012.

80. Engelmayr GC, Rabkin E, Sutherland FWH, et al. The independent role of cyclic flexure in the early in vitro development of an engineered heart valve tissue. *Biomaterials*. 2005;26(2):175-87. Available at: http://www.ncbi.nlm.nih.gov/pubmed/15207464. Accessed March 19, 2012.

81. Karran EH, Young TJ, Markwell RE, Harper GP. In vivo model of cartilage degradation--effects of a matrix metalloproteinase inhibitor. *Annals of the rheumatic diseases*. 1995;54(8):662-9. Available at: http://www.pubmedcentral.nih.gov/articlerender.fcgi?artid=1009964&tool=pmcentrez&rendertype=abstract. Accessed April 8, 2012.

82. Ketchedjian A, Jones AL, Krueger P, et al. Recellularization of decellularized allograft scaffolds in ovine great vessel reconstructions. *The Annals of thoracic surgery*. 2005;79(3):888-96; discussion 896. Available at: http://www.ncbi.nlm.nih.gov/pubmed/15734400. Accessed April 8, 2012.

83. Hilbert SL, Luna RE, Zhang J, et al. Allograft heart valves: the role of apoptosis-mediated cell loss. *The Journal of thoracic and cardiovascular surgery*. 1999;117(3):454-62. Available at: http://www.ncbi.nlm.nih.gov/pubmed/10047647. Accessed April 8, 2012.

84. Röhm E. RESOMER® Biodegradable Polymers for Medical Device Applications Research | Sigma-Aldrich.com. Available at: http://www.sigmaaldrich.com/materials-science/polymer-science/resomer.html. Accessed April 19, 2012.

85. Gilbert TW, Stewart-Akers AM, Simmons-Byrd A, Badylak SF. Degradation and remodeling of small intestinal submucosa in canine Achilles tendon repair. *The Journal of bone and joint surgery. American volume*. 2007;89(3):621-30. Available at: http://www.ncbi.nlm.nih.gov/pubmed/17332112. Accessed April 9, 2012.

86. Report F, Panel A. AVMA Guidelines on Euthanasia. *Methods*. 2007;(June).

87. Nygren A, Kondo C, Clark RB, Giles WR. Voltage-sensitive dye mapping in Langendorff-perfused rat hearts. *American journal of physiology. Heart and circulatory physiology*. 2003;284(3):H892-902. Available at: http://www.ncbi.nlm.nih.gov/pubmed/12424095. Accessed April 8, 2012.

88. Qin H, Kay MW, Chattipakorn N, et al. Effects of heart isolation, voltage-sensitive dye, and electromechanical uncoupling agents on ventricular fibrillation. *American journal of physiology. Heart and circulatory physiology*. 2003;284(5):H1818-26. Available at: http://www.ncbi.nlm.nih.gov/pubmed/12679330. Accessed April 7, 2012.

89. Efimov IR, Nikolski VP, Salama G. Optical imaging of the heart. *Circulation research*. 2004;95(1):21-33. Available at: http://www.ncbi.nlm.nih.gov/pubmed/15242982. Accessed March 21, 2012.

90. Durst CA, Cuchiara MP, Mansfield EG, West JL, Grande-Allen KJ. Flexural characterization of cell encapsulated PEGDA hydrogels with applications for tissue engineered heart valves. *Acta biomaterialia*. 2011;7(6):2467-76. Available at: http://www.ncbi.nlm.nih.gov/pubmed/21329770. Accessed April 8, 2012.

91. Sharpe WN, Pulskamp J, Gianola DS, et al. Strain Measurements of Silicon Dioxide Microspecimens by Digital Imaging Processing. *Experimental Mechanics*. 2007;47(5):649-658. Available at: http://www.springerlink.com/index/10.1007/s11340-006-9010-z. Accessed April 8, 2012.

92. Kiernan JA. *Histological and Histochemical Methods: Theory and Practice*. Scion; 2008:606. Available at: http://books.google.com/books?id=sNRNPgAACAAJ&pgis=1. Accessed April 8, 2012.

93. Ruifrok AC, Johnston DA. Quantification of histochemical staining by color deconvolution. *Analytical and quantitative cytology and histology / the International*

Academy of Cytology [and] American Society of Cytology. 2001;23(4):291-9. Available at: http://www.ncbi.nlm.nih.gov/pubmed/11531144. Accessed March 15, 2012.

94. Chung S, Dzeja PP, Faustino RS, et al. Mitochondrial oxidative metabolism is required for the cardiac differentiation of stem cells. *Nature clinical practice. Cardiovascular medicine*. 2007;4 Suppl 1:S60-7. Available at: http://www.pubmedcentral.nih.gov/articlerender.fcgi?artid=3232050&tool=pmcentrez&rendertype=abstract. Accessed April 8, 2012.

95. Hoshino T, Fujiwara H, Kawai C, Hamashima Y. Myocardial fiber diameter and regional distribution in the ventricular wall of normal adult hearts, hypertensive hearts and hearts with hypertrophic cardiomyopathy. *Circulation*. 1983;67(5):1109-16. Available at: http://www.ncbi.nlm.nih.gov/pubmed/6682019. Accessed April 8, 2012.

96. Dorin RP, Pohl HG, De Filippo RE, Yoo JJ, Atala A. Tubularized urethral replacement with unseeded matrices: what is the maximum distance for normal tissue regeneration? *World journal of urology*. 2008;26(4):323-6. Available at: http://www.ncbi.nlm.nih.gov/pubmed/18682960. Accessed April 8, 2012.

97. Lehr EJ, Rayat GR, Chiu B, et al. Decellularization reduces immunogenicity of sheep pulmonary artery vascular patches. *The Journal of thoracic and cardiovascular surgery*. 2011;141(4):1056-62. Available at: http://www.ncbi.nlm.nih.gov/pubmed/20637475. Accessed April 8, 2012.

98. Usui Y, Goff SG, Sauvage LR, et al. Effect of healing on compliance of porous Dacron grafts. *Annals of vascular surgery*. 1988;2(2):120-6. Available at: http://www.ncbi.nlm.nih.gov/pubmed/2973803. Accessed April 8, 2012.

99. Grande-Allen KJ, Barber JE, Klatka KM, et al. Mitral valve stiffening in end-stage heart failure: evidence of an organic contribution to functional mitral regurgitation. *The Journal of thoracic and cardiovascular surgery*. 2005;130(3):783-90. Available at: http://www.ncbi.nlm.nih.gov/pubmed/16153929. Accessed April 8, 2012.

100. Ota T, Gilbert TW, Badylak SF, Schwartzman D, Zenati MA. Electromechanical characterization of a tissue-engineered myocardial patch derived from extracellular matrix. *The Journal of thoracic and cardiovascular surgery*. 2007;133(4):979-85. Available at: http://www.ncbi.nlm.nih.gov/pubmed/17382638. Accessed April 8, 2012.

101. Parker KK, Ingber DE. Extracellular matrix, mechanotransduction and structural hierarchies in heart tissue engineering. *Philosophical transactions of the Royal Society of London. Series B, Biological sciences*. 2007;362(1484):1267-79. Available at: http://rstb.royalsocietypublishing.org/cgi/content/abstract/362/1484/1267. Accessed March 19, 2012.

102. Li Z, Guan J. Hydrogels for Cardiac Tissue Engineering. *Polymers*. 2011;3(2):740-761. Available at: http://www.mendeley.com/research/hydrogels-cardiac-tissue-engineering/. Accessed April 3, 2012.

103. Mummery CL, Davis RP, Krieger JE. Challenges in using stem cells for cardiac repair. *Science translational medicine*. 2010;2(27):27ps17. Available at: http://www.ncbi.nlm.nih.gov/pubmed/20393186. Accessed April 8, 2012.

104. Gupta V, Werdenberg JA, Lawrence BD, et al. Reversible secretion of glycosaminoglycans and proteoglycans by cyclically stretched valvular cells in 3D culture. *Annals of biomedical engineering*. 2008;36(7):1092-103. Available at: http://www.ncbi.nlm.nih.gov/pubmed/18425579. Accessed April 19, 2012.

105. de Vries RBM, Oerlemans A, Trommelmans L, Dierickx K, Gordijn B. Ethical aspects of tissue engineering: a review. *Tissue engineering. Part B, Reviews*. 2008;14(4):367-75. Available at: http://www.ncbi.nlm.nih.gov/pubmed/18834330. Accessed April 8, 2012.

106. Discher DE, Mooney DJ, Zandstra PW. Growth factors, matrices, and forces combine and control stem cells. *Science (New York, N.Y.)*. 2009;324(5935):1673-7. Available at: http://www.pubmedcentral.nih.gov/articlerender.fcgi?artid=2847855&tool=pmcentrez&rendertype=abstract. Accessed March 1, 2012.

107. Commission E. Need for a legislative framework for Human tissue engineering and tissue-engineered products. *October*. 2002;(June):1-5.

108. Sulmasy DP. Within you/without you: biotechnology, ontology, and ethics. *Journal of general internal medicine*. 2008;23 Suppl 1:69-72. Available at: http://www.pubmedcentral.nih.gov/articlerender.fcgi?artid=2150626&tool=pmcentrez&rendertype=abstract. Accessed April 8, 2012.

109. Paola FA, Walker RM. Deactivating the implantable cardioverter-defibrillator: a biofixture analysis. *Southern medical journal*. 2000;93(1):20-3. Available at: http://www.ncbi.nlm.nih.gov/pubmed/10653059. Accessed April 8, 2012.

110. Trommelmans L, Selling J, Dierickx K. A critical assessment of the directive on tissue engineering of the European union. *Tissue engineering*. 2007;13(4):667-72. Available at: http://www.ncbi.nlm.nih.gov/pubmed/17253926. Accessed April 8, 2012.

111. Deplazes A, Huppenbauer M. Synthetic organisms and living machines : Positioning the products of synthetic biology at the borderline between living and non-living matter. *Systems and synthetic biology*. 2009;3(1-4):55-63. Available at: http://www.pubmedcentral.nih.gov/articlerender.fcgi?artid=2759422&tool=pmcentrez&rendertype=abstract. Accessed March 1, 2012.

112. Lutter G, Metzner A, Jahnke T, et al. Percutaneous tissue-engineered pulmonary valved stent implantation. *The Annals of thoracic surgery*. 2010;89(1):259-63. Available at: http://www.ncbi.nlm.nih.gov/pubmed/20103248. Accessed April 8, 2012.

113. Anon. The Ethics of Synthetic Biology and Emerging Technologies Presidential Commission for the Study of Bioethical Issues. 2010.

114. Gregory J, McCullough LB. *John Gregory's Writings on Medical Ethics and Philosophy of Medicine (Google eBook)*. Springer; 1998:254. Available at: http://books.google.com/books?id=KogYEYUGhV8C&pgis=1. Accessed April 8, 2012.

115. Eggink AJ, Roelofs LAJ, Feitz WFJ, et al. Delayed intrauterine repair of an experimental spina bifida with a collagen biomatrix. *Pediatric neurosurgery*. 2008;44(1):29-35. Available at: http://www.ncbi.nlm.nih.gov/pubmed/18097188. Accessed April 8, 2012.

116. Hope RA, Hope T, Savulescu J, Hendrick J. *Medical Ethics and Law: The Core Curriculum*. Elsevier Health Sciences; 2008:270. Available at: http://books.google.com/books?id=DOPfK6LvGR0C&pgis=1. Accessed April 8, 2012.

APPENDIX 1

1. heart.m

The following program allows you to apply a x and y- dim mean filter over the data. The inputs into the program are the start and end times, the range of x and y pixels and the mean filter across a certain x and y dimension. The output is the graph of the data in plot format for each averaged pixel. The output is saved as an image and evaluated.

```
function heart(prefix,directory,stime,etime,xps,yps,xpe,ype,x,y,dig)
ndirectory = directory;
t1 = stime:etime;
disp(ndirectory);
xval = xpe-xps+1;
yval = ype-yps+1;
col = (mod(xval,x)-(xval))/-x;
row = (mod(yval,y)-(yval))/-y;
intense =zeros(stime-etime+1,row*col);
t = '.tif';

digit = '0';
for i = 1:dig-2
    digit = strcat('0',digit);
end
counter = 1;
 for i = 1:etime-stime+1
        val1 = 10^(counter-1);
        val2 = 10^counter;
        if i>=val1 && i<val2
            n = strcat(digit,num2str(i));
        else
            counter = counter+1;
            digit= digit(1:dig-(counter));
            n = strcat(digit,num2str(i));
        end
         file = strcat(ndirectory,'\',prefix,'-',n,t);
         I = imread(file);
         Inew = I(yps:ype,xps:xpe);
         imshow(Inew)
         for j = 1:y:ype-yps+1
             for k = 1:x:xpe-xps+1
                 aver = mean(mean(Inew(j:j+(y-1),k:k+(x-1))));
                 act = col*(j-1)+(k);
                 intense(i,act)= aver;
             end
         end
        if(floor(i/1000)==i/1000)
         disp(i)
        end
end
```

```
figure('OuterPosition',[0,0,1333,1000],'Name',strcat(directory,'-
',prefix))
subplot
for i =1:row*col
subplot(row,col,i)
plot(t1,intense(:,i))
end
saveas(gcf,strcat(directory,'-',prefix,'.tif'))
end
```

2. slopecalc.m

The following code checks the data for the slope, to see regions where action potentials could begin.

```
y = size(data,1);
x = size(data,2);
t = size(data,3);

for i =1:y
    for j = 1:x
        for k = 1:t-6
            p = polyfit([1:6],data(k:k+5),1);
            slope(i,j,k)= p(1);
    end
    end
end
```

3. runall.m

The following program allows you to input a certain folder and calculates the phase shift, absolute, frequencies, and time shift values of the images within the files. You can edit the start and end values within the code. A Gaussian convolution kernel is added to help filter the image data. Absv returns the absolute value of the fourier transform of the data. Freqv is the maximum frequency for the fourier transform for that pixel. This helps identify the most significant signals in the data. Phav returns the phase values to show where in the phase the signals are and timesv is calculated from the phase. All values are saved in values.mat

```
function [phav,absv,freqv,timesv] = runall()
```

```
listing = dir('*.tif');
pics = size(listing);
[m n] = size(imread(listing(1).name));
data = zeros(m,n,pics);
for i = 1:pics
    data(:,:,i) = imread(listing(i).name);
end

ti = 1;
tf = pics;
xs = 1;
xe = n;
ys = 1;
ye = m;

disp('gaussian convolution kernel')
t1 = ti:tf;
data = double(data);
[x y t]= size(data);
for i = 1:t
    I = data(:,:,i);
    H = fspecial('gaussian',[3 3],0.631);
    filtdata(:,:,i) = imfilter(I,H,'replicate');
    if(floor(i/1000)*1000==i)
        disp(i)
    end
end

disp('fourier')

cropdata = data(ys:ye,xs:xe,ti:tf);
for x = 1:xe-xs+1
    for y = 1:ye-ys+1
        val = fft(double(squeeze(cropdata(y,x,:))));
        absv(y,x,:) = abs(val);
        [maxval,loc]=max(absv(y,x,:));
        freqv(y,x) = loc;
        phav(y,x) = phase(val(loc));
        timesv(y,x) = phav(y,x)/(2*pi)*freqv(y,x);
    end
end
save('values');
clear all
end
```

APPENDIX 2

The following MATLAB code was used to analyze the displacement of charcoal dots applied to the tissue and generate maps that illustrate regional tissue strain (descriptions only, digital file due to length).

1. Filelist_generator.m

```
function [FileNameBase,PathNameBase,filenamelist]=filelist_generator

% Code to construct a list of 9999 or less filenames
% Programmed by Rob, changed by Chris. Automatic filelist generation
% and image time aquisition added by Chris.
% Last revision: 12/25/06
```

2. Grid_generator.m

```
function [grid_x,grid_y]=grid_generator(FileNameBase,PathNameBase);

% Code to generate the DIC analysis grid
% Completely rewritten by Chris
% Programmed first by Dan and Rob
%
% Last revision: 12/27/06

% The grid_generator function will help you create grids of markers.
The
% dialog has different options allowing you to create a marker grid
which is rectangular,
% circular, a line or two rectangels of a shape or contains only of two
% markers. After choosing one of the shapes you will be asked for the
base
% image which is typically your first image. After opening that image
you
% will be asked to click at the sites of interest and the markers will
be
% plotted on top of your image. You can choose if you want to keep
these
% markers or if you want to try again.
% It has to be noted that you can
% always generate your own marker positions. Therefore the marker
position
% in pixel has to be saved as a text based format where the x-position
is
% saved as grid_x.dat and the y-position saved as grid_y.dat.
%
```

2. Displacement.m

```
% Initialize data
% written by Chris and Dan

% Displacement.m allows you to analyze the data you aquiered with the
% correlation, fitting or mean routine. It only needs the validx and
% validy and can calculate strain from it. Before you start you should
% consider cleaning up the data as described in the guide. After that
step
% you can analyze parts of your data, or the full set. Try to use also
the
% console command, e.g. if you want to analyze only image 100-110 since
% something really interesting happend there, load validx and validy
into
% your workspace and call
% displacement(validx(:,100:110),validy(:,100:110));
% In this case displacement only loads the important images and you can
% clean this part of your data set.

function
[validx,validy,displx,disply]=delete_jumpers(validx,validy,displx,displ
y);

% written by Chris Durst

% This is a filter which helps to find jumpy data points which are
% oscillating or stop moving.
% The Filter starts by finding the next 10 datapoint neighbours
% (num_neighbours), calculates their mean position and then plots the
% difference between each data point and its neighbours versus image
% number. If a data point is jumping around it will show up as a spike.
But
% be careful, one bad one will also affect his neighbours, therefore
its
% worthwhile to use this filter step by step.
```

APPENDIX 3

1. Macro to quantify DAB intensity

```
// Find threshold value
macro "control [1]" {

open();

dir = getDirectory("image");
name = getTitle;
mainimage=name;

choices = newArray("Native", "Patch", "Transition");
Dialog.create("Select choice");
Dialog.addMessage("Select area of anaylsis. ");
Dialog.addChoice("-->", choices);
Dialog.show();
choice2 = Dialog.getChoice();

Dialog.create("Number of ROI?");
Dialog.addMessage("Enter the number of selections to be analyzed");
Dialog.addNumber("# of selections", 0);
Dialog.show();
m = Dialog.getNumber();

//run("Duplicate...", "title=ROI");

for (i=0; i<m; i++) {
      title = "ROI";
      msg = "After selecting ROI with the brush tool, click \"OK\".";
      waitForUser(title, msg);

      roiManager("add");
      roiManager("Show All");
}

roiManager("OR");
run("Clear Outside");
roiManager("Delete");
roiManager("Deselect");

title = "Preview";
msg = "After previewing image for areas to be removed, click \"OK\".";
waitForUser(title, msg);

choices = newArray("Yes", "No");
var choice ="";

Dialog.create("Select choice");
Dialog.addMessage("Are there any areas that need to be removed?");
Dialog.addChoice("-->", choices);
Dialog.show();
choice = Dialog.getChoice();

if (choice == "Yes") {
      title = "Removal";
```

```
	msg = "After selecting area to be removed with the brush tool,
click \"OK\".";
	waitForUser(title, msg);

	roiManager("add");
	roiManager("Show All");

	breakcheck = 1;
	while(breakcheck == 1) {
		Dialog.create("Select choice");
		Dialog.addMessage("Are there any areas that need to be
removed?");
		Dialog.addChoice("-->", choices);
		Dialog.show();
		choice = Dialog.getChoice();

		if  (choice == "Yes") {
			title = "Removal";
			msg = "After selecting area to be removed with the
brush tool, click \"OK\".";
			waitForUser(title, msg);

				roiManager("add");
		}
		else {
			breakcheck = 0;
			roiManager("OR");
			run("Clear");
			roiManager("Delete");
		}
	}
}

if (choice2 == "Native") {
	pathoutlines=dir+name + "-native-roi";
	saveAs("tiff", pathoutlines);
}
else if (choice2 == "Patch") {
	pathoutlines=dir+name + "-patch-roi";
	saveAs("tiff", pathoutlines);
}

run("Subtract Background...", "rolling=150 light sliding");
run("Colour Deconvolution", "vectors=[H DAB]");
close();
//run("8-bit");

run("Threshold...");
title = "Threshold";
msg = "Use the \"Threshold\" tool to\nadjust the threshold, after
recording value, click \"OK\".";
waitForUser(title, msg);

close();
close();
close();
close();
}
```

```
}


// Perform Analysis
macro "dabquant [2]" {

open();

dir = getDirectory("image");
name = getTitle;
mainimage=name;

choices = newArray("Native", "Patch", "Transition");
Dialog.create("Select choice");
Dialog.addMessage("Select area of anaylsis. ");
Dialog.addChoice("-->", choices);
Dialog.show();
choice2 = Dialog.getChoice();

Dialog.create("Number of ROI?");
Dialog.addMessage("Enter the number of selections to be analyzed");
Dialog.addNumber("# of selections", 0);
Dialog.show();
m = Dialog.getNumber();

run("Duplicate...", "title=ROI");

for (i=0; i<m; i++) {
      title = "ROI";
      msg = "After selecting ROI with the brush tool, click \"OK\".";
      waitForUser(title, msg);

      roiManager("add");
      roiManager("Show All");
}

roiManager("OR");
run("Clear Outside");
roiManager("Delete");

choices = newArray("Yes", "No");
var choice ="";

Dialog.create("Select choice");
Dialog.addMessage("Are there any areas that need to be removed?");
Dialog.addChoice("-->", choices);
Dialog.show();
choice = Dialog.getChoice();

if (choice == "Yes") {
      title = "Removal";
      msg = "After selecting area to be removed with the brush tool,
click \"OK\".";
      waitForUser(title, msg);

      roiManager("add");
      roiManager("Show All");
```

```
	breakcheck = 1;
	while(breakcheck == 1) {
		Dialog.create("Select choice");
		Dialog.addMessage("Are there any areas that need to be
removed?");
		Dialog.addChoice("-->", choices);
		Dialog.show();
		choice = Dialog.getChoice();

		if  (choice == "Yes") {
			title = "Removal";
			msg = "After selecting area to be removed with the
brush tool, click \"OK\".";
			waitForUser(title, msg);

				roiManager("add");
		}
		else {
			breakcheck = 0;
			roiManager("OR");
			run("Clear");
			//roiManager("Delete");
		}
	}
}

if (choice2 == "Native") {
	pathoutlines=dir+name + "-native-roi";
	saveAs("tiff", pathoutlines);
}
else if (choice2 == "Patch") {
	pathoutlines=dir+name + "-patch-roi";
	saveAs("tiff", pathoutlines);
}
else if (choice2 == "Transition") {
	pathoutlines=dir+name + "-transition-roi";
	saveAs("tiff", pathoutlines);
}

run("Subtract Background...", "rolling=150 light sliding");
run("Colour Deconvolution", "vectors=[H DAB]");
close();

rename("dabimage");
run("Duplicate...", "title=DAB");
//run("8-bit");

run("Threshold...");
Dialog.create("Threshold values");
Dialog.addMessage("Enter the lower and upper threshold limits");
Dialog.addNumber("Lower_Threshold", 0);
Dialog.addNumber("Upper_Threshold", 255);
Dialog.show();
Lower_Threshold = Dialog.getNumber();
Upper_Threshold = Dialog.getNumber();
setThreshold(Lower_Threshold, Upper_Threshold);

run("Convert to Mask");
```

```
run("Fill Holes");


run("Set Measurements...", "area mean min display redirect=dabimage
decimal=3");
run("Analyze Particles...", "size=40.0-Infinity circularity=0.00-1.00
show=Outlines display include");

outlines=getTitle;
selectWindow(outlines);
run("Copy");
close();

if (choice2 == "Native") {
      measurename = name + "-native.xls";
      measurepath=dir+measurename;
      saveAs("Measurements", measurepath);
      run("Close");
      close();
      selectWindow(mainimage);
      setPasteMode("AND");
      run("Paste");
      pathoutlines=dir+name + "-native-outlines";
      saveAs("tiff", pathoutlines);
}
else if (choice2 == "Patch") {
      measurename = name + "-patch.xls";
      measurepath=dir+measurename;
      saveAs("Measurements", measurepath);
      run("Close");
      close();
      selectWindow(mainimage);
      setPasteMode("AND");
      run("Paste");
      pathoutlines=dir+name + "-patch-outlines";
      saveAs("tiff", pathoutlines);
}

roiManager("delete");

close();
close();
close();
close();
close();

}
}


// Find Area
macro "area [3]" {

open();

dir = getDirectory("image");
name = getTitle;
```

```
mainimage=name;

run("Subtract Background...", "rolling=150 light sliding");
run("Colour Deconvolution", "vectors=[H DAB]");
close();
rename("area");
run("Convert to Mask");
run("Set Measurements...", "area mean min display redirect=area
decimal=3");
run("Analyze Particles...", "size=40.0-Infinity circularity=0.00-1.00
show=Outlines display");

index = lastIndexOf(name, ".");

if (index!=-1) {
name = substring(name, 0, index);
measurename = name + "-a.xls";
measurepath=dir+measurename;
saveAs("Measurements", measurepath);
pathoutlines=dir+name + "-a-outlines";
saveAs("tiff", pathoutlines);
run("Clear Results");

close();
close();
close();
close();
close();
close();
}
}
```